



MONASH University

**Fabrication and Characterization of Ordered
Plasmonic Metal Nanostructures for Sensing and
Electrocatalytic Applications**

Kun Chen

B.Eng. (with Honours)

A thesis submitted for the degree of Doctor of Philosophy at
Monash University in 2017
School of Chemistry

Copyright notice

© The author (2017).

Except as provided in the Copyright Act 1968, this thesis may not be reproduced in any form without the written permission of the author.

I certify that I have made all reasonable efforts to secure copyright permissions for third-party content included in this thesis and have not knowingly added copyright content to my work without the owner's permission.

Abstract

Due to their unique physicochemical and plasmonic properties, metal nanostructures have attracted great interest in various research fields. This thesis focuses on the fabrication of Cu-based ordered nanostructures for applications in surface-enhanced Raman spectroscopy (SERS) and electrochemical reduction of CO₂. Surface-enhanced Raman spectroscopy is a powerful spectroscopic technique with single molecule sensitivity and has emerged as a useful tool in chemical and biological sensing. Previous research has shown that coinage metals (Au, Ag, Cu) normally generate much stronger SERS enhancements than transition metals because the free-electrons in these metals can be effectively excited by visible light. To further understand this phenomenon and to synthesise SERS substrates with strong SERS enhancement and excellent reproducibility, this research started on fabricating large-scale and highly ordered Cu nanorod arrays as cost-effective SERS substrates. It was found that ordered Cu nanorod arrays can be used as cheap and effective SERS substrates in their own right by effectively tuning the gap size between neighboring nanorods to sub-10 nm and increasing the packing density of nanorods, with a detection of benzenethiol as low as 10⁻¹⁰ M. By sputtering a very thin layer of Ag nanoparticles on the surface of the Cu nanorod arrays, the detection limit of benzenethiol could be further enhanced, achieving reproducible signals at concentrations as low as 10⁻¹⁵ M. This hybrid configuration provides not only strong Raman-active sites over the whole substrate but also efficient binding sites for the capture of analyte molecules at the “hot” spots.

For the first time, SERS nanotechnology has been applied for urea detection, an important molecule in biological and medical fields. SERS substrate based Au/Cu hybrid nanostructure arrays were synthesized. By effectively optimizing the gap size between neighbouring nanorods, a high density of hot-spots was generated, enabling the substrates to detect urea signals at a concentration as low as 1 mM with great reproducibility.

Electrocatalytically converting CO₂ to hydrocarbons is a very attractive way to use the excess electricity generated from renewable energies. Cu has been considered as one of the most active materials for CO₂ conversion. This research went on to apply the Cu nanowire arrays to the

electrochemical reduction of CO₂. It was found that Cu nanowires tend to favour hydrogen evolution reaction over CO₂ reduction. By sputter-coating a thin layer of Au on top, the current density as well as Faradaic efficiency (FE) of CO were remarkably enhanced. At an overpotential of 540 mV with respect to the formation of CO, the Au-coated Cu nanowires catalyse the formation of syngas, a very useful gas mixture, with high efficiency and stability.

This research went on to synthesise ordered nanoporous Cu membranes and used them as electrodes for CO₂ reduction for the first time. In aqueous electrolyte, non-flow-through Cu membranes gave very high current densities, but produced only H₂, suggesting that the reaction was mass-transfer limited. When ionic liquid was added to the electrolyte, these flow-through membranes could catalyse the formation of CO at an overpotential as low as 90 mV. The combination of a flow-through Cu membrane catalyst and ionic liquid in the electrolyte produced syngas with high efficiency and stability at an overpotential of 390 mV.

Ultimately, this thesis was able to demonstrate various methods to synthesise different kinds of Cu-based ordered metal nanostructures, and apply them to various applications, such as sensing and electrochemical reduction of CO₂.

Declaration

This thesis contains no material which has been accepted for the award of any other degree or diploma at any university or equivalent institution and that, to the best of my knowledge and belief, this thesis contains no material previously published or written by another person, except where due reference is made in the text of the thesis.



Signature:

Print Name: ...Kun Chen.....

Date:1/9/17.....

Publications during enrolment

- **K. Chen**, X. Zhang, Y. Zhang, D. Y. Lei, H. Li, T. Williams and D. R. MacFarlane, *Advanced Materials Interfaces*, **2016**, 3.
- **K. Chen**, X. Zhang and D. R. MacFarlane, *Chemical Communications*, **2017**, 53, 7949-7952.
- **K. Chen**, X. Zhang, T. Williams, L. Bourgeois and D. R. MacFarlane, *Electrochimica Acta*, **2017**, 239, 84-89.
- M. Ali, F. Zhou, **K. Chen**, C. Kozur, C. Xiao, L. Bourgeois, X. Zhang and D.R.MacFarlane, *Nature communications*, **2016**, 7
- M. Kar, Z. Ma, L. M. Azofra, **K. Chen**, M. Forsyth and D. R. MacFarlane, *Chemical communications*, **2016**, 52, 4033-4036

Thesis including published works declaration

I hereby declare that this thesis no material which has been accepted for the award of any other degree or diploma at any university or equivalent institution and that, to the best of my knowledge and belief, this thesis contains no material previously published or written by another person, except where due reference is made in the test of the thesis.

This thesis includes 3 original papers published in peer reviewed journals and 1 submitted publication. The core theme of the thesis is “Fabrication and Characterization of Ordered Plasmonic Metal Nanostructures for Sensing and Electrocatalytic Applications”. The ideas, development and writing up of all the papers in the thesis were the principal responsibility of myself, the candidate, working within the School of Chemistry under the supervision of Prof. Douglas MacFarlane and Dr. Xinyi Zhang.

(The inclusion of co-authors reflects the fact that the work came from active collaboration between researchers and acknowledges input into team-based research.)

In the case of the four experimental chapters my contribution to the work involved involves the following:

Thesis Chapter	Publication Title	Status	Nature and % of student contribution	Co-author name(s) Nature and % of Co-author's contribution*	Co-author, Monash student Y/N*
2	<i>Highly Ordered Ag/Cu Hybrid Nanostructure Arrays for Ultrasensitive Surface-Enhanced Raman Spectroscopy</i>	<i>Published</i>	<i>85%. Concept, collecting and analysing data, and writing first draft</i>	<i>Doug MacFarlane, key idea and manuscript editing 5% Xinyi Zhang, key ideas and manuscript editing 5% Yongliang Zhan,,input into simulation 2% Dang Yuan Lei, input into simulation 1% Haitao Li, Input into SEM 1% Tim Williams, input into TEM analysis 1%</i>	<i>No</i>
3	<i>Ultrasensitive surface-enhanced Raman scattering detection of urea by highly ordered Au/Cu hybrid nanostructure arrays</i>	<i>Published</i>	<i>90%. Concept, collecting and analysing data, and writing first draft</i>	<i>Doug MacFarlane, key idea and manuscript editing 5% Xinyi Zhang, key ideas and manuscript editing 5%</i>	<i>No</i>
4	<i>Electrochemical reduction of CO₂ on core-shell Cu/Au nanostructure arrays for syngas production</i>	<i>Published</i>	<i>85%. Concept, collecting and analysing data, and writing first draft</i>	<i>Doug MacFarlane, key idea and manuscript editing 5% Xinyi Zhang, key ideas and manuscript editing 7% Tim Williams, input in TEM analysis 1% Laure Bourgeois, input into TEM images 2%</i>	<i>No</i>

5	<i>Electrochemical production of syngas from CO₂ on nanoporous flow-through Cu membranes in ionic liquid electrolyte</i>	<i>submitted</i>	<i>90%. Concept, collecting and analysing data, and writing first draft</i>	<i>Doug MacFarlane, key idea and manuscript editing 5% Xinyi Zhang, key ideas and manuscript editing 5%</i>	<i>No</i>
---	---	------------------	---	---	-----------

I have/ have not renumbered sections of submitted or published papers in order to generate a consistent presentation within the thesis.

Student Signature:

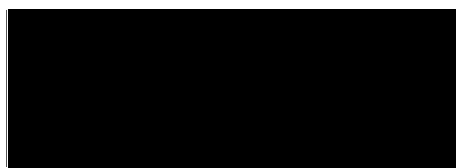


Date: 1/9/17

The undersigned hereby certify that the above declaration correctly reflects the nature and extent of the student and co-authors' contributions to this work.

Main Supervisor signature:

Date: 1/9/17



Acknowledgements

I would like to thank my supervisors, Doug and Xinyi, for their constant input, advice and support over the course of my Ph.D. Also, thanks to my third supervisor Tim for his help in TEM. Everyone in and around the Macfarlane offices have made this journey a joy and I don't know what I would have done without them. I would also like to thank my parents for their support of my PhD overseas.

Table of Content

Chapter 1 Introduction

1. Metal nanostructures	2
2. Preparation of metal nanostructures.....	3
3. Potential applications of metal nanostructures.....	5
3.1. Surface-enhanced Raman spectroscopy.....	6
3.2 Electrochemical reduction of CO ₂	10
3.3 Other applications	24
4. Aims of this project and structure of thesis.....	26

Chapter 2 Highly ordered Ag/Cu hybrid nanostructure Arrays for ultrasensitive surface-enhanced Raman spectroscopy

1. General Overview.....	42
2. Paper “Highly Ordered Ag/Cu Hybrid Nanostructure Arrays for Ultrasensitive Surface-Enhanced Raman Spectroscopy”	43
3. Supplementary Information.....	50

Chapter 3 Ultrasensitive surface-enhanced Raman scattering detection of urea by highly ordered Au/Cu hybrid nanostructure arrays

1. General Overview.....	64
2. Paper “Highly Ultrasensitive Surface-enhanced Raman Scattering Detection of Urea by Highly Ordered Au/Cu Hybrid Nanostructure Arrays”	65
3. Supplementary Information	69

Chapter 4 Electrochemical reduction of CO₂ on core-shell Cu/Au nanostructure arrays for syngas production

1. General Overview.....	78
2. Paper “Electrochemical Reduction of CO ₂ on Core-shell Cu/Au Nanostructure Arrays for Syngas Production”	79
3. Supplementary Information.....	85

Chapter 5 Electrochemical production of syngas from CO₂ on nanoporous

flow-through Cu membranes in ionic liquid electrolyte

1. General Overview.....	96
2. Paper “Electrochemical production of syngas from CO ₂ on nanoporous flow-through Cu membranes in ionic liquid electrolyte”	97
3. Supplementary Information.....	104

Chapter 6 Conclusions and Future Work

1. Conclusions.....	113
2. Future Work.....	114

Chapter 1

Introduction

Introduction

1. Metal nanostructures

In recent years, metal nanostructures have attracted great interest in various research fields because of their unique physicochemical and plasmonic properties [1, 2]. Among them, Au, Ag, and Cu nanostructures are of particular interest. These metal nanostructures have been widely used in electronics and catalysis. Recently, the interaction between metal nanostructures and light — plasmonics — has attracted much attention [3-7]. “Plasmonic” nanostructured metals have strong interactions with incident light, and are capable of converting light into a localized electric field called a localized surface plasmon [8]. By controlling the size and shape of the metal nanostructures, the localized surface plasmon effect can be significantly enhanced [9]. Applications of plasmonic effects include surface enhanced Raman spectroscopy (SERS), single molecule spectroscopy, super lenses, nanoscale lasing, plasmon-enhanced fluorescence, enhancement of non-linear optical signals, plasmon assisted photo lithography, quantum computing, light harvesting, photocatalysis, and biochemical sensing, leading to particular interest in nanoplasmonics [10-24]. As well as this, plasmonic metallic nanostructures are excellent candidates for photo- and electro- chemical catalysts; their advantages include plasmon induced hot electrons, extremely high surface areas and good catalytic activities for a variety of reactions.

This thesis focuses on preparation and characterization of metal nanostructures for two specific application areas: sensing (through surface enhanced Raman scattering, SERS) and energy (as electrodes for carbon dioxide reduction). This introduction firstly reviews methods used to produce metal nanostructures, emphasising how the shapes and sizes of particles can be controlled. Then the fundamentals of the SERS effect are introduced, followed by a brief review of nanostructured metals for SERS. Finally, CO₂ electroreduction is discussed, including the requirements for catalysts, and the particular advantages of nanostructured metals and hybrid materials for this application are indicated.

2. Preparation of metal nanostructures

Various methods have been developed to control the shape and size of synthesised nanostructures [25]. Much effort has also been devoted to making nanostructures that are cheap, environmentally friendly, and efficient. Figure 1 summarizes the various preparation methods that have been used so far to synthesise different types of metal nanostructures. Because Ag nanostructures have plasmon resonance in the visible light range, leading to potential applications in a wide range of technologies, most of the synthetic methods discussed below will be in reference to Ag.

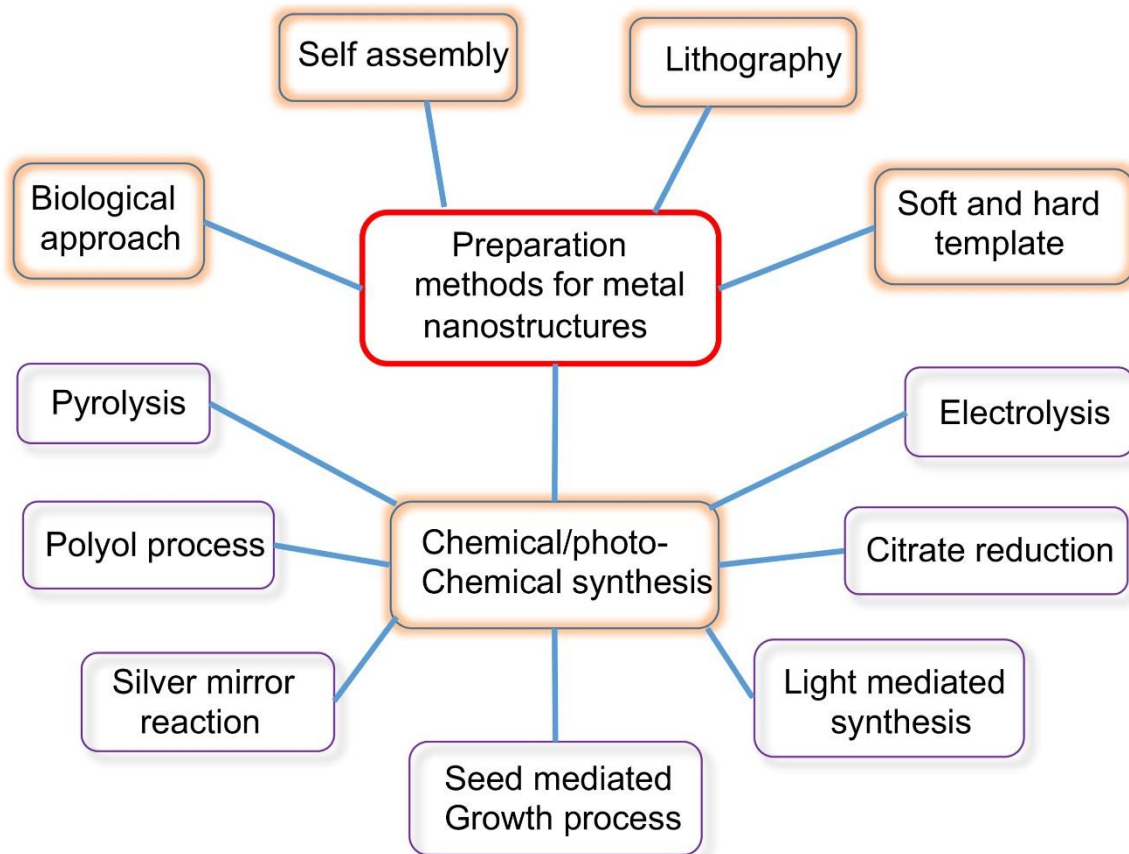


Figure 1. The various methods for synthesis of metal nanostructures.

2.1. Chemical and photochemical synthesis

The size and shape of metal nanostructures have a significant impact on their optical properties. Several methods have been developed to prepare nanostructures with controlled size and shape [26-28]. For example, one common method to synthesise Ag colloidal solutions is citrate reduction of Ag⁺ ions [29-31], where a calculated amount of sodium citrate is added into an aqueous solution of silver nitrate and heated. Through controlling the pH, spherical, triangular and rod like nanoparticles, with sizes between 20 and 500 nm, can be formed [32, 33]. Polyol synthesis is another well-known method to synthesise a variety of Ag nanostructures with different sizes and shapes [27, 34-37]. Generally speaking, a Ag salt precursor and capping agents are added into polyols for nucleation and growth of Ag nanostructures. Reaction temperature and reactant concentrations are very important factors that have a strong impact on the final reaction products. Other chemical and photochemical synthesis methods include light-mediated synthesis [38-45], electrolysis and pyrolysis [46, 47], and seed-mediated synthesis [48-51]. More complex nanostructures generally require the use of templates.

2.2. Soft- and hard-template mediated synthesis

Template-based synthesis is a very versatile way of fabricating nanostructures. [52] Templates can be either “soft” or “hard”. Normally, surfactants are used as soft templates, while porous anodic aluminium oxide (AAO) membrane is a typical hard template. Many researchers have used template assisted methods to synthesise metal nanostructures including nanowires,[52-55] nanorods,[56-58] and nanoplates.[59-63] Advantages of template-assisted synthesis include good control of the size and shape of the final products, and mild reaction conditions.[64-66]

2.3. Other synthetic methods

Assisted self-assembly process has also been used to make different metal nanostructures from nanoparticles [67-69]. Compared with other methods, this process is able to generate large structures at microscale. Another common way to make nanostructures is the hydrothermal process [70-72], which usually requires high temperature for reactions to occur. Recently, living microorganisms such as fungi

and bacteria were also used to synthesise different kinds of metal nanoparticles [73-78]. This biological approach has great potential for large-scale applications since it provides good control over the size of the nanostructures and is also environmentally friendly.

3. Potential applications of metal nanostructures

Metal nanostructures are promising materials for various potential applications. Recently many advanced applications (such as super lenses, lasers, and phase changing materials[14, 79, 80]) are also emerging. Figure 2 summarizes various potential applications of metal nanostructures. This chapter will discuss in detail about two specific applications, namely surface-enhanced Raman spectroscopy (SERS) and electrochemical reduction of CO₂, which are the focus of this thesis. In the end of the chapter, a brief introduction will be given to other potential applications of metal nanostructures.

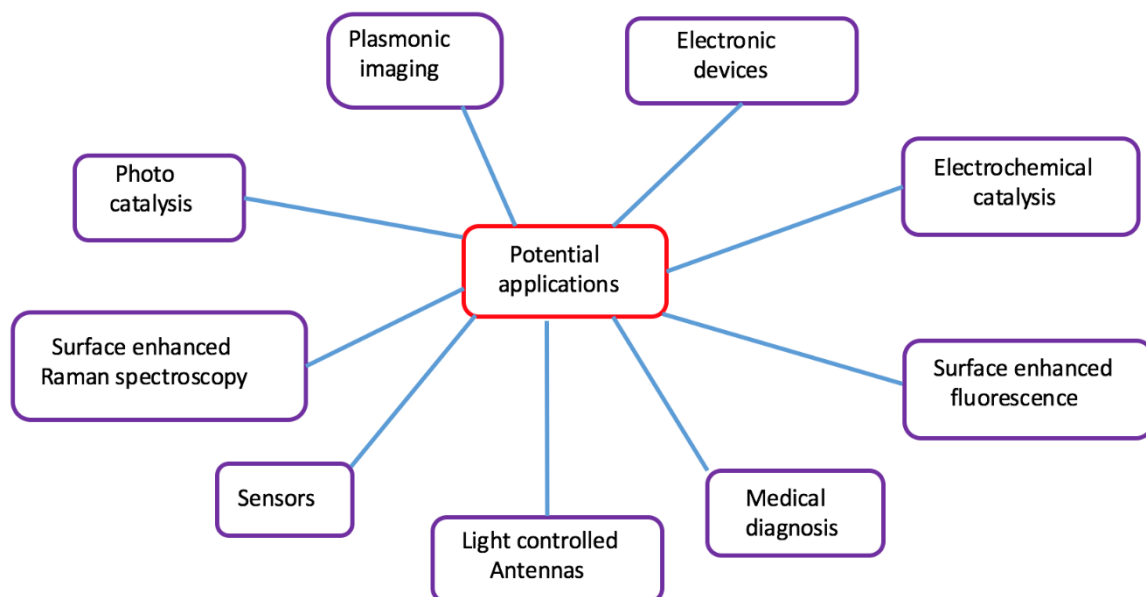


Figure 2. Potential applications of metal nanostructures.

3.1. Surface-enhanced Raman spectroscopy

The discovery of surface-enhanced Raman spectroscopy (SERS) nearly 40 years ago has sparked great interest in the scientific community [81-83]. When light interacts with a molecule, some photons undergo inelastic or Raman scattering [84]. Although most incident photons do not lose any energy when scattered, a tiny portion of the scattered photons have different energies because of the energy exchange involved in the scattering process. These energy changes reflect the characteristic energies of the vibrational modes of a certain molecule. Because different functional groups have different vibrational energies, Raman scattering is a very selective technique, making it extremely useful to identify unknown molecules [85, 86]. However, due to the very weak signals, the application of Raman scattering technique had been quite limited until the arrival of the SERS technique.

Because of its huge advantages in diagnostic testing, sensing, counterterrorism, corrosion monitoring and immunology, ever since the first discovery of SERS, tremendous efforts have been devoted to understanding the underlying physical phenomenon responsible for the dramatic enhancement of the intensity of the Raman signals [87-90]. Due to technical advances (such as nanotechnology advancement and single-molecule detection) and social needs (health care, chemical sensing), the scientific interest in SERS has been particularly strong recently [91, 92]. Most researchers are using noble metals (Ag, Au, and Cu) as SERS substrates because they have plasmon resonance in the visible spectrum. The main obstacle for practical applications of SERS-based sensors is the lack of simple synthetic methods to make reproducible SERS substrates with high sensitivity and reliability.

3.1.1. Electromagnetic and chemical SERS enhancement

To improve the performance of SERS substrates requires a deep understanding of the mechanisms of SERS enhancement. After much debate, it has been widely accepted that there are two kinds of SERS enhancements: electromagnetic and chemical enhancement. Electromagnetic enhancement accounts for the major part of the SERS enhancement, and the localized surface plasmon resonance (LSPR) generated in the near-field of metallic nanostructures is responsible for the greatly enhanced Raman signals [9, 93-100]. Because of the excitation of the LSPR, the local electromagnetic field ($|E|$) is enhanced,

resulting in significant SERS effect. Since the Raman scattering enhancement is proportional to $|E|^4$, it is possible to get a very high SER enhancement with only a modest increase in the electromagnetic field intensity [101]. Nevertheless, the SERS enhancement effects are very localized. As the distance between the analyte and metal nanoparticles increases, the SERS effects decay rapidly, making it a very surface-sensitive technique [102]. Chemical effect is another mechanism responsible for the SER enhancement. Due to the interaction with the metal nanoparticle, the electronic states of the analyte molecule are either broadened or shifted, resulting in additional SER enhancement known as chemical enhancement [101].

3.1.2. Electromagnetic enhancement of SERS effect by metal nanostructures

3.1.2.1. Size and Shape of the Metal Nanostructure

The SERS enhancement is highly dependent on the size, shape, surrounding environment, and nature of the metal nanostructures [103-110]. It is necessary that the dimension of the metal nanostructures is much smaller than the wavelength of the incident light. It has been found that most SERS-active systems often have structures in the range of 5-100 nm, while a size of 20-70 nm usually gives the highest SERS enhancements [111]. When the size is too small (less than 5 nm), the electronic scattering becomes the dominant force, depleting the electrical conductivity and therefore the SERS effect [111].

The size of the nanoparticles can also cause shift in the plasmon resonance frequencies [112]. When the source frequency is in resonance with the plasmon band, a maximum electric-field enhancement is observed [113]. Xia et al. have carried out a series of experiments to test the SERS enhancement of sharp Ag nanocubes [114]. They found out that larger particle size (around 100 nm) led to higher SER enhancement, mainly due to the resonance between the laser source and the plasmon band. The exposed crystal planes and shape of metal nanostructures also play a vital role in the SERS effects. Zhang and co-workers found out that, compared with metal nanowires, metal nanoparticles show higher SER enhancement, and the effects of crystal facets are even more dramatic [115].

It has been generally accepted that the surface plasmon band for an elongated nanoparticle has two components: longitudinal and transverse [116]. Thus, nanoparticles with sharp edges and corners normally have higher SERS enhancement because of the optical antenna effect [114].

3.1.2.2. Distance dependence of SERS intensity

The distance dependence of the SERS effect is considered as the most important feature of this technique. In the case of chemical enhancement, it is necessary for the analyte to be adsorbed to the metal nanostructure surface for the electron transfer to occur. However, when it comes to the electromagnetic enhancement, the mechanism is quite different. It is important to know that the fine geometrical features of the metal nanostructures play a vital role in the distance dependence effect [117]. Besides, the coupling of plasmons lead to an amplified polarization, thereby significantly increasing the SERS enhancement [118-121].

A lot of studies have been carried out to estimate the distance dependencies. Van et al. used atomic layer deposition (ALD) as spacer layer between the substrate and the analyte molecules [122, 123]. The authors concluded that the SERS intensity decreases by a factor of 10 with an increased distance of 2.8 nm. Some researchers also employed electron beam lithography (EBL) to investigate the distance dependence of the plasmonic coupling [115, 124-126]. Su and co-workers demonstrated that there is an exponential decay of the SERS intensity as a function of the interparticle distance [127].

3.1.2.3. Complex metal nanostructures

Ever since the report on single-molecule SERS experiments [12, 99], tremendous effects have been devoted to investigating the origin of the very high enhancement factor (EF) and developing novel metal nanostructures with high sensitivity and reproducibility [128, 129].

Although the EBL method is a versatile way of fabricating nanostructures with desired dimensions, the high cost makes it unsuitable for large scale applications. Therefore, a significant amount of attention has been focused on developing various methods (such as colloidal lithography[130-132], block copolymer lithography[133, 134], electron beam lithography [135, 136], nanoimprint lithography

[137, 138], and laser interference lithography [139-142]) to make complex nanostructures for SERS applications.

Young et al. successfully used a reactive ion etching method to make glass nanopillar arrays with silver nanoislands as SERS substrate. They concluded that their SERS substrate has a much higher EF (over 10^7) and greater signal reproducibility than previous studies [143]. Meng and colleagues show that by making highly ordered core/shell nanoporous Au/Au nanorod arrays as substrate, the SERS sensitivity could be further enhanced [144]. They used a porous AAO template-assisted method to co-electrodeposit Au-Ag alloy nanorods inside the nanochannels of the AAO template (as shown in Figure 3a). The porous Au nanorods were achieved by carefully dealloying the Ag using a concentrated HNO_3 solution (Figure 3b). After electrodepositing an ultrathin layer of Ag on the porous Au nanorods, core/shell nanoporous Au/Ag nanorod arrays were successfully synthesised (Figure 3c). They demonstrated that their SERS substrate was able to detect R6G and PCBs with extremely high sensitivities and great reproducibility.

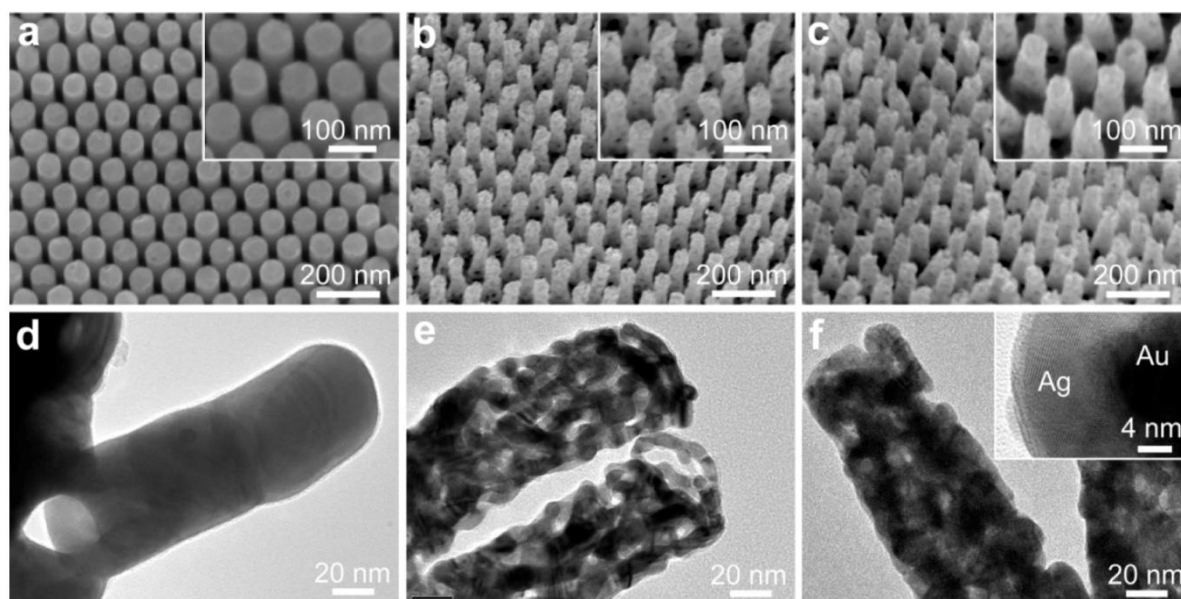


Figure 3. Structural characterizations of the nanorods after different fabrication steps. (a-c) SEM observations and enlarged views (insets) of the solid Au–Ag alloy nanorod arrays, the nanoporous Au nanorod arrays and the core@shell nanoporous Au@Ag nanorod arrays, respectively. (d–f) TEM images of the corresponding individual nanorods shown in (a–c). Reproduced with permission from Ref. [144].

Apart from nanorods based SERS substrates, Zhang et al. demonstrated that hierarchical porous plasmonic metamaterials are also great substrates for SERS applications [145]. They used AAO and poly (methyl methacrylate) (PMMA) as templates to make the desired ordered porous metal nanostructure, as shown in Figure 4a. By using lyotropic liquid-crystal (LLC) phases as mesostructure templates, they successfully synthesised hierarchical porous Au membrane as powerful SER substrate, which has a detection limit of 10^{-13} M for benzenethiol.

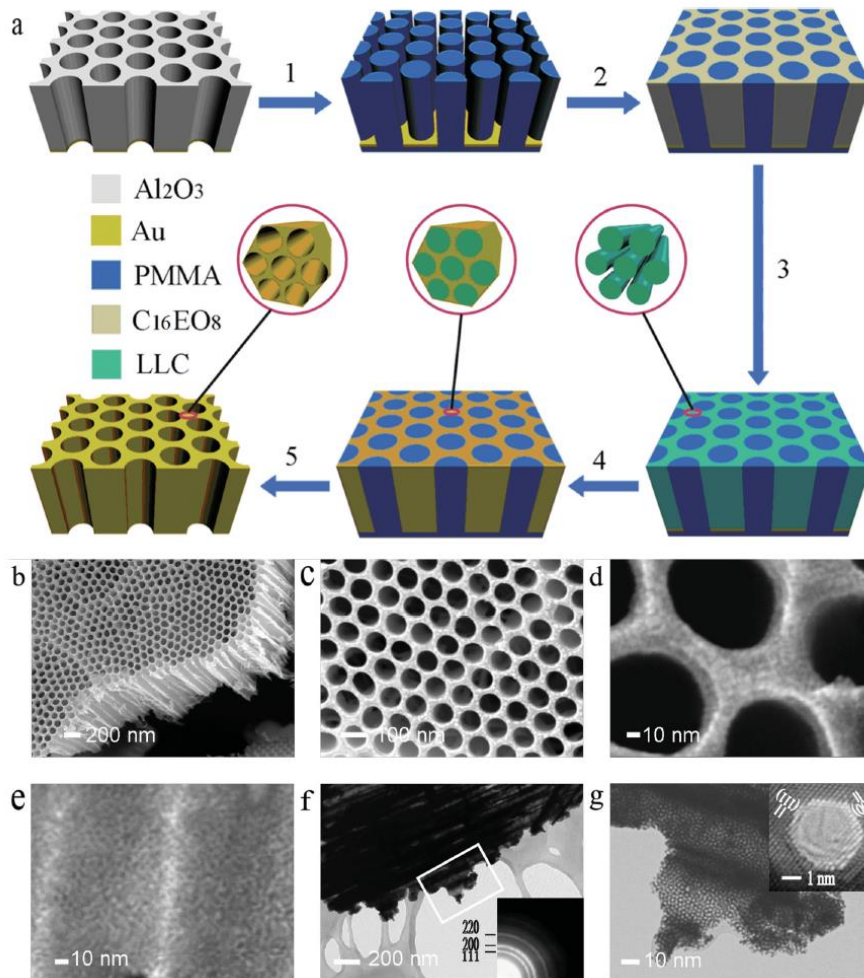


Figure 4. Fabrication and characterization of hierarchically ordered porous metamaterials. a) Schematic illustration of the preparation procedures. b,c) SEM images of oblique (b) and plain (c) views of an as-prepared membrane and d,e) its high-resolution images of plain (d) and cross-sectional views (e). f) TEM image of cross-sectional view of the membrane and its corresponding electronic diffraction pattern (inset). g) TEM image of the region indicated in (f) with the HRTEM image of a single mesopore shown in the inset. Reproduced with permission from Ref. [145].

3.2. Electrochemical reduction of CO₂

To satisfy human kind's insatiable appetite for energy, fossil fuels including petroleum, coal and natural gas are being burned at an alarming rate, which releases over 30 billion tons of carbon dioxide (CO₂) into our atmosphere annually. The pre-industrial level of CO₂ level was only about 270 ppm, but now the number has climbed up to 400 ppm. This kind of dramatic increase poses a huge threat to the delicate ecosystem of our planet. As a well-known greenhouse gas, CO₂ traps the sun's heat and is mainly responsible for causing various climate changes. Therefore, there is an urgent need to reduce the CO₂ amount produced annually and to convert CO₂ into valuable fuels in order to develop our society in a sustainable manner.

The ideal way of CO₂ conversion is to use renewable energy sources to reduce CO₂ produced in refineries, power plants and petrochemical plants into useful chemicals [146, 147]. To achieve this goal huge efforts have been devoted to investigating CO₂ reduction reaction using photochemical [148-150], thermochemical [151-153], and electrochemical approaches over the past decades [154-156].

Among the photocatalytically active systems for CO₂ reduction that have been reported so far, they all suffer from the problem of low selectivity and production rate, and are therefore not economically viable [157]. The thermochemical CO₂ conversion often requires high pressures and temperatures. An equivalent amount of hydrogen is also necessary to proceed the reaction, which means it can be energetically problematic to implement on a large scale [158].

On the contrary, the electrochemical reduction of CO₂ has attracted most of the attention of the scientific community. The main advantages of this process include the ambient reaction conditions, the controllable reaction rates, and the easy separation of the products [159].

Among potential electrocatalysts for electrochemical reduction of CO₂, bulk metals have been studied extensively over the past decades. Hori has written a detailed review about the different properties of bulk metallic catalysts for CO₂ reduction [160]. Recently, nanostructured metallic electrocatalysts have attracted particular attention due to some of their clear advantages over their bulky counterparts. One obvious advantage is that nanostructured materials usually have much bigger surface

areas, which in turn provide many more active surface sites. It has been generally accepted that the catalytic activity of heterogeneous catalysts is proportional to the amount of surface active sites they have, making it an effective way of boosting the catalytic performance by simply nanostructuring the materials. Moreover, some reports also show that nanostructured electrocatalysts tend to have improved catalytic stability [161, 162]. The main reason for this enhanced performance is due to the fact that increased surface area gives the electrocatalysts a high tolerance to the heavy metal impurities in the electrolyte, which often leads to a gradual decrease of the catalytic activity of the electrocatalysts [163]. While bulk catalysts are susceptible to even a ppm level of impurities, nanostructured electrocatalysts are better posed to deal with the impurities problem due to their much increased surface area. In addition, edge and low-coordinated sites are ubiquitous among nanostructured catalysts, which give them very different catalytic properties [164, 165].

3.2.1. Thermodynamics and kinetics of the CO₂ reduction reaction

To improve the performance of CO₂ reduction requires a deep understanding of the underlying mechanisms involved in the process. As the end final product of burning fossil fuels, CO₂ is thermodynamically stable [166, 167]. It also imposes huge challenges to convert it kinetically, since it requires a very high initial activation energy [168]. CO₂^{•-}, a key intermediate species, requires a potential as negative as -1.9 V versus the standard hydrogen electrode (SHE) to make the reaction happen in aqueous media (pH=7) [147, 169, 170]. However, several proton-assisted multiple-electron process are much easier to occur at relatively more positive potentials [160]. Various C1 and C2 products of CO₂ reduction reaction, such as CH₄, CO, C₂H₄, have been identified by using different catalysts and electrolytes [171-177]. Table 1 shows the thermodynamic redox potentials for different products [178]. These half-reaction potentials only show the minimum thermodynamic potential needed to push the reaction forward and are also dependent on the electrolyte used [179-182]. The thermodynamic potentials alone cannot possibly predict the reaction kinetics, including the reaction energy and pathway.

Electrochemical thermodynamic half-reactions	Electrode potentials (V vs. SHE) under standard conditions
$\text{CO}_2(\text{g}) + 4\text{H}^+ + 4\text{e}^- \rightarrow \text{C}(\text{s}) + 2\text{H}_2\text{O}(\text{l})$	0.210
$\text{CO}_2(\text{g}) + 2\text{H}_2\text{O}(\text{l}) + 4\text{e}^- \rightarrow \text{C}(\text{s}) + 4\text{OH}^-$	-0.627
$\text{CO}_2(\text{g}) + 2\text{H}^+ + 2\text{e}^- \rightarrow \text{HCOOH}(\text{l})$	-0.250
$\text{CO}_2(\text{g}) + 2\text{H}_2\text{O}(\text{l}) + 2\text{e}^- \rightarrow \text{HCOO}^-(\text{aq}) + \text{OH}^-$	-1.078
$\text{CO}_2(\text{g}) + 2\text{H}^+ + 2\text{e}^- \rightarrow \text{CO}(\text{g}) + \text{H}_2\text{O}(\text{l})$	-0.106
$\text{CO}_2(\text{g}) + 2\text{H}_2\text{O}(\text{l}) + 2\text{e}^- \rightarrow \text{CO}(\text{g}) + 2\text{OH}^-$	-0.934
$\text{CO}_2(\text{g}) + 4\text{H}^+ + 4\text{e}^- \rightarrow \text{CH}_2\text{O}(\text{l}) + 4\text{OH}^-$	-0.898
$\text{CO}_2(\text{g}) + 6\text{H}^+ + 6\text{e}^- \rightarrow \text{CH}_3\text{OH}(\text{l}) + \text{H}_2\text{O}(\text{l})$	0.016
$\text{CO}_2(\text{g}) + 5\text{H}_2\text{O}(\text{l}) + 6\text{e}^- \rightarrow \text{CH}_3\text{OH}(\text{l}) + 6\text{OH}^-$	-0.812
$\text{CO}_2(\text{g}) + 8\text{H}^+ + 8\text{e}^- \rightarrow \text{CH}_4(\text{g}) + \text{H}_2\text{O}(\text{l})$	0.169
$\text{CO}_2(\text{g}) + 6\text{H}_2\text{O}(\text{l}) + 8\text{e}^- \rightarrow \text{CH}_4(\text{g}) + 8\text{OH}^-$	-0.659
$2\text{CO}_2(\text{g}) + 2\text{H}^+ + 2\text{e}^- \rightarrow \text{H}_2\text{C}_2\text{O}_2(\text{aq})$	-0.500
$2\text{CO}_2(\text{g}) + 2\text{e}^- \rightarrow \text{C}_2\text{O}_4^{2-}(\text{aq})$	-0.590
$2\text{CO}_2(\text{g}) + 12\text{H}^+ + 12\text{e}^- \rightarrow \text{CH}_2\text{CH}_2(\text{g}) + 4\text{H}_2\text{O}(\text{l})$	0.064
$2\text{CO}_2(\text{g}) + 8\text{H}_2\text{O}(\text{l}) + 12\text{e}^- \rightarrow \text{CH}_2\text{CH}_2(\text{g}) + 12\text{OH}^-$	-0.764
$2\text{CO}_2(\text{g}) + 12\text{H}^+ + 12\text{e}^- \rightarrow \text{CH}_2\text{CH}_2\text{OH}(\text{l}) + 3\text{H}_2\text{O}(\text{l})$	0.084
$2\text{CO}_2(\text{g}) + 9\text{H}_2\text{O}(\text{l}) + 12\text{e}^- \rightarrow \text{CH}_2\text{CH}_2\text{OH}(\text{l}) + 12\text{OH}^-$	-0.744

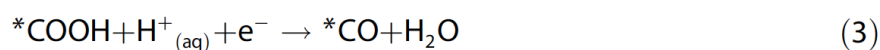
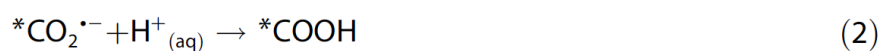
Table 1. The electrode potentials for numerous electrochemical CO₂ reduction half-reactions in aqueous solution at standard experimental conditions. Reproduced with permission from Ref. [178].

Generally speaking, CO₂ reduction in aqueous media competes with hydrogen evolution reaction (HER), which occurs at a similar thermodynamic potential (0 V vs. SHE) but requires a much lower overpotential [159]. This competing reaction makes converting CO₂ efficiently and selectively a major scientific challenge [183-189]. Therefore, ideal electrocatalysts for CO₂ reduction should be able to suppress HER, while driving CO₂ reduction at low overpotentials with high reaction rates [190-193].

3.2.2. Metal nanostructures for CO₂ reduction

As one of the most well studied metals, Ag is known for being capable of selectively converting CO₂ into CO in an aqueous media. More importantly, compared with other metal surfaces, it only requires a relatively small overpotential to push the reaction forward. One possible reason why CO₂ reduction

reaction is more favourable on the Ag surface is that it possesses appropriate binding energy to CO and COOH [194]. Another factor is that the Ag surface's binding energy to atomic H is so low that the competing HER is suppressed [195]. According to Hori's report in 1994, polycrystalline Ag surface is capable of reducing CO₂ to CO with a Faradaic efficiency of around 80% at -0.97 V versus the reversible hydrogen electrode (RHE). H₂ and a trace amount of formate were the other products detected [190]. The adsorption of CO₂^{•-} in different electrolytic media and product selectivity were investigated extensively by the authors, and they subsequently proposed a reaction scheme as shown in Equations (1)-(4):



In those equations * represents either a vacant catalytically active site or a surface-bound species. More recently, with the help of a highly sensitive custom reactor, Hatsukade et al. completed a more comprehensive evaluation of polycrystalline Ag surface at room temperature in aqueous electrolyte, as shown in Figure 5 [196]. Their results indicate that the optimal potential window is around -1.0 to -1.2 V versus RHE, when the driving force is large enough for the reaction, but not too big as to produce significant amount of H₂. Notably, they also reported the formation of methanol and ethanol on an Ag surface for the first time. This work forms the baseline for subsequent studies of CO₂ on a Ag surface in aqueous media.

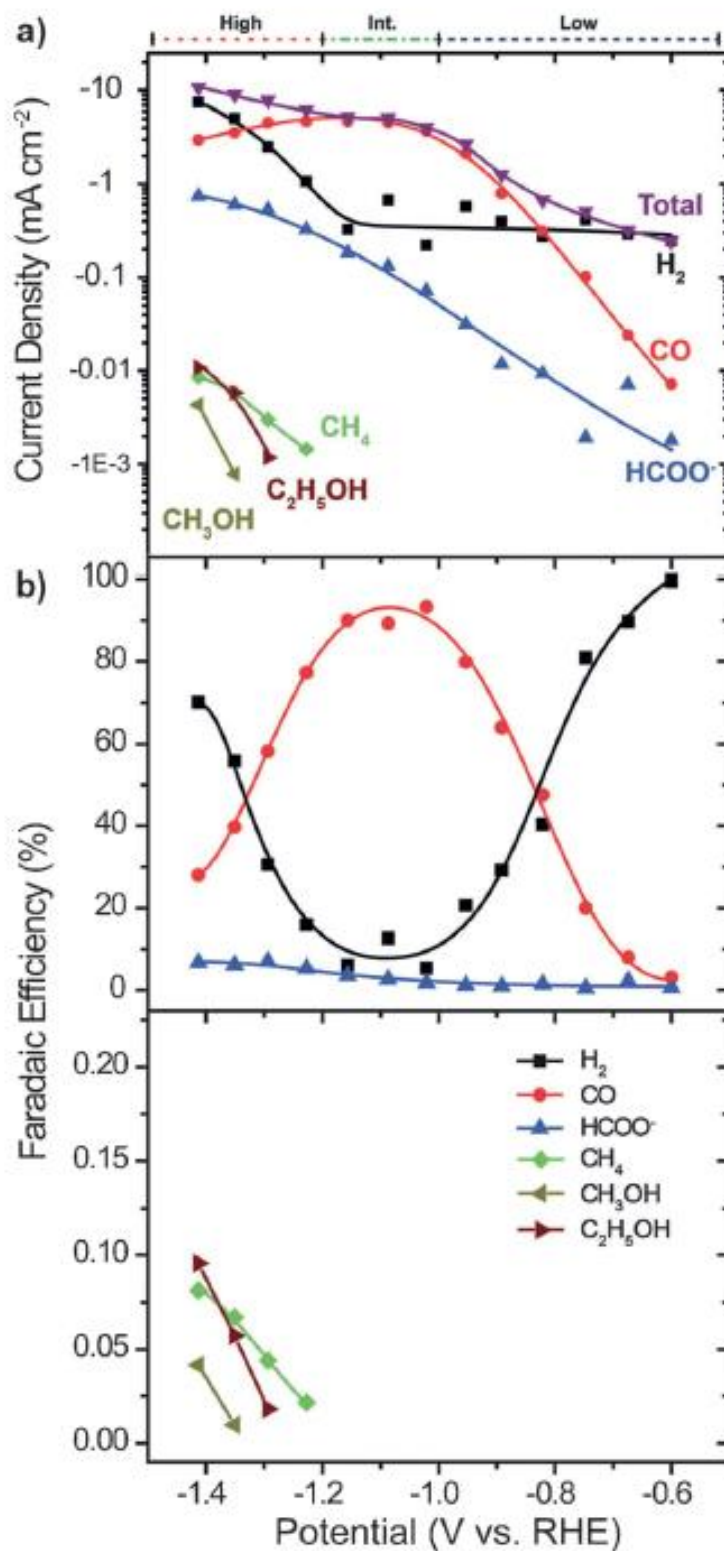


Figure 5. a) Tafel plot of the partial current density to each product. Indications for the low-, intermediate-, and high-overpotential regions are shown above the plot. b) Faradaic efficiency for each product as a function of potential. Reproduced with permission from Ref. [196].

Due to the good performance of Ag surface for CO₂ reduction, it becomes quite natural to test the catalytic performance of nanostructured Ag materials. Lu et al. used a de-alloy procedure to fabricate a nanoporous Ag catalyst with curved inner surfaces [162]. The resulting catalyst was able to achieve a significantly high current density of 20 mA cm⁻² under a relatively low overpotential (-0.6 V vs. RHE). According to this study, the intrinsic activity of nanoporous Ag surface is more than 20 times higher than that of the polycrystalline surface. The main reason for this increased activity is that on a highly curved nanoporous Ag surface, Ag (110) and Ag (221) are more prevalent. Those low-coordinated Ag atoms are capable of reducing the activation energy required to convert CO₂ to CO₂^{•-}. Notably, the experimental study conducted by Hoshi et al. also supports this theory [197].

Au is known as one of the best performing catalysts to convert CO₂ to CO selectively. Understandably, the extremely high price remains a big obstacle for Au to be applied on a large scale. Nevertheless, due to its stable electrochemical properties and high catalytic activity, Au is an ideal material for fundamental study. Zhu et al. synthesised a series of Au nanoparticles with different sizes of 4, 6, 8 and 10 nm and demonstrated that the edges sites on the Au nanoparticle surface favours CO₂ reduction while the corners sites favours the HER [198]. They concluded that the 8 nm Au nanoparticles provide an optimum number of edge sites to reduce CO₂ into CO while minimise the number of corner sites that favour HER.

To this day, metallic Cu is the best known material that is capable of converting CO₂ into a variety of hydrocarbons [199]. Although due to its low catalytic activity and poor selectivity, Cu has not been considered as an ideal catalyst for CO₂ reduction, it is still worthwhile to have a deep understanding of the unique ability of Cu to catalyse hydrocarbon formation, which would provide invaluable aid to the design of future catalysts for CO₂ reduction. With the help of a highly sensitive electrochemical cell and modern characterization techniques, Kual et al. recently re-evaluated the catalytic performance of polycrystalline Cu for CO₂ reduction, providing a better mechanistic understanding of the reaction [200]. According to their study, only four major products (CO, methane, ethylene, and formate) are observed in the low overpotential region (-0.6 to -0.8 V vs. RHE). But when the overpotential becomes higher (-0.9 to -1.15 V vs. RHE), more C1-C3 hydrocarbon products are produced. Besides, at very high

overpotential region (over -1.15 V vs RHE), all products but methane are suppressed while HER is promoted. To explain the phenomenon, the authors proposed several plausible pathways for to generate C2 and C3 products. However, further experimental work is certainly needed to give a better understanding of the reduction mechanism on polycrystalline Cu surface.

Interestingly, some studies have shown that by making nanostructured Cu electrocatalysts, their ability to reduce CO₂ was significantly reduced, while the HER was greatly promoted [201, 202]. Reske and colleagues studied the catalytic performance of Cu nanoparticles with different particle sizes (2-15 nm) for CO₂ reduction [201]. Compared with polycrystalline Cu, a significant increase of FE of H₂ can be clearly observed. After conducting a modelling study, the authors proposed that due to the presence of low-coordinated atoms, there is a stronger surface binding to CO₂ intermediates (*CO₂ or *COOH) and H_{aq}, which facilitates the H-H bond formation and makes HER the dominant pathway. Nevertheless, more studies are required to fully understand the size-dependent mechanism.

Similar phenomena were also observed in other Cu nanostructures. Sen et al. have synthesised a nanofoam with nanoscale dendritic walls for CO₂ reduction [202]. Their results show that as in the case of Cu nanoparticles, HER is greatly enhanced compared with a bulk Cu surface. As for the production of hydrocarbons, only trace amounts of C1-C3 products were detected (shown in Figure 6).

Making nanostructured Cu catalyst is clearly not a trivial thing, however currently the relationship between material dimensions and the CO₂ reduction mechanism is not well understood yet. Further experimental modelling is still needed to provide deep insights into the mechanism.

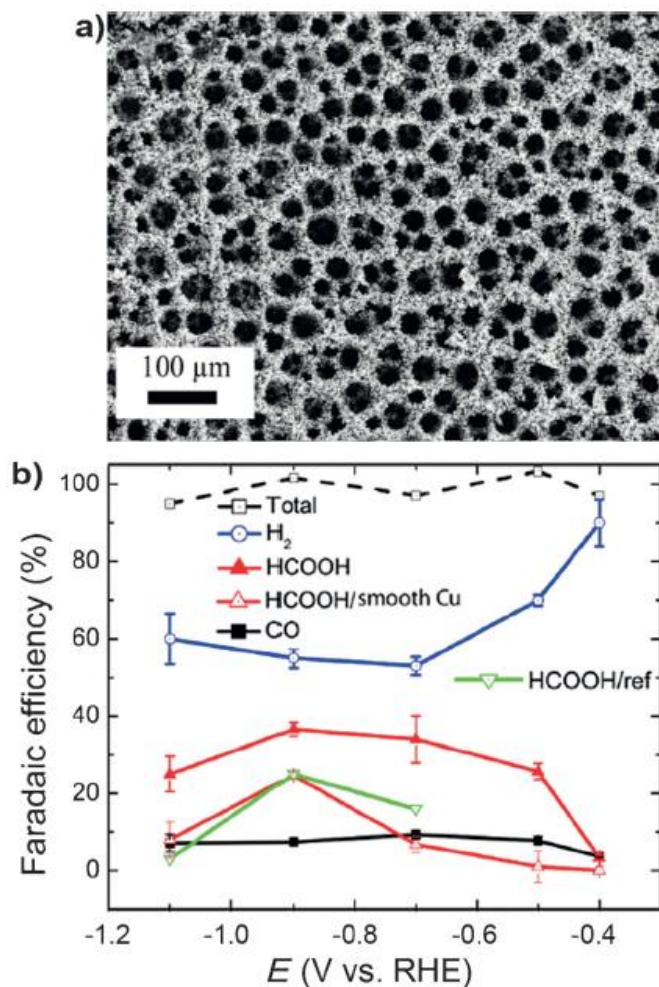


Figure 6. a) SEM image of a Cu foam deposited electrochemically. b) The corresponding product distribution as a function of applied potential. Reproduced with permission from Ref. [202].

One of the most successful measures employed recently to improve the catalytic performance of metallic catalysts was the oxidation and subsequent reduction of bulk metals. This process is capable of modifying the catalytic surface and creating more active sites. It was first proposed by Frese whose results showed increased methanol production [183]. More recently, by using much higher oxidation temperatures, Li et al. demonstrated much enhanced catalytic activity and stability of oxidized polycrystalline Cu foils [161]. After heating a Cu foil at 500 °C for 12 h in the oven, the resulting catalyst had a very rough surface structure and produced mainly CO and formate at much lower overpotentials than the untreated counterpart, as shown in Figure 7. According to the authors, the main reason for this significant improvement might be the presence of Cu¹ and surface defect sites, which

are likely to improve the formation of $\text{CO}_2^{\bullet-}$ intermediates while suppressing the HER. Nevertheless, it is difficult to draw conclusions about the improved catalytic activity per site, since the increase in the surface area is much larger than the improvement of its catalytic activity.

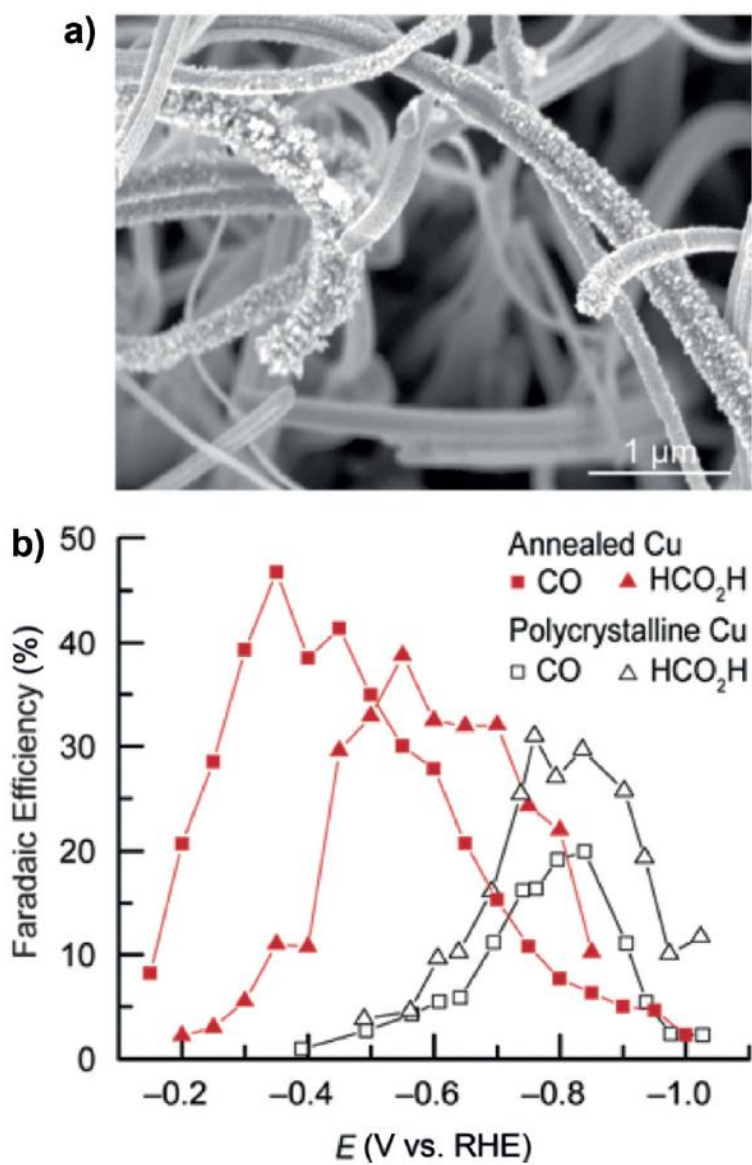


Figure 7. a) SEM image of a polycrystalline Cu foil annealed at 500°C for 12h. b) The corresponding Faradaic efficiencies for the production of CO and HCO₂H as a function of applied potentials. Reproduced with permission from Ref. [161].

The same technique has also been successfully applied to polycrystalline Au foils. Chen et al. showed that by intentionally oxidizing and reducing Au foils, the catalytic activity was significantly enhanced [203]. The resulting Au catalyst showed much higher CO production at much lower overpotentials compared with bulk Au. This enhanced performance is due to the increase of surface area and improved stabilization of $\text{CO}_2^{\bullet-}$ intermediate.

Sn has also attracted a lot of interest for CO_2 reduction. Bulk Sn is capable of reducing CO_2 primarily to formate at relatively high overpotentials. Recently, Zhang et al. showed that by reducing SnO_2 nanoparticles, the catalytic activity and selectivity to formate were enhanced [204]. The authors concluded that the size of the SnO_2 particles had a big role in the surface-species binding energy, and a maximum catalytic activity was achieved using 5 nm SnO_2 particles. Besides, Chen et al. also investigated the performance of electrodeposited Sn/ SnO_x nanoclusters as catalysts for CO_2 reduction [205]. In their study, they showed that compared with bulk Sn, the Sn/ SnO_x sites were capable of improving the catalytic performance with high efficiency and selectivity.

3.2.3. Hybrid metallic catalysts

Atoms nearby can also have a significant impact on the electronic properties of individual atoms. In the case of monoatomic catalyst, this phenomenon is not very evident since all atoms have very similar electronic properties. However, when it comes to bimetallic catalysts, the interaction of the two elements can have a major impact on the catalytic activity of the surface. Because of this, these kinds of hybrid metallic catalysts have been extensively investigated in order to improve the efficiency and selectivity of CO_2 reduction. One study showed that at -1.1 V vs. NHE Ru-Pd catalyst was able to convert CO_2 to formic acid with a current density of 80 mA cm^{-2} and a FE of approximately 90% [206]. Rasul et al. synthesised Cu-In alloy catalysts and tested them for CO_2 reduction reaction [207]. The authors concluded that the addition of In was able to suppress the HER and increase the efficiency of CO_2 reduction. At -0.5 V vs. RHE, the FE of CO formation exceeded 90%, higher than In or Cu alone.

In another work, Au-Cu hybrid catalysts were investigated by controlling the alloy composition [208]. The results revealed that the FE of methane and ethylene increased with the increase in the Cu content.

To explain this phenomenon, the authors proposed that synergistic geometric and electronic effects might have played important roles. Kortlever et al. have also synthesised Pd-Pt hybrid catalysts for CO₂ reduction. The authors reported that at a very low overpotential (-0.4 V vs. RHE) the catalysts were able to reduce CO₂ into formic acid with high efficiency (5 mA cm⁻² current density) and selectivity (88% FE) [209].

3.2.4. Nanostructured electrocatalysis in ionic liquids

Another way to reduce the energy barrier and increase the efficiency for CO₂ reduction is to add certain ionic liquids (ILs) to the electrolyte. Rosen et al. demonstrated that by forming a complex with the CO₂^{•-} intermediate, certain IL ions are able to reduce the energy barrier of CO₂ reduction [168]. According to this reference, the CO₂^{•-} can form a complex with the ionic liquid anion and move the potential for the formation of CO₂^{•-} in the positive direction, which greatly decreases the activation energy for the reduction of CO₂ to CO. The authors investigated the catalytic behaviour of Ag nanoparticles in an 18 mol % 1-ethyl-3-methylimidazolium tetrafluoroborate (EMIM-BF₄) solution. At an overpotential as low as 0.17 V (1.5 V in applied voltage), the reaction started to occur, with a Faradaic efficiency close to 100% for the production of CO. Figure 8 shows how the free energy of the system changes during the reaction.

Rosen et al. also examined the relationship between the water content in the EMIM-BF₄ solution and the catalytic performance [210]. In nearly dry IL electrolyte, the Faradaic efficiency of CO was very low. But when the water content was increased to around 90 mol %, the FE of CO increased to almost 100%, and the total current density increased from around 2 mA/cm² to over 10 mA/cm². Further increasing the water content only led to a rapid promotion of HER, causing the decrease of both current density and FE of CO. This result indicates that an appropriate amount of H₂O in EMIM-BF₄ electrolyte promotes the CO₂ reduction reaction, as the hydrolysis of BF₄⁻ provides greater proton availability. It also shows that EMIM cation is capable of inhibiting the HER even at very high water concentrations.

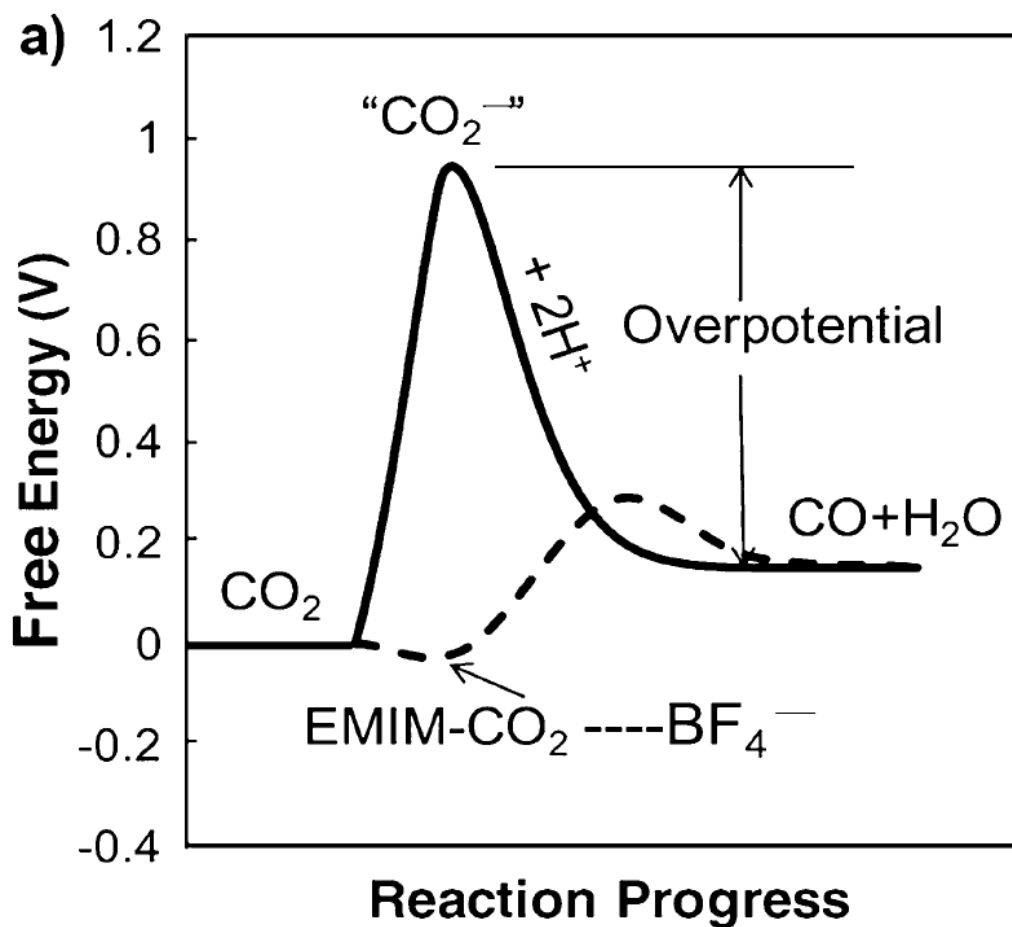


Figure 8. A schematic of how the free energy of the system changes during the reaction in water or acetonitrile (solid line) or EMIM-BF₄ (dashed line). Reproduced with permission from Ref. [168].

Salehi-Khojin et al. examined the effect of the size of the Ag nanoparticles in CO₂ reduction in an IL media [211]. The electrolyte they used was EMIM-BF₄ with 75 μM of water content. As the particle size decreased from 200 to 5 nm, there was a significant increase in the current density, which was expected because a smaller particle size means a larger surface area and more active sites. Nevertheless, when the particle size decreased further to 1 nm, there was a dramatic decrease in the current density. The authors proposed that a change of binding energy to certain intermediates is likely to be the cause of this observed abnormality.

According to some studies, IL electrolytes are also capable of changing the selectivity of product in the CO₂ reduction reaction. In aqueous media, Bi was reported to be a good catalyst for formate formation. However, DiMeglio et al. showed by conducting CO₂ reduction in an IL electrolyte, their Bi

film became CO selective [212]. This change of activity after the introduction of IL can be clearly observed in Figure 9.

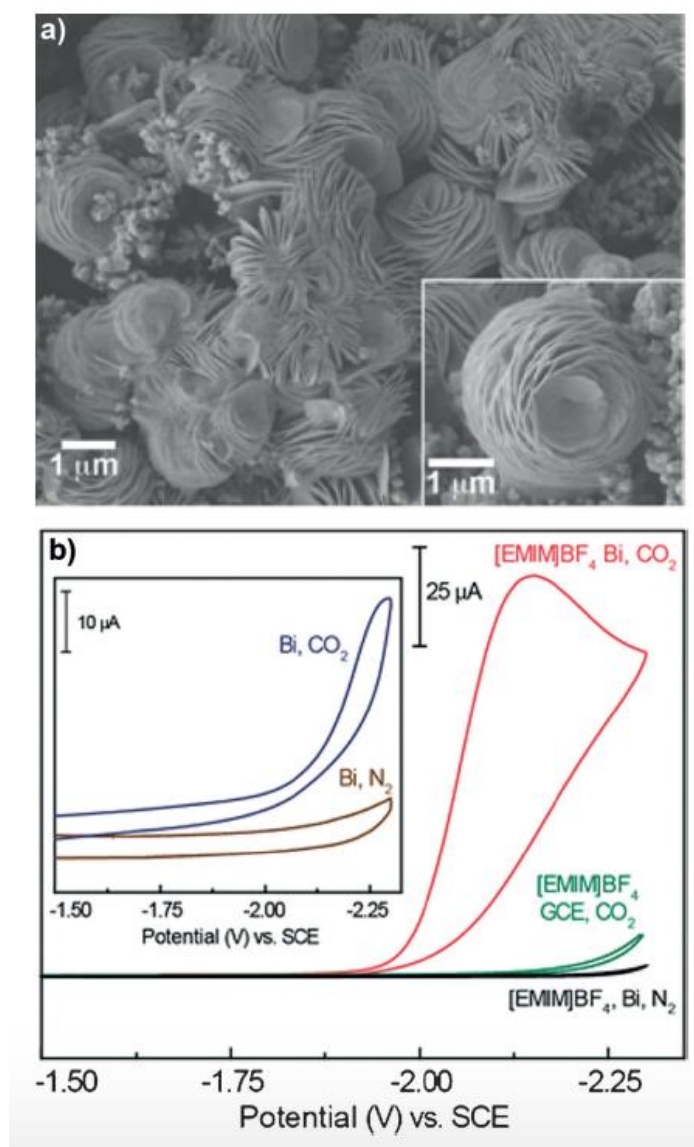


Figure 9. a) SEM image of a Bi thin film deposited on a GCE. b) CV traces recorded for Bi-deposited and bare GCEs in MeCN that contained 20 mm EMIM-BF₄. Inset: Bi-deposited GCE in MeCN without the IL. Reproduced with permission from Ref. [212].

3.3. Other applications

3.3.1. Photo catalysis

Due to their unique optical, catalytic, electronic and mechanical properties, novel functional nanomaterials have attracted great attention recently. The world is currently combating against many environmental and energy problems, which makes it of particular interest to develop novel catalysts that can catalyse desirable chemical formations using light. Plasmonic metal nanostructures often have very large surface areas, leading to increased catalytic activity. Using a green renewable energy source such as solar energy to convert CO₂ and N₂ into useful organic products in the presence of cheap and effective photocatalysts has been considered as the most desirable solution to the energy crisis we are likely to face [213].

Based on the nature of photocatalysis, it can be divided into two types, namely homogeneous photocatalysis and heterogeneous photocatalysis. A desirable photocatalytic system normal requires a big band gap, large surface area, suitable morphology, good stability and reusability [214-216]. Metal oxides, such as oxides of chromium, titanium, zinc and vanadium, are among the best known photocatalysts. The combination of light absorption properties, electronic structure, and excited lifetimes of metal oxides means they are good candidates for photocatalysts. Nevertheless, it remains extremely difficult to find a stable system with a desirable band for visible absorption. Although a lot of research has been carried out on metal oxide such as TiO₂ and ZnO, the wide band gap means their potential as photocatalysts is relatively limited since UV light only accounts for around 4% of the whole solar spectrum [217].

3.3.2. Surface-enhanced Fluorescence (SEF)

Fluorescence technique is widely applied in various fields such as optical devices, microscopy imaging, and medical diagnosis. Scientists are showing great interest in using SEF when it comes to the detection of single molecule. Surface modes and near field coupling between excited fluorophores are two main factors affecting the performance of SEF [218, 219]. It is worth pointing out that surfaces of plasmonic

nanostructure with localized surface plasmons are excellent substrates for efficient SEF. Similar to SERS, molecular distance from plasmonic nanostructures also has a great impact on the SEF experiments [220, 221].

3.3.3. Surface based electronic devices

Surface plasmons are also very important in transmitting information on computer chips. Plasmonic nanostructures are capable of supporting very high frequencies (over 100 THz), while the conventional wires can only hold 10 GHz. Due to this unique feature of extremely high frequency, plasmonic nanostructures are very useful to the development of various electronics like plasmonsters [222]. Lithographic techniques are often employed to develop different kinds of electronic devices due to their advantages in overcoming the problems involving geometry, location, and orientation [223, 224].

4. Aims of this project and structure of thesis

The general aim of this project is to develop novel metal nanostructures based on Cu for different kinds of applications. Cu was chosen for this investigation because it is relatively cheap and it has been demonstrated to be an active material for sensing and CO₂ reduction.

This thesis is divided into 6 chapters, as follows:

Chapter 1: Introduction.

Chapter 2: This chapter focuses on the fabrication of Cu nanorod arrays as well as Ag/Cu hybrid nanostructure arrays as highly sensitive and cost-effective substrates for SERS application. Coinage metals (Au, Ag, Cu) normally generate much stronger SERS enhancements than transition metals because the free-electrons in these metals can be effectively excited by visible light. So far, only a few studies have probed the performance of Cu nanostructures for SERS applications. In this chapter, the effects of the distance between neighbouring Cu nanorods as well as Ag sputtering coating are studied and the conditions will be optimized to achieve the highest SERS sensitivity.

Chapter 3: This chapter investigates the performance of Au/Cu hybrid nanostructure arrays as cost-effective and highly sensitive surface-enhanced Raman scattering substrates for the detection of urea, an important molecule in biological and medical fields. Colorimetric method is by far the most common method used for urea detection, but it requires reagent mixing and multiple incubation steps, rendering it unsuitable for quick monitoring. So it is important to have an alternative way to detect the urea concentration. In this chapter, SERS technique is employed to detect the concentration of urea solution with high sensitivity and reproducibility.

Chapter 4: This chapter studies the performance of Cu based nanowire arrays for the electrochemical reduction of CO₂. As one of the main end products of combustion, carbon dioxide is considered as the primary cause of global warming. Considering the fact that metallic Cu is the only known material that

is capable of converting CO₂ into a variety of hydrocarbons, and that both the size and structure of the electrodes could have massive impacts on the CO₂ reduction paths, it is worthwhile to explore the catalytic activity of three-dimensional nanostructured Cu electrode. This chapter examines for the first time the reduction of CO₂ on Cu/Au core-shell nanowire arrays.

Chapter 5: This chapter discusses the synthesis of ordered Cu nanoporous and examines the performance of the Cu membranes as electrodes for the electrochemical reduction of CO₂. In order to suppress the hydrogen reduction reaction, ionic liquids have been introduced as electrolytes for the reaction. The performance of flow-through porous Cu membranes for CO₂ reduction in an ionic liquid medium has been investigated and evaluated.

Chapter 6: General conclusions from chapter 2-5 and future work.

- [1] C. Rao, G. Kulkarni, P.J. Thomas, P.P. Edwards, Size-dependent chemistry: properties of nanocrystals, *Chemistry—A European Journal*, 8 (2002) 28-35.
- [2] M.I. Stockman, Nanoplasmonics: The physics behind the applications, *Physics Today*, 64 (2011) 39-44.
- [3] V.M. Shalaev, Transforming Light, *Science*, 322 (2008) 384-386.
- [4] M.L. Brongersma, V.M. Shalaev, The Case for Plasmonics, *Science*, 328 (2010) 440-441.
- [5] D.K. Gramotnev, S.I. Bozhevolnyi, Plasmonics beyond the diffraction limit, *Nature photonics*, 4 (2010) 83-91.
- [6] S. Lal, S. Link, N.J. Halas, Nano-optics from sensing to waveguiding, *Nature photonics*, 1 (2007) 641-648.
- [7] J.A. Schuller, E.S. Barnard, W. Cai, Y.C. Jun, J.S. White, M.L. Brongersma, Plasmonics for extreme light concentration and manipulation, *Nature materials*, 9 (2010) 193-204.
- [8] S. Hayashi, Near-Field Optics and Surface Plasmon Polaritons, *Topics in Applied Physics*, 81 (2001) 71.
- [9] W.L. Barnes, A. Dereux, T.W. Ebbesen, Surface plasmon subwavelength optics, *Nature*, 424 (2003) 824-830.
- [10] N.M. Nanocrystals, Plasmon Electron Transfer Photochemistry and Single-Molecule Raman Spectroscopy Brus, Louis, *Accounts of Chemical Research*, 41 (2008) 1742-1749.
- [11] J. Jiang, K. Bosnick, M. Maillard, L. Brus, Single molecule Raman spectroscopy at the junctions of large Ag nanocrystals, *ACS Publications*, 2003.
- [12] S. Nie, S.R. Emory, Probing single molecules and single nanoparticles by surface-enhanced Raman scattering, *science*, 275 (1997) 1102-1106.
- [13] S. Kühn, U. Håkanson, L. Rogobete, V. Sandoghdar, Enhancement of single-molecule fluorescence using a gold nanoparticle as an optical nanoantenna, *Physical review letters*, 97 (2006) 017402.
- [14] H.A. Atwater, A. Polman, Plasmonics for improved photovoltaic devices, *Nature materials*, 9 (2010) 205-213.
- [15] M. Moskovits, Surface-enhanced Raman spectroscopy: a brief retrospective, *Journal of Raman Spectroscopy*, 36 (2005) 485-496.
- [16] Y. Zakharko, T. Nychporuk, L. Bonacina, M. Lemiti, V. Lysenko, Plasmon-enhanced nonlinear optical properties of SiC nanoparticles, *Nanotechnology*, 24 (2013) 055703.
- [17] W. Zhou, M. Dridi, J.Y. Suh, C.H. Kim, D.T. Co, M.R. Wasielewski, G.C. Schatz, T.W. Odom, Lasing action in strongly coupled plasmonic nanocavity arrays, *Nature nanotechnology*, 8 (2013) 506-511.
- [18] D. Shao, S. Chen, Surface-plasmon-assisted nanoscale photolithography by polarized light, *Applied physics letters*, 86 (2005) 253107.
- [19] S. Pillai, K. Catchpole, T. Trupke, M. Green, Surface plasmon enhanced silicon solar cells, *Journal of applied physics*, 101 (2007) 093105.
- [20] W. Hou, S.B. Cronin, A review of surface plasmon resonance-enhanced photocatalysis, *Advanced Functional Materials*, 23 (2013) 1612-1619.
- [21] M.E. Stewart, C.R. Anderton, L.B. Thompson, J. Maria, S.K. Gray, J.A. Rogers, R.G. Nuzzo, Nanostructured plasmonic sensors, *Chemical reviews*, 108 (2008) 494-521.
- [22] N. Fang, H. Lee, C. Sun, X. Zhang, Sub-diffraction-limited optical imaging with a silver superlens, *Science*, 308 (2005) 534-537.

- [23] P.V. Kamat, Photophysical, photochemical and photocatalytic aspects of metal nanoparticles, ACS Publications, 2002.
- [24] Y. Tian, T. Tatsuma, Mechanisms and applications of plasmon-induced charge separation at TiO₂ films loaded with gold nanoparticles, *Journal of the American Chemical Society*, 127 (2005) 7632-7637.
- [25] U.Y. Qazi, R. Javaid, A Review on Metal Nanostructures: Preparation Methods and Their Potential Applications, *Advances in Nanoparticles*, 5 (2016) 27.
- [26] Y. Sun, Y. Xia, Shape-controlled synthesis of gold and silver nanoparticles, *Science*, 298 (2002) 2176-2179.
- [27] A. Tao, P. Sinsermsuksakul, P. Yang, Polyhedral silver nanocrystals with distinct scattering signatures, *Angewandte Chemie International Edition*, 45 (2006) 4597-4601.
- [28] K.E. Korte, S.E. Skrabalak, Y. Xia, Rapid synthesis of silver nanowires through a CuCl₂-mediated polyol process, *Journal of Materials Chemistry*, 18 (2008) 437-441.
- [29] A.L. Koh, K. Bao, I. Khan, W.E. Smith, G. Kothleitner, P. Nordlander, S.A. Maier, D.W. McComb, Electron energy-loss spectroscopy (EELS) of surface plasmons in single silver nanoparticles and dimers: influence of beam damage and mapping of dark modes, *ACS Nano*, 3 (2009) 3015-3022.
- [30] J.P. Camden, J.A. Dieringer, Y. Wang, D.J. Masiello, L.D. Marks, G.C. Schatz, R.P. Van Duyne, Probing the structure of single-molecule surface-enhanced Raman scattering hot spots, *Journal of the American Chemical Society*, 130 (2008) 12616-12617.
- [31] Z.S. Pillai, P.V. Kamat, What factors control the size and shape of silver nanoparticles in the citrate ion reduction method?, *The Journal of Physical Chemistry B*, 108 (2004) 945-951.
- [32] A. Henglein, M. Giersig, Formation of colloidal silver nanoparticles: capping action of citrate, *The Journal of Physical Chemistry B*, 103 (1999) 9533-9539.
- [33] X. Dong, X. Ji, H. Wu, L. Zhao, J. Li, W. Yang, Shape control of silver nanoparticles by stepwise citrate reduction, *The Journal of Physical Chemistry C*, 113 (2009) 6573-6576.
- [34] B. Wiley, Y. Sun, Y. Xia, Synthesis of silver nanostructures with controlled shapes and properties, *Accounts of Chemical Research*, 40 (2007) 1067-1076.
- [35] Y. Xia, Y. Xiong, B. Lim, S.E. Skrabalak, Shape-Controlled synthesis of metal nanocrystals: simple chemistry meets complex physics?, *Angewandte Chemie International Edition*, 48 (2009) 60-103.
- [36] B.J. Wiley, Z. Wang, J. Wei, Y. Yin, D.H. Cobden, Y. Xia, Synthesis and electrical characterization of silver nanobeams, *Nano Letters*, 6 (2006) 2273-2278.
- [37] A.R. Tao, S. Habas, P. Yang, Shape control of colloidal metal nanocrystals, *Small*, 4 (2008) 310-325.
- [38] U.Y. Qazi, S. Kajimoto, H. Fukumura, Effect of sodium dodecyl sulfate on the formation of silver nanoparticles by biphotonic reduction of silver nitrate in water, *Chemistry Letters*, 43 (2014) 1693-1695.
- [39] P. Lim, R. Liu, P. She, C. Hung, H. Shih, Synthesis of Ag nanospheres particles in ethylene glycol by electrochemical-assisted polyol process, *Chemical physics letters*, 420 (2006) 304-308.
- [40] J. Zhang, S. Li, J. Wu, G.C. Schatz, C.A. Mirkin, Plasmon-Mediated Synthesis of Silver Triangular Bipyramids, *Angewandte Chemie*, 121 (2009) 7927-7931.
- [41] A.V. Kabashin, P. Delaporte, A. Pereira, D. Grojo, R. Torres, T. Sarnet, M. Sentis, Nanofabrication with pulsed lasers, *Nanoscale research letters*, 5 (2010) 454.

- [42] X. Zheng, W. Xu, C. Corredor, S. Xu, J. An, B. Zhao, J.R. Lombardi, Laser-induced growth of monodisperse silver nanoparticles with tunable surface plasmon resonance properties and a wavelength self-limiting effect, *The Journal of Physical Chemistry C*, 111 (2007) 14962-14967.
- [43] C. Xue, G.S. Métraux, J.E. Millstone, C.A. Mirkin, Mechanistic study of photomediated triangular silver nanoprism growth, *Journal of the American Chemical Society*, 130 (2008) 8337-8344.
- [44] R. Jin, Y. Cao, C.A. Mirkin, K. Kelly, G.C. Schatz, J. Zheng, Photoinduced conversion of silver nanospheres to nanoprisms, *Science*, 294 (2001) 1901-1903.
- [45] E. Haro-Poniatowski, N. Batina, M. Acosta-García, M. Pohl-Alfaro, P. Castillo-Ocampo, C. Ricolleau, E. Fort, UV-Laser irradiation effects on silver nanostructures, *Radiation Effects & Defects in Solids*, 162 (2007) 491-499.
- [46] V.K. Sharma, R.A. Yngard, Y. Lin, Silver nanoparticles: green synthesis and their antimicrobial activities, *Advances in colloid and interface science*, 145 (2009) 83-96.
- [47] Q. Zhang, H. Liu, X. Wang, X. Shi, X. Duan, Fabrication and characterization of nano silver powder prepared by spray pyrolysis, *Journal of Wuhan University of Technology-Mater. Sci. Ed.*, 24 (2009) 871.
- [48] Q. Zhang, W. Li, C. Moran, J. Zeng, J. Chen, L.-P. Wen, Y. Xia, Seed-mediated synthesis of Ag nanocubes with controllable edge lengths in the range of 30– 200 nm and comparison of their optical properties, *Journal of the American Chemical Society*, 132 (2010) 11372-11378.
- [49] N.R. Jana, L. Gearheart, C.J. Murphy, Seed-mediated growth approach for shape-controlled synthesis of spheroidal and rod-like gold nanoparticles using a surfactant template, *Advanced Materials*, 13 (2001) 1389.
- [50] B. Pietrobon, M. McEachran, V. Kitaev, Synthesis of size-controlled faceted pentagonal silver nanorods with tunable plasmonic properties and self-assembly of these nanorods, *ACS nano*, 3 (2008) 21-26.
- [51] Y. Sun, Y. Yin, B.T. Mayers, T. Herricks, Y. Xia, Uniform silver nanowires synthesis by reducing AgNO₃ with ethylene glycol in the presence of seeds and poly (vinyl pyrrolidone), *Chemistry of Materials*, 14 (2002) 4736-4745.
- [52] A. Thomas, F. Goettmann, M. Antonietti, Hard templates for soft materials: creating nanostructured organic materials, *Chemistry of Materials*, 20 (2008) 738-755.
- [53] A. Kryukov, A. Stroyuk, N. Zin'chuk, A. Korzhak, S.Y. Kuchmii, Optical and catalytic properties of Ag₂S nanoparticles, *Journal of Molecular Catalysis A: Chemical*, 221 (2004) 209-221.
- [54] X. Zheng, L. Zhu, A. Yan, X. Wang, Y. Xie, Controlling synthesis of silver nanowires and dendrites in mixed surfactant solutions, *Journal of colloid and interface science*, 268 (2003) 357-361.
- [55] J. Zhang, B. Han, M. Liu, D. Liu, Z. Dong, J. Liu, D. Li, J. Wang, B. Dong, H. Zhao, Ultrasonication-induced formation of silver nanofibers in reverse micelles and small-angle X-ray scattering studies, *The Journal of Physical Chemistry B*, 107 (2003) 3679-3683.
- [56] N.R. Jana, L. Gearheart, C.J. Murphy, Wet chemical synthesis of silver nanorods and nanowires of controllable aspect ratio Electronic supplementary information (ESI) available: UV–VIS spectra of silver nanorods. *Chemical Communications*, (2001) 617-618.
- [57] Y. Liu, Y. Chu, L. Yang, D. Han, Z. Lü, A novel solution-phase route for the synthesis of crystalline silver nanowires, *Materials Research Bulletin*, 40 (2005) 1796-1801.
- [58] C. Ni, P.A. Hassan, E.W. Kaler, Structural characteristics and growth of pentagonal silver nanorods prepared by a surfactant method, *Langmuir*, 21 (2005) 3334-3337.

- [59] M. Maillard, S. Giorgio, M.-P. Pileni, Tuning the size of silver nanodisks with similar aspect ratios: synthesis and optical properties, *The Journal of Physical Chemistry B*, 107 (2003) 2466-2470.
- [60] W. Zhang, X. Qiao, J. Chen, Synthesis of silver nanoparticles—effects of concerned parameters in water/oil microemulsion, *Materials Science and Engineering: B*, 142 (2007) 1-15.
- [61] D.O. Yener, J. Sindel, C.A. Randall, J.H. Adair, Synthesis of nanosized silver platelets in octylamine-water bilayer systems, *Langmuir*, 18 (2002) 8692-8699.
- [62] S. Chen, D.L. Carroll, Synthesis and characterization of truncated triangular silver nanoplates, *Nano letters*, 2 (2002) 1003-1007.
- [63] D. Wang, C. Song, Z. Hu, X. Zhou, Synthesis of silver nanoparticles with flake-like shapes, *Materials Letters*, 59 (2005) 1760-1763.
- [64] R.P. Bagwe, K.C. Khilar, Effects of intermicellar exchange rate on the formation of silver nanoparticles in reverse microemulsions of AOT, *Langmuir*, 16 (2000) 905-910.
- [65] Z. Zhang, R.C. Patel, R. Kothari, C.P. Johnson, S.E. Friberg, P.A. Aikens, Stable silver clusters and nanoparticles prepared in polyacrylate and inverse micellar solutions, *The Journal of Physical Chemistry B*, 104 (2000) 1176-1182.
- [66] W. Zhang, X. Qiao, J. Chen, Q. Chen, Self-assembly and controlled synthesis of silver nanoparticles in SDS quaternary microemulsion, *Materials Letters*, 62 (2008) 1689-1692.
- [67] H. Duan, D. Wang, D.G. Kurth, H. Möhwald, Directing self-assembly of nanoparticles at water/oil interfaces, *Angewandte Chemie International Edition*, 43 (2004) 5639-5642.
- [68] B.A. Korgel, S. Fullam, S. Connolly, D. Fitzmaurice, Assembly and self-organization of silver nanocrystal superlattices: ordered “soft spheres”, *The Journal of Physical Chemistry B*, 102 (1998) 8379-8388.
- [69] J.E. Martin, J.P. Wilcoxon, J. Odinek, P. Provencio, Control of the interparticle spacing in gold nanoparticle superlattices, *The Journal of Physical Chemistry B*, 104 (2000) 9475-9486.
- [70] A.-X. Yin, W.-C. Liu, J. Ke, W. Zhu, J. Gu, Y.-W. Zhang, C.-H. Yan, Ru nanocrystals with shape-dependent surface-enhanced Raman spectra and catalytic properties: controlled synthesis and DFT calculations, *Journal of the American Chemical Society*, 134 (2012) 20479-20489.
- [71] B. Liu, H.C. Zeng, Hydrothermal synthesis of ZnO nanorods in the diameter regime of 50 nm, *Journal of the American Chemical Society*, 125 (2003) 4430-4431.
- [72] Y. Yang, X.L. Zhong, Q. Zhang, L.G. Blackstad, Z.W. Fu, Z.Y. Li, D. Qin, The role of etching in the formation of Ag nanoplates with straight, curved and wavy edges and comparison of their SERS properties, *Small*, 10 (2014) 1430-1437.
- [73] M. Kowshik, N. Deshmukh, W. Vogel, J. Urban, S.K. Kulkarni, K. Paknikar, Microbial synthesis of semiconductor CdS nanoparticles, their characterization, and their use in the fabrication of an ideal diode, *Biotechnology and Bioengineering*, 78 (2002) 583-588.
- [74] V. Bansal, P. Poddar, A. Ahmad, M. Sastry, Room-temperature biosynthesis of ferroelectric barium titanate nanoparticles, *Journal of the American Chemical Society*, 128 (2006) 11958-11963.
- [75] V. Bansal, D. Rautaray, A. Ahmad, M. Sastry, Biosynthesis of zirconia nanoparticles using the fungus *Fusarium oxysporum*, *Journal of Materials Chemistry*, 14 (2004) 3303-3305.
- [76] B. Ankamwar, M. Chaudhary, M. Sastry, Gold nanotriangles biologically synthesised using tamarind leaf extract and potential application in vapor sensing, *Synthesis and Reactivity in Inorganic, Metal-Organic and Nano-Metal Chemistry*, 35 (2005) 19-26.

- [77] V. Armendariz, I. Herrera, M. Jose-yacaman, H. Troiani, P. Santiago, J.L. Gardea-Torresdey, Size controlled gold nanoparticle formation by Avena sativa biomass: use of plants in nanobiotechnology, *Journal of Nanoparticle Research*, 6 (2004) 377-382.
- [78] M. Sastry, A. Ahmad, M.I. Khan, R. Kumar, Biosynthesis of metal nanoparticles using fungi and actinomycete, *Current science*, 85 (2003) 162-170.
- [79] B.P. Rand, P. Peumans, S.R. Forrest, Long-range absorption enhancement in organic tandem thin-film solar cells containing silver nanoclusters, *Journal of Applied Physics*, 96 (2004) 7519-7526.
- [80] H. Shen, P. Bienstman, B. Maes, Plasmonic absorption enhancement in organic solar cells with thin active layers, *Journal of Applied Physics*, 106 (2009) 073109.
- [81] D.L. Jeanmaire, R.P. Van Duyne, Surface Raman spectroelectrochemistry: Part I. Heterocyclic, aromatic, and aliphatic amines adsorbed on the anodized silver electrode, *Journal of Electroanalytical Chemistry and Interfacial Electrochemistry*, 84 (1977) 1-20.
- [82] M. Fleischmann, P.J. Hendra, A.J. McQuillan, Raman spectra of pyridine adsorbed at a silver electrode, *Chemical Physics Letters*, 26 (1974) 163-166.
- [83] M.G. Albrecht, J.A. Creighton, Anomalously intense Raman spectra of pyridine at a silver electrode, *J. Am. Chem. Soc.*, 99 (1977) 5215-5217.
- [84] K. Kneipp, H. Kneipp, I. Itzkan, R.R. Dasari, M.S. Feld, Ultrasensitive chemical analysis by Raman spectroscopy, *Chemical reviews*, 99 (1999) 2957-2976.
- [85] C. Casiraghi, S. Pisana, K. Novoselov, A. Geim, A. Ferrari, Raman fingerprint of charged impurities in graphene, *Applied Physics Letters*, 91 (2007) 233108.
- [86] M. Hashimoto, T. Araki, S. Kawata, Molecular vibration imaging in the fingerprint region by use of coherent anti-Stokes Raman scattering microscopy with a collinear configuration, *Optics Letters*, 25 (2000) 1768-1770.
- [87] A. Otto, I. Mrozek, H. Grabhorn, W. Akemann, Surface-enhanced Raman scattering, *Journal of Physics: Condensed Matter*, 4 (1992) 1143.
- [88] A. Campion, Raman spectroscopy of molecules adsorbed on solid surfaces, *Annual Review of Physical Chemistry*, 36 (1985) 549-572.
- [89] M. Moskovits, Surface-enhanced spectroscopy, *Reviews of modern physics*, 57 (1985) 783.
- [90] P. Kambhampati, C. Child, M.C. Foster, A. Campion, On the chemical mechanism of surface enhanced Raman scattering: experiment and theory, *The Journal of chemical physics*, 108 (1998) 5013-5026.
- [91] J. Homola, Surface plasmon resonance sensors for detection of chemical and biological species, *Chemical reviews*, 108 (2008) 462-493.
- [92] C. McDonagh, C.S. Burke, B.D. MacCraith, Optical chemical sensors, *Chemical reviews*, 108 (2008) 400-422.
- [93] W. Knoll, Interfaces and thin films as seen by bound electromagnetic waves, *Annual Review of Physical Chemistry*, 49 (1998) 569-638.
- [94] L.J. Sherry, S.-H. Chang, G.C. Schatz, R.P. Van Duyne, B.J. Wiley, Y. Xia, Localized surface plasmon resonance spectroscopy of single silver nanocubes, *Nano letters*, 5 (2005) 2034-2038.
- [95] T.R. Jensen, M.D. Malinsky, C.L. Haynes, R.P. Van Duyne, Nanosphere lithography: tunable localized surface plasmon resonance spectra of silver nanoparticles, *The Journal of Physical Chemistry B*, 104 (2000) 10549-10556.
- [96] E. Ringe, J.M. McMahon, K. Sohn, C. Cogley, Y. Xia, J. Huang, G.C. Schatz, L.D. Marks, R.P. Van Duyne, Unraveling the effects of size, composition, and substrate on the localized

surface plasmon resonance frequencies of gold and silver nanocubes: a systematic single-particle approach, *The Journal of Physical Chemistry C*, 114 (2010) 12511-12516.

[97] P. Lee, D. Meisel, Adsorption and surface-enhanced Raman of dyes on silver and gold sols, *J. Phys. Chem*, 86 (1982) 3391-3395.

[98] G.C. Schatz, Theoretical studies of surface enhanced Raman scattering, *Accounts of Chemical Research*, 17 (1984) 370-376.

[99] K. Kneipp, Y. Wang, H. Kneipp, L.T. Perelman, I. Itzkan, R.R. Dasari, M.S. Feld, Single molecule detection using surface-enhanced Raman scattering (SERS), *Physical review letters*, 78 (1997) 1667.

[100] A. Campion, P. Kambhampati, Surface-enhanced Raman scattering, *Chemical Society Reviews*, 27 (1998) 241-250.

[101] T.Y. Jeon, D.J. Kim, S.-G. Park, S.-H. Kim, D.-H. Kim, Nanostructured plasmonic substrates for use as SERS sensors, *Nano Convergence*, 3 (2016) 18.

[102] M. Moskovits, D. DiLella, K. Maynard, Surface Raman spectroscopy of a number of cyclic aromatic molecules adsorbed on silver: selection rules and molecular reorientation, *Langmuir*, 4 (1988) 67-76.

[103] A. Indrasekara, S. Meyers, S. Shubeita, L. Feldman, T. Gustafsson, L. Fabris, Gold nanostar substrates for SERS-based chemical sensing in the femtomolar regime, *Nanoscale*, 6 (2014) 8891-8899.

[104] F. Tian, F. Bonnier, A. Casey, A.E. Shanahan, H.J. Byrne, Surface enhanced Raman scattering with gold nanoparticles: effect of particle shape, *Analytical Methods*, 6 (2014) 9116-9123.

[105] D.-K. Lim, K.-S. Jeon, J.-H. Hwang, H. Kim, S. Kwon, Y.D. Suh, J.-M. Nam, Highly uniform and reproducible surface-enhanced Raman scattering from DNA-tailorable nanoparticles with 1-nm interior gap, *Nature nanotechnology*, 6 (2011) 452-460.

[106] A. Indrasekara, B.J. Paladini, D.J. Naczynski, V. Starovoytov, P.V. Moghe, L. Fabris, Dimeric Gold Nanoparticle Assemblies as Tags for SERS-Based Cancer Detection, *Advanced healthcare materials*, 2 (2013) 1370-1376.

[107] Y. Shin, J. Song, D. Kim, T. Kang, Facile Preparation of Ultrasmall Void Metallic Nanogap from Self-Assembled Gold–Silica Core–Shell Nanoparticles Monolayer via Kinetic Control, *Advanced Materials*, 27 (2015) 4344-4350.

[108] N. Pazos-Perez, C.S. Wagner, J.M. Romo-Herrera, L.M. Liz-Marzán, F.J. García de Abajo, A. Wittemann, A. Fery, R.A. Alvarez-Puebla, Organized Plasmonic Clusters with High Coordination Number and Extraordinary Enhancement in Surface-Enhanced Raman Scattering (SERS), *Angewandte Chemie International Edition*, 51 (2012) 12688-12693.

[109] T. Thai, Y. Zheng, S.H. Ng, S. Mudie, M. Altissimo, U. Bach, Self-Assembly of Vertically Aligned Gold Nanorod Arrays on Patterned Substrates, *Angewandte Chemie International Edition*, 51 (2012) 8732-8735.

[110] H.-Y. Chen, M.-H. Lin, C.-Y. Wang, Y.-M. Chang, S. Gwo, Large-scale hot spot engineering for quantitative SERS at the single-molecule scale, *Journal of the American Chemical Society*, 137 (2015) 13698-13705.

[111] H. Ko, S. Singamaneni, V.V. Tsukruk, Nanostructured surfaces and assemblies as SERS media, *Small*, 4 (2008) 1576-1599.

[112] S.K. Ghosh, T. Pal, Interparticle coupling effect on the surface plasmon resonance of gold nanoparticles: from theory to applications, *Chemical reviews*, 107 (2007) 4797-4862.

- [113] E. Hutter, J.H. Fendler, Exploitation of localized surface plasmon resonance, *Advanced Materials*, 16 (2004) 1685-1706.
- [114] J.M. McLellan, A. Siekkinen, J. Chen, Y. Xia, Comparison of the surface-enhanced Raman scattering on sharp and truncated silver nanocubes, *Chemical Physics Letters*, 427 (2006) 122-126.
- [115] W. Rechberger, A. Hohenau, A. Leitner, J. Krenn, B. Lamprecht, F. Aussenegg, Optical properties of two interacting gold nanoparticles, *Optics communications*, 220 (2003) 137-141.
- [116] L.J. Sherry, R. Jin, C.A. Mirkin, G.C. Schatz, R.P. Van Duyne, Localized surface plasmon resonance spectroscopy of single silver triangular nanoprisms, *Nano letters*, 6 (2006) 2060-2065.
- [117] B. Kennedy, S. Spaeth, M. Dickey, K. Carron, Determination of the distance dependence and experimental effects for modified SERS substrates based on self-assembled monolayers formed using alkanethiols, *The Journal of Physical Chemistry B*, 103 (1999) 3640-3646.
- [118] J.J. Storhoff, R. Elghanian, R.C. Mucic, C.A. Mirkin, R.L. Letsinger, One-pot colorimetric differentiation of polynucleotides with single base imperfections using gold nanoparticle probes, *Journal of the American Chemical Society*, 120 (1998) 1959-1964.
- [119] P.K. Jain, W. Qian, M.A. El-Sayed, Ultrafast electron relaxation dynamics in coupled metal nanoparticles in aggregates, *The Journal of Physical Chemistry B*, 110 (2006) 136-142.
- [120] J.J. Storhoff, A.A. Lazarides, R.C. Mucic, C.A. Mirkin, R.L. Letsinger, G.C. Schatz, What controls the optical properties of DNA-linked gold nanoparticle assemblies?, *Journal of the American Chemical Society*, 122 (2000) 4640-4650.
- [121] C. Jiang, S. Markutsya, V.V. Tsukruk, Collective and individual plasmon resonances in nanoparticle films obtained by spin-assisted layer-by-layer assembly, *Langmuir*, 20 (2004) 882-890.
- [122] J.A. Dieringer, A.D. McFarland, N.C. Shah, D.A. Stuart, A.V. Whitney, C.R. Yonzon, M.A. Young, X. Zhang, R.P. Van Duyne, Introductory lecture surface enhanced Raman spectroscopy: new materials, concepts, characterization tools, and applications, *Faraday discussions*, 132 (2006) 9-26.
- [123] A.V. Whitney, J.W. Elam, S. Zou, A.V. Zinovev, P.C. Stair, G.C. Schatz, R.P. Van Duyne, Localized surface plasmon resonance nanosensor: a high-resolution distance-dependence study using atomic layer deposition, *The Journal of Physical Chemistry B*, 109 (2005) 20522-20528.
- [124] B. Lamprecht, G. Schider, R. Lechner, H. Ditlbacher, J. Krenn, A. Leitner, F. Aussenegg, Metal nanoparticle gratings: influence of dipolar particle interaction on the plasmon resonance, *Physical review letters*, 84 (2000) 4721.
- [125] M. Salerno, N. Felidj, J. Krenn, A. Leitner, F. Aussenegg, J. Weeber, Near-field optical response of a two-dimensional grating of gold nanoparticles, *Physical Review B*, 63 (2001) 165422.
- [126] J. Krenn, A. Dereux, J. Weeber, E. Bourillot, Y. Lacroute, J. Goudonnet, G. Schider, W. Gotschy, A. Leitner, F. Aussenegg, Squeezing the optical near-field zone by plasmon coupling of metallic nanoparticles, *Physical Review Letters*, 82 (1999) 2590.
- [127] K.-H. Su, Q.-H. Wei, X. Zhang, J. Mock, D.R. Smith, S. Schultz, Interparticle coupling effects on plasmon resonances of nanogold particles, *Nano letters*, 3 (2003) 1087-1090.

- [128] V. Myroshnychenko, J. Rodríguez-Fernández, I. Pastoriza-Santos, A.M. Funston, C. Novo, P. Mulvaney, L.M. Liz-Marzán, F.J.G. de Abajo, Modelling the optical response of gold nanoparticles, *Chemical Society Reviews*, 37 (2008) 1792-1805.
- [129] H. Xu, J. Aizpurua, M. Käll, P. Apell, Electromagnetic contributions to single-molecule sensitivity in surface-enhanced Raman scattering, *Physical Review E*, 62 (2000) 4318.
- [130] T.Y. Jeon, S.-G. Park, S.Y. Lee, H.C. Jeon, S.-M. Yang, Shape control of Ag nanostructures for practical SERS substrates, *ACS applied materials & interfaces*, 5 (2013) 243-248.
- [131] N.G. Greeneltch, M.G. Blaber, A.-I. Henry, G.C. Schatz, R.P. Van Duyne, Immobilized nanorod assemblies: fabrication and understanding of large area surface-enhanced Raman spectroscopy substrates, *Analytical chemistry*, 85 (2013) 2297-2303.
- [132] H. Im, K.C. Bantz, S.H. Lee, T.W. Johnson, C.L. Haynes, S.H. Oh, Self-Assembled Plasmonic Nanoring Cavity Arrays for SERS and LSPR Biosensing, *Advanced Materials*, 25 (2013) 2678-2685.
- [133] W. Lee, S.Y. Lee, R.M. Briber, O. Rabin, Self-Assembled SERS Substrates with Tunable Surface Plasmon Resonances, *Advanced Functional Materials*, 21 (2011) 3424-3429.
- [134] W.J. Cho, Y. Kim, J.K. Kim, Ultrahigh-density array of silver nanoclusters for SERS substrate with high sensitivity and excellent reproducibility, *ACS nano*, 6 (2011) 249-255.
- [135] L. Feng, Y.-L. Xu, W.S. Fegadolli, M.-H. Lu, J.E. Oliveira, V.R. Almeida, Y.-F. Chen, A. Scherer, Experimental demonstration of a unidirectional reflectionless parity-time metamaterial at optical frequencies, *Nature materials*, 12 (2013) 108-113.
- [136] A.J. Pasquale, B.r.M. Reinhard, L. Dal Negro, Concentric necklace nanolenses for optical near-field focusing and enhancement, *Acs Nano*, 6 (2012) 4341-4348.
- [137] F.S. Ou, M. Hu, I. Naumov, A. Kim, W. Wu, A.M. Bratkovsky, X. Li, R.S. Williams, Z. Li, Hot-spot engineering in polygonal nanofinger assemblies for surface enhanced Raman spectroscopy, *Nano letters*, 11 (2011) 2538-2542.
- [138] D. Chanda, K. Shigeta, T. Truong, E. Lui, A. Mihi, M. Schulmerich, P.V. Braun, R. Bhargava, J.A. Rogers, Coupling of plasmonic and optical cavity modes in quasi-three-dimensional plasmonic crystals, *Nature communications*, 2 (2011) 479.
- [139] S.-G. Park, J.-D. Kwon, C.-W. Mun, B. Cho, C.S. Kim, M. Song, D.-H. Kim, T.Y. Jeon, H.C. Jeon, Fabrication of Au-decorated 3D ZnO nanostructures as recyclable SERS substrates, *SENSORS*, 2014 IEEE, IEEE, 2014, pp. 1387-1390.
- [140] H.C. Jeon, C.J. Heo, S.Y. Lee, S.M. Yang, Hierarchically Ordered Arrays of Noncircular Silicon Nanowires Featured by Holographic Lithography Toward a High-Fidelity Sensing Platform, *Advanced Functional Materials*, 22 (2012) 4268-4274.
- [141] T.Y. Jeon, H.C. Jeon, S.Y. Lee, T.S. Shim, J.D. Kwon, S.G. Park, S.M. Yang, 3D hierarchical architectures prepared by single exposure through a highly durable colloidal phase mask, *Advanced Materials*, 26 (2014) 1422-1426.
- [142] T.Y. Jeon, S.G. Park, D.H. Kim, S.H. Kim, Standing-Wave-Assisted Creation of Nanopillar Arrays with Vertically Integrated Nanogaps for SERS-Active Substrates, *Advanced Functional Materials*, 25 (2015) 4681-4688.
- [143] Y.J. Oh, K.H. Jeong, Glass Nanopillar Arrays with Nanogap-Rich Silver Nanoislands for Highly Intense Surface Enhanced Raman Scattering, *Advanced Materials*, 24 (2012) 2234-2237.

- [144] B. Chen, G. Meng, Q. Huang, Z. Huang, Q. Xu, C. Zhu, Y. Qian, Y. Ding, Green synthesis of large-scale highly ordered core@ shell nanoporous Au@ Ag nanorod arrays as sensitive and reproducible 3D SERS substrates, *ACS applied materials & interfaces*, 6 (2014) 15667-15675.
- [145] X. Zhang, Y. Zheng, X. Liu, W. Lu, J. Dai, D.Y. Lei, D.R. MacFarlane, Hierarchical Porous Plasmonic Metamaterials for Reproducible Ultrasensitive Surface-Enhanced Raman Spectroscopy, *Advanced Materials*, 27 (2015) 1090-1096.
- [146] R. Angamuthu, P. Byers, M. Lutz, A.L. Spek, E. Bouwman, Electrocatalytic CO₂ Conversion to Oxalate by a Copper Complex, *Science*, 327 (2010) 313-315.
- [147] Z. Chen, J.J. Concepcion, M.K. Brennaman, P. Kang, M.R. Norris, P.G. Hoertz, T.J. Meyer, Splitting CO₂ into CO and O₂ by a single catalyst, *Proceedings of the National Academy of Sciences*, 109 (2012) 15606-15611.
- [148] A.J. Morris, G.J. Meyer, E. Fujita, Molecular approaches to the photocatalytic reduction of carbon dioxide for solar fuels, *Accounts of Chemical Research*, 42 (2009) 1983-1994.
- [149] E.E. Barton, D.M. Rampulla, A.B. Bocarsly, Selective solar-driven reduction of CO₂ to methanol using a catalyzed p-GaP based photoelectrochemical cell, *Journal of the American Chemical Society*, 130 (2008) 6342-6344.
- [150] C. Wang, Z. Xie, K.E. deKrafft, W. Lin, Doping metal-organic frameworks for water oxidation, carbon dioxide reduction, and organic photocatalysis, *Journal of the American Chemical Society*, 133 (2011) 13445-13454.
- [151] W.C. Chueh, C. Falter, M. Abbott, D. Scipio, P. Furler, S.M. Haile, A. Steinfeld, High-Flux Solar-Driven Thermochemical Dissociation of CO₂ and H₂O Using Nonstoichiometric Ceria, *Science*, 330 (2010) 1797-1801.
- [152] B. Xu, Y. Bhawe, M.E. Davis, Spinel Metal Oxide-Alkali Carbonate-Based, Low-Temperature Thermochemical Cycles for Water Splitting and CO₂ Reduction, *Chemistry of Materials*, 25 (2013) 1564-1571.
- [153] D. Arifin, V.J. Aston, X. Liang, A.H. McDaniel, A.W. Weimer, CoFe₂O₄ on a porous Al₂O₃ nanostructure for solar thermochemical CO₂ splitting, *Energy & Environmental Science*, 5 (2012) 9438-9443.
- [154] E.E. Benson, C.P. Kubiak, A.J. Sathrum, J.M. Smieja, Electrocatalytic and homogeneous approaches to conversion of CO₂ to liquid fuels, *Chemical Society Reviews*, 38 (2009) 89-99.
- [155] M. Rakowski Dubois, D.L. Dubois, Development of molecular electrocatalysts for CO₂ reduction and H₂ production/oxidation, *Accounts of Chemical Research*, 42 (2009) 1974-1982.
- [156] C. Costentin, M. Robert, J.-M. Savéant, Catalysis of the electrochemical reduction of carbon dioxide, *Chemical Society Reviews*, 42 (2013) 2423-2436.
- [157] D. Cialla, A. März, R. Böhme, F. Theil, K. Weber, M. Schmitt, J. Popp, Surface-enhanced Raman spectroscopy (SERS): progress and trends, *Analytical and bioanalytical chemistry*, 403 (2012) 27-54.
- [158] P. Furler, J. Scheffe, M. Gorbar, L. Moes, U. Vogt, A. Steinfeld, Solar thermochemical CO₂ splitting utilizing a reticulated porous ceria redox system, *Energy & Fuels*, 26 (2012) 7051-7059.
- [159] Q. Lu, J. Rosen, F. Jiao, Nanostructured metallic electrocatalysts for carbon dioxide reduction, *ChemCatChem*, 7 (2015) 38-47.
- [160] Y. Hori, Electrochemical CO₂ reduction on metal electrodes, *Modern aspects of electrochemistry*, Springer 2008, pp. 89-189.

- [161] C.W. Li, M.W. Kanan, CO₂ reduction at low overpotential on Cu electrodes resulting from the reduction of thick Cu₂O films, *Journal of the American Chemical Society*, 134 (2012) 7231-7234.
- [162] Q. Lu, J. Rosen, Y. Zhou, G.S. Hutchings, Y.C. Kimmel, J.G. Chen, F. Jiao, A selective and efficient electrocatalyst for carbon dioxide reduction, *Nature communications*, 5 (2014).
- [163] Y. Hori, H. Konishi, T. Futamura, A. Murata, O. Koga, H. Sakurai, K. Oguma, "Deactivation of copper electrode" in electrochemical reduction of CO₂, *Electrochimica Acta*, 50 (2005) 5354-5369.
- [164] J. Kibsgaard, Z. Chen, B.N. Reinecke, T.F. Jaramillo, Engineering the surface structure of MoS₂ to preferentially expose active edge sites for electrocatalysis, *Nature materials*, 11 (2012) 963-969.
- [165] C. Chen, Y. Kang, Z. Huo, Z. Zhu, W. Huang, H.L. Xin, J.D. Snyder, D. Li, J.A. Herron, M. Mavrikakis, Highly crystalline multimetallic nanoframes with three-dimensional electrocatalytic surfaces, *Science*, 343 (2014) 1339-1343.
- [166] D.A. Tryk, T. Yamamoto, M. Kokubun, K. Hirota, K. Hashimoto, M. Okawa, A. Fujishima, Recent developments in electrochemical and photoelectrochemical CO₂ reduction: involvement of the (CO₂)⁻² dimer radical anion, (2001).
- [167] D.A. Tryk, T. Yamamoto, M. Kokubun, K. Hirota, K. Hashimoto, M. Okawa, A. Fujishima, Recent developments in electrochemical and photoelectrochemical CO₂ reduction: involvement of the (CO₂)⁻² dimer radical anion, *Applied organometallic chemistry*, 15 (2001) 113-120.
- [168] B.A. Rosen, A. Salehi-Khojin, M.R. Thorson, W. Zhu, D.T. Whipple, P.J. Kenis, R.I. Masel, Ionic liquid-mediated selective conversion of CO₂ to CO at low overpotentials, *Science*, 334 (2011) 643-644.
- [169] K. Chandrasekaran, L.M. Bockris, In-situ spectroscopic investigation of adsorbed intermediate radicals in electrochemical reactions: CO₂- on platinum, *Surface science*, 185 (1987) 495-514.
- [170] J.M. Bockris, J. Wass, On the photoelectrocatalytic reduction of carbon dioxide, *Materials chemistry and physics*, 22 (1989) 249-280.
- [171] D. Summers, K. Frese, MECHANISTIC ASPECTS OF THE ELECTROCHEMICAL REDUCTION OF CO₂, CO, AND CH₃OH TO CH₄ AT RU ELECTRODES, ABSTRACTS OF PAPERS OF THE AMERICAN CHEMICAL SOCIETY, AMER CHEMICAL SOC 1155 16TH ST, NW, WASHINGTON, DC 20036, 1987, pp. 246-COLL.
- [172] M. Gattrell, N. Gupta, A. Co, A review of the aqueous electrochemical reduction of CO₂ to hydrocarbons at copper, *Journal of Electroanalytical Chemistry*, 594 (2006) 1-19.
- [173] X. Nie, W. Luo, M.J. Janik, A. Asthagiri, Reaction mechanisms of CO₂ electrochemical reduction on Cu (111) determined with density functional theory, *Journal of Catalysis*, 312 (2014) 108-122.
- [174] R.J. Lim, M. Xie, M.A. Sk, J.-M. Lee, A. Fisher, X. Wang, K.H. Lim, A review on the electrochemical reduction of CO₂ in fuel cells, metal electrodes and molecular catalysts, *Catalysis Today*, 233 (2014) 169-180.
- [175] K. Dhar, C. Cavallotti, Investigation of the initial steps of the electrochemical reduction of CO₂ on Pt electrodes, *The Journal of Physical Chemistry A*, 118 (2014) 8676-8688.
- [176] J.P. Jones, G. Prakash, G.A. Olah, Electrochemical CO₂ reduction: recent advances and current trends, *Israel Journal of Chemistry*, 54 (2014) 1451-1466.

- [177] M. Karamad, H.A. Hansen, J. Rossmeisl, J.K. Nørskov, Mechanistic pathway in the electrochemical reduction of CO₂ on RuO₂, *ACS Catalysis*, 5 (2015) 4075-4081.
- [178] A.J. Bard, R. Parsons, J. Jordan, Standard potentials in aqueous solution, CRC press 1985.
- [179] M. Todoroki, K. Hara, A. Kudo, T. Sakata, Electrochemical reduction of high pressure CO₂ at Pb, Hg and In electrodes in an aqueous KHCO₃ solution, *Journal of Electroanalytical Chemistry*, 394 (1995) 199-203.
- [180] A. Murata, Y. Hori, Product selectivity affected by cationic species in electrochemical reduction of CO₂ and CO at a Cu electrode, *Bulletin of the Chemical Society of Japan*, 64 (1991) 123-127.
- [181] L. Sun, G.K. Ramesha, P.V. Kamat, J.F. Brennecke, Switching the reaction course of electrochemical CO₂ reduction with ionic liquids, *Langmuir*, 30 (2014) 6302-6308.
- [182] Y. Oh, X. Hu, Ionic liquids enhance the electrochemical CO₂ reduction catalyzed by MoO₃, *Chemical Communications*, 51 (2015) 13698-13701.
- [183] K.W. Frese, Electrochemical reduction of CO₂ at intentionally oxidized copper electrodes, *Journal of the Electrochemical Society*, 138 (1991) 3338-3344.
- [184] S.A. Wander, A. Miedaner, B.C. Noll, R.M. Barkley, D.L. DuBois, Chelate Bite Effects for [Pd (triphosphine)(solvent)](BF₄)₂ Complexes in Electrochemical CO₂ Reduction and the Heterolytic Cleavage of Molecular Hydrogen, *Organometallics*, 15 (1996) 3360-3373.
- [185] K. Hara, A. Tsuneto, A. Kudo, T. Sakata, Change in the product selectivity for the electrochemical CO₂ reduction by adsorption of sulfide ion on metal electrodes, *Journal of Electroanalytical Chemistry*, 434 (1997) 239-243.
- [186] S. Kaneco, K. Iiba, K. Ohta, T. Mizuno, A. Saji, Electrochemical reduction of CO₂ on Au in KOH+ methanol at low temperature, *Journal of Electroanalytical Chemistry*, 441 (1998) 215-220.
- [187] S. Kaneco, K. Iiba, K. Ohta, T. Mizuno, A. Saji, Electrochemical reduction of CO₂ at an Ag electrode in KOH-methanol at low temperature, *Electrochimica acta*, 44 (1998) 573-578.
- [188] M.-J. Cheng, Y. Kwon, M. Head-Gordon, A.T. Bell, Tailoring Metal-Porphyrin-Like Active Sites on Graphene to Improve the Efficiency and Selectivity of Electrochemical CO₂ Reduction, *The Journal of Physical Chemistry C*, 119 (2015) 21345-21352.
- [189] J. Wu, R.M. Yadav, M. Liu, P.P. Sharma, C.S. Tiwary, L. Ma, X. Zou, X.-D. Zhou, B.I. Yakobson, J. Lou, Achieving highly efficient, selective, and stable CO₂ reduction on nitrogen-doped carbon nanotubes, *ACS nano*, 9 (2015) 5364-5371.
- [190] Y. Hori, H. Wakebe, T. Tsukamoto, O. Koga, Electrocatalytic process of CO selectivity in electrochemical reduction of CO₂ at metal electrodes in aqueous media, *Electrochimica Acta*, 39 (1994) 1833-1839.
- [191] K. Hara, A. Tsuneto, A. Kudo, T. Sakata, Electrochemical Reduction of CO₂ on a Cu Electrode under High Pressure Factors that Determine the Product Selectivity, *Journal of the Electrochemical Society*, 141 (1994) 2097-2103.
- [192] R. Kas, R. Kortlever, A. Milbrat, M.T. Koper, G. Mul, J. Baltrusaitis, Electrochemical CO₂ reduction on Cu₂O-derived copper nanoparticles: controlling the catalytic selectivity of hydrocarbons, *Physical Chemistry Chemical Physics*, 16 (2014) 12194-12201.
- [193] J. Xie, Y. Huang, H. Yu, Tuning the catalytic selectivity in electrochemical CO₂ reduction on copper oxide-derived nanomaterials, *Frontiers of Environmental Science & Engineering*, 9 (2015) 861-866.

- [194] H.A. Hansen, J.B. Varley, A.A. Peterson, J.K. Nørskov, Understanding trends in the electrocatalytic activity of metals and enzymes for CO₂ reduction to CO, *The journal of physical chemistry letters*, 4 (2013) 388-392.
- [195] W. Sheng, M. Myint, J.G. Chen, Y. Yan, Correlating the hydrogen evolution reaction activity in alkaline electrolytes with the hydrogen binding energy on monometallic surfaces, *Energy & Environmental Science*, 6 (2013) 1509-1512.
- [196] T. Hatsukade, K.P. Kuhl, E.R. Cave, D.N. Abram, T.F. Jaramillo, Insights into the electrocatalytic reduction of CO₂ on metallic silver surfaces, *Physical Chemistry Chemical Physics*, 16 (2014) 13814-13819.
- [197] N. Hoshi, M. Kato, Y. Hori, Electrochemical reduction of CO₂ on single crystal electrodes of silver Ag (111), Ag (100) and Ag (110), *Journal of electroanalytical chemistry*, 440 (1997) 283-286.
- [198] W. Zhu, R. Michalsky, Ö. Metin, H. Lv, S. Guo, C.J. Wright, X. Sun, A.A. Peterson, S. Sun, Monodisperse Au nanoparticles for selective electrocatalytic reduction of CO₂ to CO, *J. Am. Chem. Soc.*, 135 (2013) 16833-16836.
- [199] A.A. Peterson, F. Abild-Pedersen, F. Studt, J. Rossmeisl, J.K. Nørskov, How copper catalyzes the electroreduction of carbon dioxide into hydrocarbon fuels, *Energy & Environmental Science*, 3 (2010) 1311-1315.
- [200] K.P. Kuhl, E.R. Cave, D.N. Abram, T.F. Jaramillo, New insights into the electrochemical reduction of carbon dioxide on metallic copper surfaces, *Energy & Environmental Science*, 5 (2012) 7050-7059.
- [201] R. Reske, H. Mistry, F. Behafarid, B. Roldan Cuenya, P. Strasser, Particle size effects in the catalytic electroreduction of CO₂ on Cu nanoparticles, *Journal of the American Chemical Society*, 136 (2014) 6978-6986.
- [202] S. Sen, D. Liu, G.T.R. Palmore, Electrochemical reduction of CO₂ at copper nanofoams, *Acs Catalysis*, 4 (2014) 3091-3095.
- [203] Y. Chen, C.W. Li, M.W. Kanan, Aqueous CO₂ reduction at very low overpotential on oxide-derived Au nanoparticles, *Journal of the American Chemical Society*, 134 (2012) 19969-19972.
- [204] S. Zhang, P. Kang, T.J. Meyer, Nanostructured tin catalysts for selective electrochemical reduction of carbon dioxide to formate, *Journal of the American Chemical Society*, 136 (2014) 1734-1737.
- [205] Y. Chen, M.W. Kanan, Tin oxide dependence of the CO₂ reduction efficiency on tin electrodes and enhanced activity for tin/tin oxide thin-film catalysts, *Journal of the American Chemical Society*, 134 (2012) 1986-1989.
- [206] N. Furuya, T. Yamazaki, M. Shibata, High performance Ru · Pd catalysts for CO₂ reduction at gas-diffusion electrodes, *Journal of Electroanalytical Chemistry*, 431 (1997) 39-41.
- [207] S. Rasul, D.H. Anjum, A. Jedidi, Y. Minenkov, L. Cavallo, K. Takanebe, A Highly Selective Copper–Indium Bimetallic Electrocatalyst for the Electrochemical Reduction of Aqueous CO₂ to CO, *Angewandte Chemie International Edition*, 54 (2015) 2146-2150.
- [208] D. Kim, J. Resasco, Y. Yu, A.M. Asiri, P. Yang, Synergistic geometric and electronic effects for electrochemical reduction of carbon dioxide using gold–copper bimetallic nanoparticles, *Nature communications*, 5 (2014).
- [209] R. Kortlever, I. Peters, S. Koper, M.T. Koper, Electrochemical CO₂ reduction to formic acid at low overpotential and with high faradaic efficiency on carbon-supported bimetallic Pd–Pt nanoparticles, *ACS Catalysis*, 5 (2015) 3916-3923.

- [210] B.A. Rosen, W. Zhu, G. Kaul, A. Salehi-Khojin, R.I. Masel, Water enhancement of CO₂ conversion on silver in 1-ethyl-3-methylimidazolium tetrafluoroborate, *Journal of The Electrochemical Society*, 160 (2013) H138-H141.
- [211] A. Salehi-Khojin, H.-R.M. Jhong, B.A. Rosen, W. Zhu, S. Ma, P.J. Kenis, R.I. Masel, Nanoparticle silver catalysts that show enhanced activity for carbon dioxide electrolysis, *The Journal of Physical Chemistry C*, 117 (2013) 1627-1632.
- [212] J. Medina-Ramos, J.L. DiMeglio, J. Rosenthal, Efficient reduction of CO₂ to CO with high current density using in situ or ex situ prepared Bi-based materials, *Journal of the American Chemical Society*, 136 (2014) 8361-8367.
- [213] H. Tong, S. Ouyang, Y. Bi, N. Umezawa, M. Oshikiri, J. Ye, Nano-photocatalytic materials: possibilities and challenges, *Advanced materials*, 24 (2012) 229-251.
- [214] E. Pelizzetti, C. Minero, Metal oxides as photocatalysts for environmental detoxification, *Comments on Inorganic Chemistry*, 15 (1994) 297-337.
- [215] T. Hisatomi, J. Kubota, K. Domen, Recent advances in semiconductors for photocatalytic and photoelectrochemical water splitting, *Chemical Society Reviews*, 43 (2014) 7520-7535.
- [216] M.R. Hoffmann, S.T. Martin, W. Choi, D.W. Bahnemann, Environmental applications of semiconductor photocatalysis, *Chemical reviews*, 95 (1995) 69-96.
- [217] A. Fujishima, Electrochemical photolysis of water at a semiconductor electrode, *nature*, 238 (1972) 37-38.
- [218] F. Tam, G.P. Goodrich, B.R. Johnson, N.J. Halas, Plasmonic enhancement of molecular fluorescence, *Nano letters*, 7 (2007) 496-501.
- [219] J.-W. Liaw, J.-H. Chen, C.-S. Chen, M.-K. Kuo, Purcell effect of nanoshell dimer on single molecule's fluorescence, *Optics express*, 17 (2009) 13532-13540.
- [220] M. Thomas, J.-J. Greffet, R. Carminati, J. Arias-Gonzalez, Single-molecule spontaneous emission close to absorbing nanostructures, *Applied physics letters*, 85 (2004) 3863-3865.
- [221] R. Carminati, J.-J. Greffet, C. Henkel, J.-M. Vigoureux, Radiative and non-radiative decay of a single molecule close to a metallic nanoparticle, *Optics Communications*, 261 (2006) 368-375.
- [222] K. Lewotsky, *The promise of plasmonics*, SPIE Professional, (2007).
- [223] R. Yan, D. Gargas, P. Yang, Nanowire photonics, *Nature photonics*, 3 (2009) 569-576.
- [224] Z. Ma, X. Zhang, X. Guo, Q. Yang, Y. Ma, L. Tong, Surface plasmon excitation in silver nanowires directly deposited on a laser diode chip, *Applied Physics Letters*, 96 (2010) 051119.

Chapter 2

**Highly ordered Ag/Cu hybrid
nanostructure arrays for ultrasensitive
surface-enhanced Raman spectroscopy**

Chapter Overview

The following chapter is a paper titled “Highly Ordered Ag/Cu Hybrid Nanostructure Arrays for Ultrasensitive Surface-Enhanced Raman Spectroscopy” published in *Advanced materials interfaces* in 2016. In this chapter, the SERS performances of ordered Cu nanorod arrays as well as Ag/Cu hybrid nanostructure arrays were studied. A two-step anodization process was used to make the porous AAO templates. Then electrodeposition of Cu nanorods was carried out inside the nanochannels of the AAO templates. After the removal of the AAO template, Cu nanorod arrays substrates were successfully synthesised. The length and the gap of the nanopores were effectively adjusted to generate the highest SERS performance.

The materials were then used as an analytical platform using benzenethiol as an example analyte. At the optimum condition, the detection limit of benzenethiol was as low as 10^{-10} M. By sputter coating a very thin layer of Ag on top of the Cu nanorod arrays, the detection limit of benzenethiol was further enhanced to 10^{-15} M. This is because, compared with Cu, the effective SERS cross section of Ag is much larger, which significantly increases the SERS sensitivity. In addition, by sputtering Ag nanoparticles, the gaps between neighbouring nanorods can be tailored into the sub-5 nm regime, which is beneficial to the improvement of the SERS sensitivity

This hybrid nanostructure shows promise as a cheap and reliable SERS substrate for ultrasensitive detection. A broader range of molecules may be selectively detected in the future by functionalization of the surface.

Highly Ordered Ag/Cu Hybrid Nanostructure Arrays for Ultrasensitive Surface-Enhanced Raman Spectroscopy

Kun Chen, Xinyi Zhang, Yongliang Zhang, Dang Yuan Lei, Haitao Li, Timothy Williams, and Douglas R. MacFarlane*

Despite significant progress recently made in this field, the practical application of surface-enhanced Raman spectroscopy (SERS) is frequently limited by the lack of highly sensitive, reproducible, and cost-effective substrates. The fabrication of SERS substrates with a consistently high density of hot-spots is a key step to address this issue. Here, a simple approach is reported for the fabrication of Ag/Cu hybrid nanostructure arrays as highly sensitive and cost-effective substrates for SERS application. By effectively tuning the gap size between neighboring nanorods to sub-10 nm and increasing the packing density of nanorods, ordered Cu nanorod arrays can be used as cheap and effective SERS substrates in their own right. After sputtering a very thin layer of Ag nanoparticles on the surface of the Cu nanorods to get sub-5 nm gaps, further field enhancement is enabled. A cascaded field enhancement has been evidenced by the electromagnetic simulations. The Ag/Cu hybrid nanostructure arrays exhibit a detection limit down to 10^{-15} M for nonresonant molecules such as benzenethiol.

1. Introduction

Surface-enhanced Raman spectroscopy (SERS) is a powerful spectroscopic technique that has potential single-molecule sensitivity and has emerged as a useful tool in chemical and biological sensing.^[1] The SERS sensitivity is dependent upon the electromagnetic field enhancement generated from the localized surface plasmon resonances close to the metal surface.^[2] The electromagnetic field enhancement is especially strong at inter-particle gaps,^[3] sharp corners or tips,^[4] and nanopores,^[1a,b,5] also known as hot spots. Since the first

observation of an SERS effect on a roughened silver electrode,^[6] tremendous effort has been devoted to developing various nanostructures, such as nanospheres,^[7] nanorods,^[8] and nanocubes,^[9] as effective SERS substrates. However, for application purposes there remains a need to develop simple and cheap methods to fabricate uniform substrates with excellent SERS sensitivity and reproducibility.^[10] One promising approach to achieving this goal is to fabricate ordered nanorod arrays using a porous anodic aluminum oxide (AAO) template.^[11] Compared with other fabrication methods, such as lithography, ion track-etched methods, or oblique angle deposition (OAD),^[12] the use of AAO membranes as the template to fabricate SERS substrates has the advantages of easy fabrication, modest cost, and great reproducibility.^[13] Moreover, the size

and neighboring gap of the nanorods can be easily tuned by changing the preparation conditions.

Previous research has shown that coinage metals (Au, Ag, and Cu) normally generate much stronger SERS enhancements than transition metals because the free electrons in these metals can be effectively excited by visible light.^[14] Therefore, nanostructured Au, Ag, and Cu are very important potential substrate source for practical SERS applications. Cu is an attractive material choice because it is cheap and prevalent in the electronics industry. However, in comparison with Au and Ag, the SERS effect of nanostructured Cu is much less investigated. This is mainly because the SERS signals from Cu are generally weaker than those from Ag or Au.^[12b] Recently, copper nanorod arrays on polymer substrates fabricated by using a guided OAD approach have exhibited a strong SERS enhancement and excellent reproducibility.^[12b] The surface plasmon resonance of Cu nanorod arrays prepared in ion track-etched polycarbonate membranes has also been investigated, and the dipolar surface plasmon resonance was found to be red-shifted with increased diameter and decreased adjacent gaps of the Cu nanorods.^[12a] Interestingly, a very recent study has shown that the enhancement factor (EF) of an all-copper plasmonic sandwich system can be as high as 1.89×10^7 ,^[8a] which is remarkably comparable to the EF of Au. Since Cu can support surface plasmon excitation by visible light,^[15] understanding the surface-induced photoprocesses on Cu nanostructures would aid not only in the design of new types of high performance SERS substrates, but

K. Chen, Dr. X. Zhang, Dr. H. Li, Prof. D. R. MacFarlane
School of Chemistry
Monash University
Clayton, Victoria 3800, Australia
E-mail: [REDACTED]

Y. Zhang, Dr. D. Y. Lei
Department of Applied Physics
The Hong Kong Polytechnic University
Hong Kong, China
Dr. T. Williams
Monash Centre for Electron Microscopy
Monash University
Clayton, Victoria 3800, Australia



DOI: 10.1002/admi.201600115

also in the development of new optoelectronic devices.^[16] In this work, we present a simple approach to fabricate large-scale and highly ordered Cu nanorod arrays with controlled gap size and packing density as cheap and effective SERS substrates. More importantly, by sputtering a very thin layer of Ag nanoparticles on the surface of the Cu nanorod arrays, we were able to further enhance the detection limit of benzenethiol, achieving reproducible signals at concentrations as low as 10^{-15} M.

2. Results and Discussion

2.1. Synthesis and Characterization of Cu Nanorod Arrays

Figure 1a shows the top-view scanning electron microscopy (SEM) image of a hole-through AAO template. The diameter of the holes and the wall thickness are ≈ 40 and 60 nm, respectively. Highly ordered arrays of vertically aligned Cu nanorods were achieved after a potentiostatic electrodeposition of Cu inside the AAO membrane (Figure 1d–f, see also Figure S1 in the Supporting Information). The nanorod length can be adjusted by controlling the electrical charge passed during the electrodeposition process. After the AAO template has been thoroughly dissolved, it can be seen that there are three Cu peaks in the X-ray diffraction (XRD) spectra of the Cu nanorod arrays, (111), (200), and (220) (Figure S2a, Supporting Information).

2.2. SERS Sensitivity of Cu Nanostructure Arrays

The SERS performance was investigated by using benzenethiol as a probe molecule. The length of the Cu nanorods

and the gap distance between them were effectively adjusted to generate the highest SERS signal intensity. According to previous research, 200 nm is thought to be the optimal length for metal nanorods to generate the highest SERS signal, and the SERS intensity diminishes at lengths longer than this.^[10] This is so because with increasing the length of the nanorod from 0 to 200 nm, the total surface area continues to increase, thus significantly enhancing the SERS intensity. However, when the length is larger than 200 nm, the electromagnetic field generated at the bottom of the metal nanorods becomes negligible. Therefore, the length of Cu nanorods in this experiment was adjusted to around 200 nm (Figure S2b, Supporting Information).

Cu nanorod arrays with different gaps between the neighboring nanorods (Figure 1d–f) were prepared by tuning the nanochannel diameter of the AAO template in diluted H_3PO_4 at 30 °C for different periods of time. When the gap distance between neighboring nanorods was about 60 nm, the detection limit of benzenethiol was only 10^{-5} M. By decreasing the gap distance, the SERS sensitivity was dramatically improved, as shown in Figure 2a. When the gap was in the sub-10 nm regime, the characteristic Raman peak at 996, 1022, and 1071 cm^{-1} for benzenethiol could be observed at concentration as low as 10^{-8} M (Figure 2b).

The diameter of the nanorods also plays a critical role in the overall SERS effect.^[4a,17] The fluorescence spectra of nanorod solutions measured with an excitation wavelength of 450 nm are displayed in Figure S3 (Supporting Information). An increase in fluorescence intensity with decreasing nanorod diameter was observed, which is probably due to the surface plasmon excitation of smaller diameter nanorods.^[18] Therefore, we explored the effect of the nanorod diameter on the SERS sensitivity by using the AAOs prepared in sulfuric acid

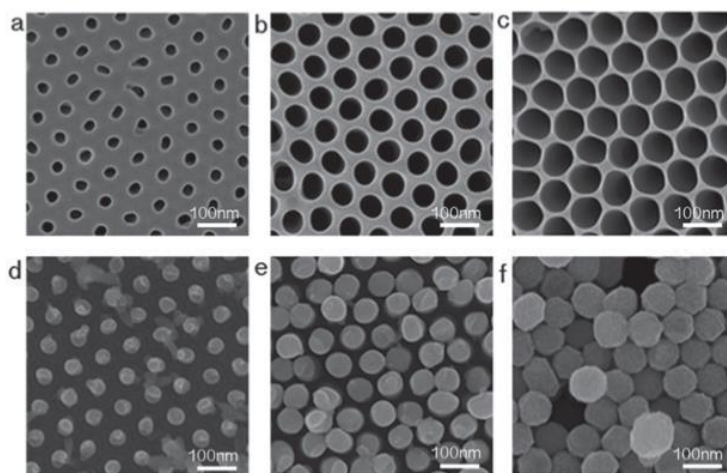


Figure 1. SEM images of AAO membranes prepared in oxalic acid electrolyte with different pore sizes and corresponding Cu nanorod arrays: a) 40 nm pore diameter and 60 nm wall thickness; b) 80 nm pore diameter and 20 nm wall thickness; c) 90 nm pore diameter and 10 nm wall thickness; d–f) SEM images of Cu nanorod arrays made from AAO membranes shown in panels (a)–(c).

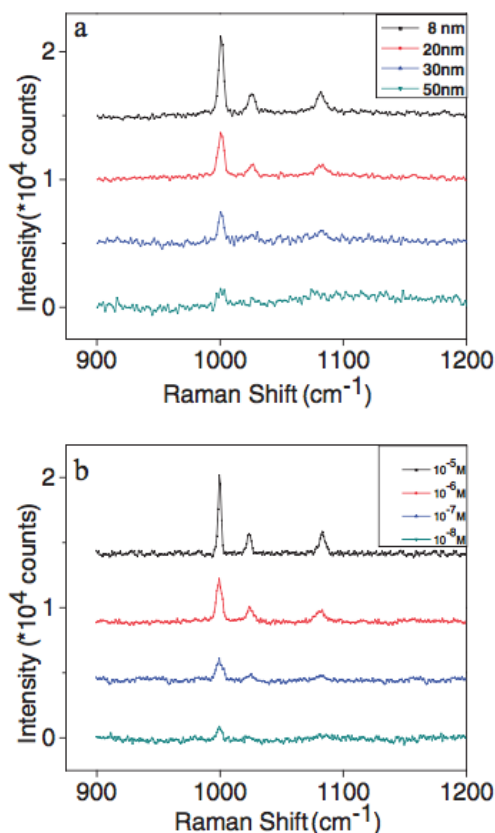


Figure 2. a) SERS spectra of 10^{-5} M benzenethiol solution adsorbed onto the Cu nanorod arrays with gap sizes of about 50, 30, 20, and 8 nm; b) Raman spectra of various benzenethiol concentrations adsorbed on the Cu nanorods substrate with a diameter of about 90 nm and a gap size of 8 nm.

electrolyte. As shown in Figure 3a–c, the holes are more closely packed, and the distance between the centers of neighboring pores is about 60 nm. By immersing the AAO membranes in 5% H_3PO_4 solution for different periods of time, we were able to control the gap size between the neighboring nanorods (Figure 3d,e). After 25 min pore enlarging, the wall thickness was below 10 nm (inset in Figure 3c) and Cu nanorod arrays with a gap size of about 6 nm were obtained using this AAO membrane (inset in Figure 3e). The SERS intensity of Raman shift at 996 cm^{-1} as a function of benzenethiol concentration with this nanorod array is plotted in Figure S4 (Supporting Information). The detection limit of benzenethiol signal was as low as 10^{-10} M with this array (Figure 4) and the EF is estimated to be 8×10^4 (Figure S6, Supporting Information). This detection limit is considerably lower than the previous reports using pure Cu as the SERS material.^[12b,19]

The SERS enhancement factor can be approximated as $EF \propto (E/E_0)^4$, where E and E_0 represent the local and incident electromagnetic fields, respectively.^[20] The enhanced electromagnetic field due to sharper tips and smaller gaps can thus significantly increase the SERS enhancement factor. There are several factors responsible for this enhanced SERS sensitivity. The Cu nanorod arrays are highly ordered over large area up to several square centimeters (Figure S7, Supporting Information). The closely packed nanorods with small diameters lead to larger number of narrow gaps per unit plane area of the substrate. The sharper tips of the nanorods also result in increased electromagnetic field at the tips.^[17] Besides, when the gaps become smaller, the plasmonic coupling among the nanorods will become more pronounced. Based on our calculation, the density of gaps on Cu nanorod array with 6 nm inter-pore distance is estimated to be 10^{11} cm^{-2} (Figure S1, Supporting Information). To the best of our knowledge, this is the highest value ever reported for a SERS substrate based on periodically arranged nanostructures.^[21] The chemical stability of Cu SERS substrates was further investigated. After the SERS experiment, the same sample was tested again under identical conditions over time and it was found that the intensity of the signal decreased about 15% over 24 h and 60% over one week (Figure S8, Supporting Information), which was further confirmed by XRD (Figure S9, Supporting Information). However, when the samples were immersed in ethanol solution for 10 days, there is no discernable change, exhibiting a good stability in ethanol.

2.3. SERS Sensitivity of Ag/Cu Hybrid Nanostructure Arrays

The SERS sensitivity was further enhanced by sputtering a very thin layer of Ag on the top of the Cu nanorod arrays, as shown in Figure 5. Cu nanorod arrays with a diameter of about 45 nm and a gap distance of 15 nm (Figure 3d) were used as the base material and subsequently adjusted the gap size by sputtering Ag nanoparticles at a rate of about 15 nm min^{-1} . When the sputtering time is 1 min, the Cu nanorods are capped with discontinuous Ag nanoparticles and the inter-tip spacing is reduced to around 12 nm (Figure 5a). The XRD and energy dispersive X-ray spectroscopy (EDS) measurements indicate that the resultant nanorods contain both Cu and Ag (Figure S10, Supporting Information), confirming that the nanorods are indeed decorated with Ag nanoparticles. With an increase in the Ag-sputtering duration, the Ag nanoparticles aggregate and the tip of each nanorod is covered by a Ag particle layer, as shown in Figure 5c. With 4 min Ag-sputtering time, the gap between neighboring nanorods is as low as 4.6 nm (Figure 5d). With further elongation of Ag-sputtering time, the number of narrow gaps decreases due to the formation of a semicontinuous Ag nanoparticle film over the surface of the Cu substrate. A typical transmission electron microscopy (TEM) image of the side view of an Ag/Cu hybrid nanorod shows that the side surface of the nanorod is dotted with many Ag nanoislands, as confirmed by the diffraction pattern (Figure 5e,f). With elongation of the sputtering time, the size and density of the Ag nanoislands increase accordingly.

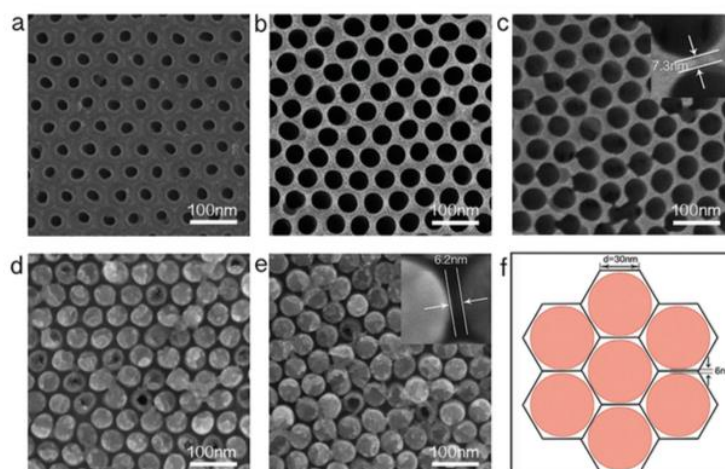


Figure 3. SEM images of AAO membranes prepared in sulfuric acid electrolyte with different pore size and corresponding Cu nanorod arrays: a–c) AAO membranes with pore enlarging time of 0, 20, and 25 min, respectively; d, e) SEM images of Cu nanorod arrays made from AAO membranes of panels (b) and (c); f) the distribution of 6 nm gaps in a unit cell.

In order to obtain an optimal SERS effect, the Ag/Cu hybrid arrays with different Ag-sputtering durations were tested by using a 10^{-13} M benzenethiol solution (Figure 6a). It can be observed that the SERS intensities increase with the Ag-sputtering duration for the first 4 min and then decrease with longer sputtering duration. These results indicate that the coupling of the localized surface plasmons between neighboring Ag nanoparticles and neighboring nanorods can be tailored by simply controlling the Ag-sputtering time.

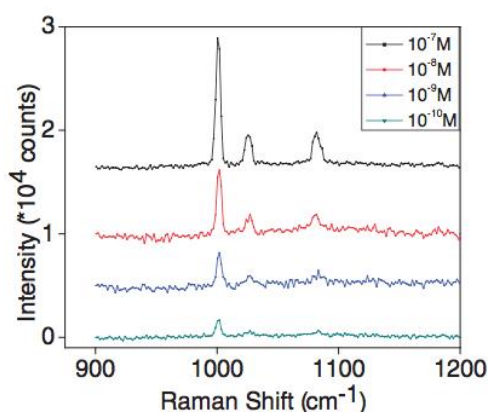


Figure 4. Raman spectra of various benzenethiol concentrations adsorbed onto copper nanorod substrate with a diameter of about 54 nm and an inter-pore distance of about 6 nm.

Under the current experimental conditions, a Ag-sputtering time of 4 min produces the optimal SERS substrate with the highest SERS sensitivity. To probe the limit of detection of this optimal substrate, the SERS spectra as a function of concentration is shown in Figure 6b. The spectral features of benzenethiol can be identified clearly even at a concentration as low as 10^{-13} M (the EF is estimated to be 1.0×10^{10} (Figure S6, Supporting Information)), demonstrating the highest sensitivity for the SERS detection. SERS intensity of Raman shift at 996 cm^{-1} as a function of benzenethiol concentration is plotted in Figure S5 in the Supporting Information. The mechanism of the Ag-based Raman enhancement can be explained as follows. First, compared with Cu, the effective SERS cross section of Ag is much larger, which significantly increases the SERS sensitivity.^[3a] In addition, by sputtering Ag nanoparticles, the gaps between neighboring nanorods can be tailored into the sub-5 nm regime, which is beneficial to the improvement of the SERS sensitivity.^[10] Finally, the plasmonic coupling among Ag nano-islands on each nanorod (Figure 5e) can also contribute to the SERS enhancement.

To gain a deeper insight into the strong SERS enhancement of the Ag-coated Cu nanorods, we have carried out a set of finite-difference time domain simulations. The structures used in simulations are schematically shown in Figure 7a for Ag/Cu hybrid nanostructure arrays, which can be modeled as a plasmonic crystal slab of triangular lattice with a rectangle unit cell in the xy plane (see the rectangle in panel (b)). The incident light has a polarization along the x direction. Other simulation details can be found in our previous paper.^[20] Figure 7b,c compares the electric field intensity enhancement profile at a surface 1 nm above the arrays of

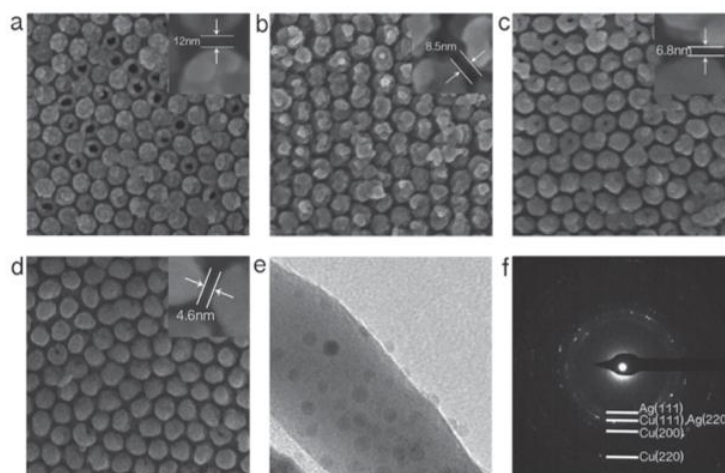


Figure 5. Top-view SEM images of Ag/Cu hybrid nanostructure arrays with different Ag-sputtering durations of a) 1 min, b) 2 min, c) 3 min, and d) 4 min. e) TEM image and f) corresponding selected-area diffraction pattern of the side surface of the Ag/Cu hybrid nanorod.

Ag and Cu nanorods, respectively. The results show that Ag has higher SERS sensitivity than Cu, which is consistent with literature.^[3a] Figure 7d depicts the field intensity enhancement distribution for Cu nanorods randomly decorated with 3 nm diameter Ag nanoparticles. For reasons of simplicity, here we have included only five Ag nanoparticles that are randomly attached at the top surface of the nanorods. Compared with pure Cu nanorods, the presence of Ag nanoparticles generates additional hot spots (white dashed circles in Figure 7d) at the edges of Cu nanorods and also increases the field intensity enhancement factor from 70 for pure Cu rods to 110 due to the reduction in the effective gap distance between neighboring nanorods. Moreover, the side views of the electric field distribution in the xz for Cu and Ag/Cu hybrid nanorods are shown in Figure S11 in the Supporting Information. It is very interesting that considerable field enhancements are observed in the bottom of the nanorods for both structures, which is in agreement with the experimental results.

2.4. SERS Signal Reproducibility of Ag/Cu Hybrid Nanostructure Arrays

In order to examine the reproducibility of the synthesized Ag/Cu hybrid substrates, we undertook a thorough statistical analysis to quantify the variation in the SERS signal intensity at different locations on one substrate (spot-to-spot variation) and between different substrates (substrate-to-substrate variation). Figure 8a shows the spot-to-spot variation distribution of the captured Raman intensities at the 996 cm^{-1} peak for a randomly selected Ag/Cu hybrid nanostructure substrate. It can be seen that the average signal intensity for

the hybrid structure is about 12300 counts with a coefficient of variation of 14.3%, exhibiting excellent signal reproducibility. To test the substrate-to-substrate SERS reproducibility, five Ag/Cu hybrid nanostructure substrates with the same nominal geometric parameters were loaded with 10^{-12} M benzenethiol and a series of Raman spectra were measured at ten different spots of each substrate to obtain an average Raman intensity. Figure 8b compares the substrate-to-substrate variation at 996 cm^{-1} in the Raman spectra for the five substrates, and the coefficient of variation is calculated as 7.6%.

3. Conclusion

In summary, we have presented a simple method to fabricate highly ordered Cu nanorod arrays over a large area. By effectively tuning the gap size between neighboring nanorods and the density of nanorods, we demonstrate that ordered Cu nanorod arrays can be used as effective SERS substrates in their own right. At the optimal condition the detection limit of benzenethiol is 10^{-10} M . The Cu nanorod arrays can be further functionalized through sputtering a thin layer of Ag nanoparticles. The integration of Ag nanoparticles into the periodic array of the copper nanorods generates a landscape of plasmon modes and offers a multiscale electromagnetic field enhancement both at the edges of the nanorods and at the interstitial gaps between the nanorods. This hybrid configuration provides not only strong Raman-active sites over the whole substrate but also efficient binding sites for the capture of analyte molecules at the “hot” spots. The Ag functionalized Cu nanorod arrays with a detection limit as low as 10^{-15} M exhibit strong SERS activities in comparison with other types of substrates

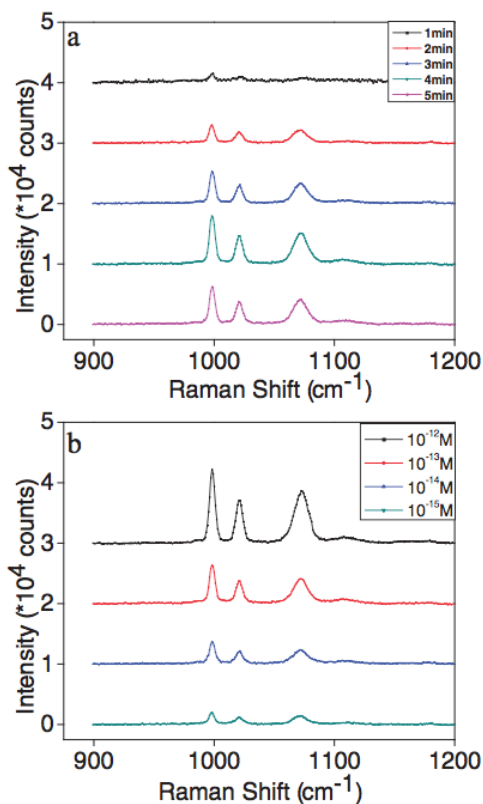


Figure 6. a) SERS spectra of 10^{-13} M benzenethiol solution adsorbed onto the Ag-capped Cu nanorod arrays with different Ag sputtering periods. b) SERS spectra of benzenethiol with different concentrations adsorbed on the Ag/Cu hybrid nanostructure arrays with Ag sputtering for 4 min.

in terms of both signal intensity and reproducibility for the detection of benzenethiol.^[20] The electromagnetic simulations provide the physical interpretation for our experimental results and clearly evidence a significant field enhancement on the Ag/Cu hybrid nanostructures. Thus, this hybrid nanostructure shows promise as a cheap and reliable SERS substrate for ultrasensitive detection. A broader range of molecules may be selectively detected by functionalization of the surface and this is the subject of ongoing research in our laboratory.

4. Experimental Section

Synthesis of Cu and Cu/Ag Hybrid Nanostructure Arrays: The porous AAO templates used in this work were prepared by a

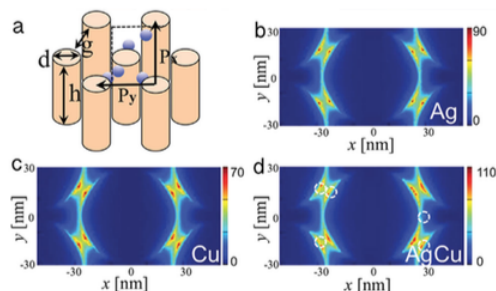


Figure 7. a) Schematic side view of an array of Cu nanorods (yellow) decorated with 2 nm diameter Ag nanoparticles (blue). The rectangle represents a unit cell of the periodic nanorod array. Simulated field intensity enhancement $[E/E_0]^2$ profile at a surface 1 nm above the b) Ag, c) Cu nanorod arrays, and d) Ag/Cu hybrid nanostructure arrays. Here, the wavelength is 633 nm, corresponding to the SERS excitation wavelength used in the experiment. In panel (d), the dashed circles represent new plasmonic hot spots due to the presence of Ag.

two-step anodization process, as described previously.^[21] High-purity (99.999%) aluminum foil of about 0.5 mm thickness was used as the starting material. An aqueous bath containing 0.2 M CuSO_4 and 0.1 M H_3BO_3 was used to prepare Cu nanorod arrays. The pH of the solution was adjusted to about 4.5 by adding 0.1 M H_2SO_4 solution. The electrodeposition was carried out at a constant potential of 0.1 V (vs Ag/AgCl) with platinum wire serving as the counter electrode at room temperature. The length of the nanorods was effectively adjusted by controlling the charge passed. After electrodeposition, the samples were washed with deionized water and the backside of the AAO membranes was electrodeposited with a thick layer of Cu to prevent the nanorods from falling apart after the removal of the AAO template, as shown schematically in Figure S1 (Supporting Information). Finally, the AAO template was fully removed by immersing the samples in 5% H_3PO_4 at 30 °C for 2 h. Ag nanoparticles were decorated onto the Cu nanorods using a Q-150TS sputtering machine at a current density of 40 mA. Ag sputtering was performed for different periods of time to tailor the gaps between neighboring nanorods for the SERS experiment. All chemical reagents used in this study were of analytical grade and were supplied by Sigma-Aldrich (Australia).

Characterization: The structure and morphology of the samples were characterized by SEM (Nova 450), EDS, TEM (Tecnai T20), and XRD (BRUKER D8-ADVANCE PXRD). The SERS measurements were conducted using benzenethiol as a typical analyte. Following the literature methodology,^[20] the analyte was adsorbed onto the surface from a fixed volume of solution (3 mL) for various periods of time. Thus, the prepared substrates were immersed in ethanol solution of varied benzenethiol concentrations and times.^[12b,20] The volume of benzenethiol solution and immersion time influence the amount of benzenethiol adsorbed on the substrate (Figures S12 and S13, Supporting Information). To ensure that adsorption equilibrium is reached on the substrate, the samples were immersed for 12 h unless otherwise indicated. Then the samples were thoroughly rinsed with deionized water and ethanol to remove any unbound benzenethiol molecules and dried in air prior to the SERS measurement. SERS spectra were measured using a confocal Raman spectrometer (RENISHAW InVia Raman Microscope) and all the Raman spectra were collected from a $1 \mu\text{m}^2$ area of the samples excited at 633 nm (laser power 1.7 mW). The exposure time for benzenethiol detection was 20 s using 10% of the laser power.

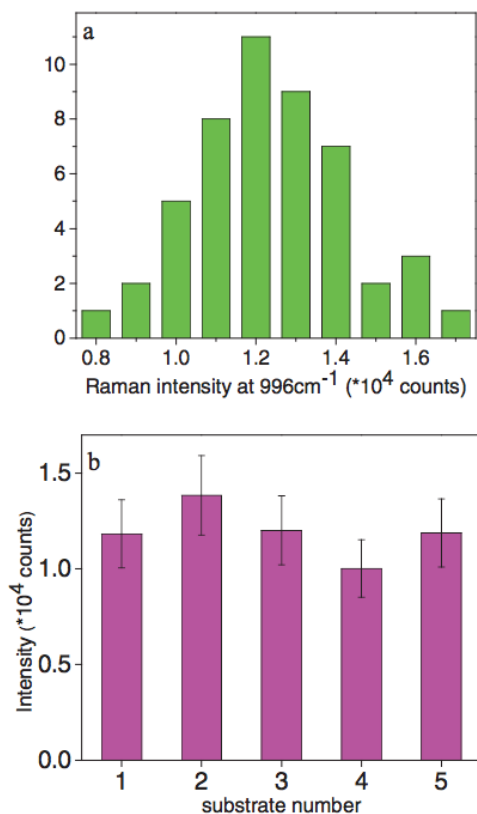


Figure 8. a) Histogram of spot-to-spot Raman intensity variation at 996 cm^{-1} for the Ag/Cu hybrid nanostructure arrays. b) Substrate-to-substrate Raman intensity variation at 996 cm^{-1} measured for five Ag/Cu hybrid substrates. Each intensity value (and error bar) represents the average (and standard deviation) of ten independently measured results at different spots. For all the measurements in panels (a) and (b), the benzenethiol concentration and loading time are $1 \times 10^{-12}\text{ M}$ and 12 h, respectively.

Supporting Information

Supporting Information is available from the Wiley Online Library or from the author.

Acknowledgements

This work was supported by the Australian Research Council (ARC), Grant No. DP 120104334. D.R.M. is grateful to the Australian Research Council for his Australian Laureate Fellowship. D.Y.L. acknowledges the support by the National Science Foundation of China (Grant No. 11474240). This work was performed in part at the Melbourne Centre for Nanofabrication (MCN) in the Victorian Node of the Australian National Fabrication Facility (ANFF) and the Monash Centre for Electron Microscopy.

- [1] a) C. Schmuck, P. Wich, B. Küstner, W. Kiefer, S. Schlücker, *Angew. Chem. Int. Ed.* **2007**, *46*, 4786; b) K. L. Wustholz, A.-I. Henry, J. M. McMahon, R. G. Freeman, N. Valley, M. E. Piotti, M. J. Natan, G. C. Schatz, R. P. V. Duyne, *J. Am. Chem. Soc.* **2010**, *132*, 10903; c) J. F. Li, Y. F. Huang, Y. Ding, Z. L. Yang, S. B. Li, X. S. Zhou, F. R. Fan, W. Zhang, Z. Y. Zhou, D. Y. Wu, *Nature* **2010**, *464*, 392.
- [2] H. Wei, H. Xu, *Nanoscale* **2013**, *5*, 10794.
- [3] a) K. Kneipp, Y. Wang, H. Kneipp, L. T. Perelman, I. Itzkan, R. R. Dasari, M. S. Feld, *Phys. Rev. Lett.* **1997**, *78*, 1667; b) G. L. Liu, Y. Lu, J. Kim, J. C. Doll, L. P. Lee, *Adv. Mater.* **2005**, *17*, 2683; c) J. J. Baumberg, T. A. Kelf, Y. Sugawara, S. Cintra, M. E. Abdelsalam, P. N. Bartlett, A. E. Russell, *Nano Lett.* **2005**, *5*, 2262; d) J. Fang, S. Du, S. Lebedkin, Z. Li, R. Kruk, M. Kappes, H. Hahn, *Nano Lett.* **2010**, *10*, 5006; e) R. Zhang, Y. Zhang, Z. Dong, S. Jiang, C. Zhang, L. Chen, L. Zhang, Y. Liao, J. Aizpurua, Y. Luo, *Nature* **2013**, *498*, 82.
- [4] a) Y. Wang, B. Yan, L. Chen, *Chem. Rev.* **2012**, *113*, 1391; b) H. Abramczyk, B. Brozek-Pluska, *Chem. Rev.* **2013**, *113*, 5766.
- [5] a) D. K. Lim, K. S. Jeon, H. M. Kim, J.-M. Nam, Y. D. Suh, *Nat. Mater.* **2009**, *9*, 60; b) D. K. Lim, K. S. Jeon, J. H. Hwang, H. Kim, S. Kwon, Y. D. Suh, J. M. Nam, *Nat. Nanotechnol.* **2011**, *6*, 452.
- [6] D. Y. Wu, J. F. Li, B. Ren, Z. Q. Tian, *Chem. Soc. Rev.* **2008**, *37*, 1025.
- [7] a) W. Li, P. H. Camargo, X. Lu, Y. Xia, *Nano Lett.* **2008**, *9*, 485; b) S. Liu, C. Jiang, B. Yang, Z. Zhang, M. Han, *RSC Adv.* **2014**, *4*, 42358; c) A. Chen, A. E. DePrince, A. Demortière, A. Joshi-Irmre, E. V. Shevchenko, S. K. Gray, U. Welp, V. K. Vlasko-Vlasov, *Small* **2011**, *7*, 2365.
- [8] a) X. Li, X. Ren, Y. Zhang, W. C. Choy, B. Wei, *Nanoscale* **2015**, *7*, 11291; b) Y. J. Oh, K. H. Jeong, *Adv. Mater.* **2012**, *24*, 2234.
- [9] P. H. Camargo, M. Rycenga, L. Au, Y. Xia, *Angew. Chem. Int. Ed.* **2009**, *48*, 2180.
- [10] B. Chen, G. Meng, Q. Huang, Z. Huang, Q. Xu, C. Zhu, Y. Qian, Y. Ding, *ACS Appl. Mater. Interfaces* **2014**, *6*, 15667.
- [11] a) H. H. Wang, C. Y. Liu, S. B. Wu, N. W. Liu, C. Y. Peng, T. H. Chan, C. F. Hsu, J. K. Wang, Y. L. Wang, *Adv. Mater.* **2006**, *18*, 491; b) G. H. Gu, J. S. Suh, *Langmuir* **2008**, *24*, 8934.
- [12] a) J. Duan, T. Cornelius, J. Liu, S. Karim, H. Yao, O. Picht, M. Rauber, S. Müller, R. Neumann, *J. Phys. Chem. C* **2009**, *113*, 13583; b) M. Keating, S. Song, G. Wei, D. Graham, Y. Chen, F. Placido, *J. Phys. Chem. C* **2014**, *118*, 4878; c) Q. Yu, P. Guan, D. Qin, G. Golden, P. M. Wallace, *Nano Lett.* **2008**, *8*, 1923.
- [13] D. Choi, Y. Choi, S. Hong, T. Kang, L. P. Lee, *Small* **2010**, *6*, 1741.
- [14] B. K. Jena, C. R. Raj, *Chem. Mater.* **2008**, *20*, 3546.
- [15] J. R. Anerna, A. G. Brolo, P. Marthandam, R. Gordon, *J. Phys. Chem. C* **2008**, *112*, 17051.
- [16] C. L. Haynes, A. D. McFarland, R. P. V. Duyne, *Anal. Chem.* **2005**, *77*, 338A.
- [17] P. Kao, N. A. Malvadkar, M. Cetinkaya, H. Wang, D. L. Allara, M. C. Demirel, *Adv. Mater.* **2008**, *20*, 3562.
- [18] P. K. Jain, I. H. El-Sayed, M. A. El-Sayed, *Nano Today* **2007**, *2*, 18.
- [19] L. Y. Chen, J. S. Yu, T. Fujita, M. W. Chen, *Adv. Funct. Mater.* **2009**, *19*, 1221.
- [20] X. Zhang, Y. Zheng, X. Liu, W. Lu, J. Dai, D. Y. Lei, D. R. MacFarlane, *Adv. Mater.* **2015**, *27*, 1090.
- [21] Y. Zheng, T. Thai, P. Reineck, L. Qiu, Y. Guo, U. Bach, *Adv. Funct. Mater.* **2013**, *23*, 1519.

ADVANCED MATERIALS INTERFACES

Supporting Information

for *Adv. Mater. Interfaces*, DOI: 10.1002/admi.201600115

Highly Ordered Ag/Cu Hybrid Nanostructure Arrays for
Ultrasensitive Surface-Enhanced Raman Spectroscopy

*Kun Chen, Xinyi Zhang, Yongliang Zhang, Dang Yuan Lei,
Haitao Li, Timothy Williams, and Douglas R. MacFarlane**

Supporting Information

Highly Ordered Ag/Cu Hybrid Nanostructure Arrays for Ultrasensitive Surface-Enhanced Raman Spectroscopy

*Kun Chen, Xinyi Zhang, Yongliang Zhang, Dangyuan Lei, Haitao Li, Tim Williams, Douglas R. MacFarlane**

S1. Calculation of density of 6nm gaps

In the hexagonally close-packed structure, there are 6 gaps of such structure around each Cu nanorod. Therefore, the number (n) of gaps around each nanorod is: $n = 6 \times \frac{1}{2} = 3$. Suppose

the center-to-center distance of the nanorods is 2d, the area of the hexagon (A) is $2\sqrt{3}d^2$.

Based on the SEM images, d is about 30 nm, so A is about $3 \times 10^{-11} \text{ cm}^2$

Therefore, the density of the sub-10 nm gaps (D) can be given as:

$$D = \frac{n}{A} = \frac{3}{3 \times 10^{-11}} = 1 \times 10^{11} \text{ cm}^{-2}$$

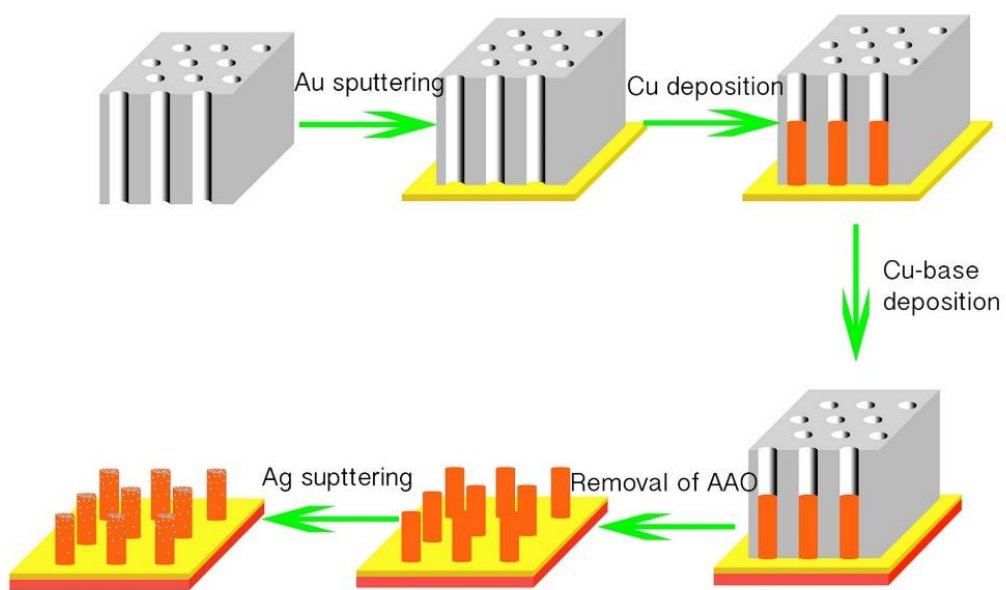


Figure S1. Schematic for the fabrication of Cu/Ag hybrid nanostructure arrays

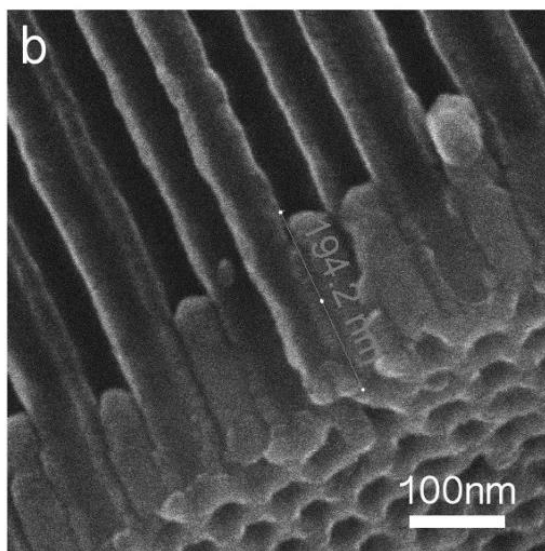
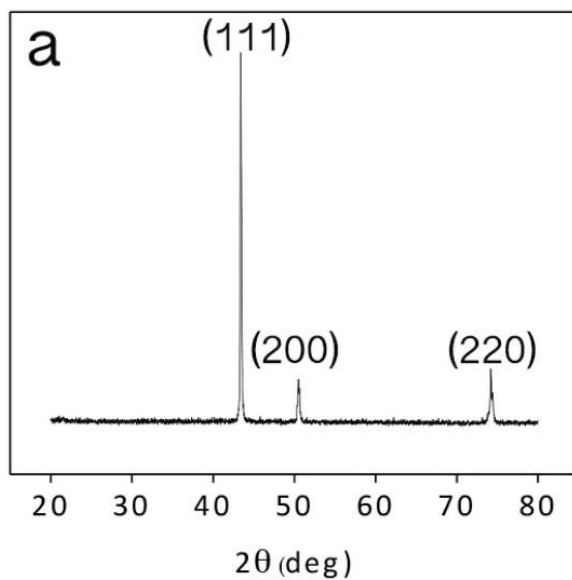


Figure S2. (a) XRD pattern of the Cu nanorod arrays; (b) Cross sectional view of the Cu nanorod arrays.

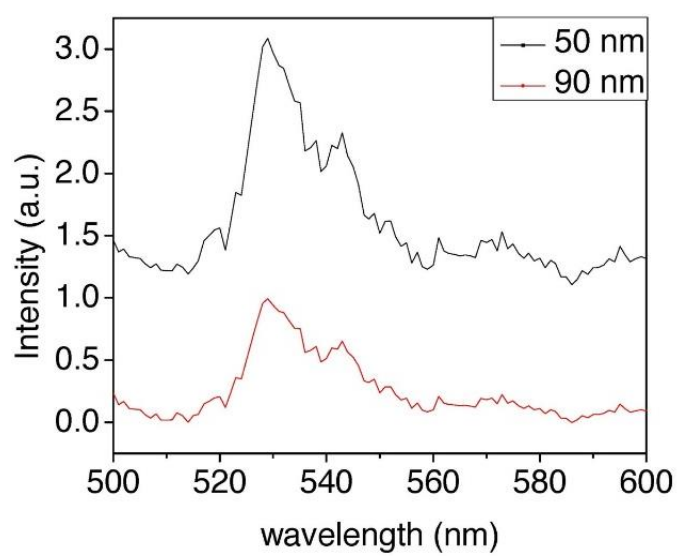


Figure S3. The fluorescence spectra of different diameter nanorods solutions ($1.0 \cdot 10^{-3} \%$) measured with an excitation wavelength of 450 nm.

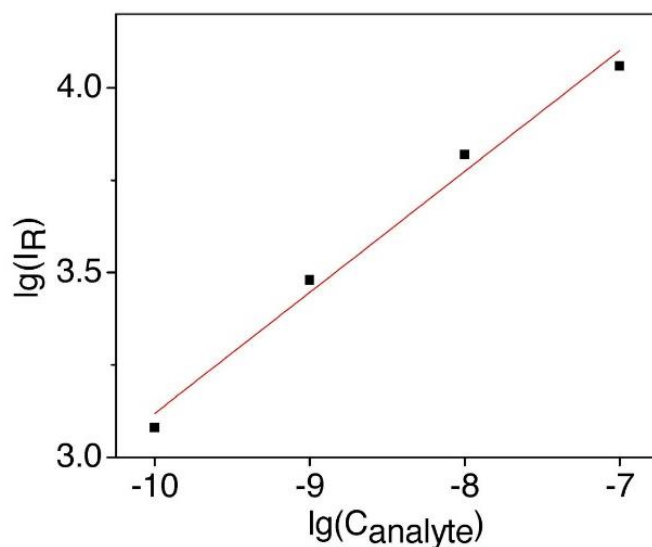


Figure S4. Raman intensity of benzenethiol adsorbed on Cu nanorod arrays (gap size about 6nm) at peak of 996 cm^{-1} as a function of benzenethiol concentration (in logarithmic scale).

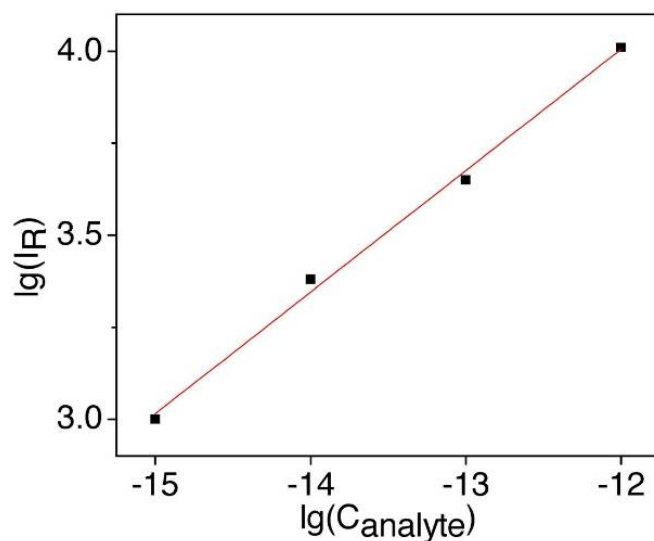


Figure S5. Raman intensity of benzenethiol adsorbed on Ag/Cu hybrid nanostructure arrays (gap size about 4.6 nm) at peak of 996 cm^{-1} as a function of benzenethiol concentration (in logarithmic scale).

Figure S4 and S5 show that the Raman intensities of the benzenethiol decrease with decreasing the loading concentration and that the benzenethiol loading follows the first-order adsorption kinetics, indicating that both the Cu nanorods substrate and Ag/Cu hybrid substrate offer sufficient binding sites for the efficient capture of the analyte from the loading solution.

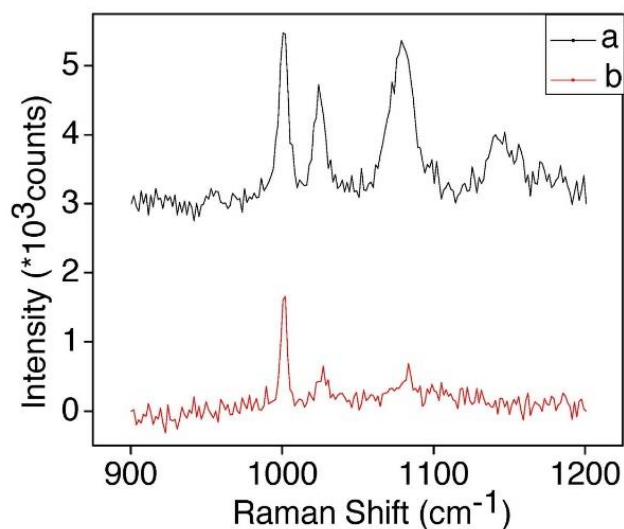


Figure S6. Spectra of benzenethiol. Curve a, SERS at 10^{-10} M benzenethiol; Curve b, 10^{-1} M benzenethiol solution as a reference.

According to previous papers,^[1] the enhancement factor (EF) can be defined by the expression $EF = (I_{\text{surface}}/I_{\text{solution}}) \times (N_{\text{solution}}/N_{\text{surface}})$, where I_{surface} and I_{solution} stand for the signal intensities of the SERS substrate and reference solution, and N_{surface} and N_{solution} are the numbers of benzenethiol molecules probed on the SERS substrate and in the reference solution, respectively.

Figure S6 shows the Raman Spectra result of 10^{-1} M reference solution, and of 10^{-10} M benzenethiol solution adsorbed on Cu nanorods substrate. The characteristic band at 996 cm^{-1} was chosen for the EF estimation. The SERS intensity (I_{surface}) was about 2485 for reference solution, and 1658 for Cu nanorods substrate. Because the SERS substrates with the size of about 1 mm^2 were immersed in benzenethiol solution for 12 h, it is assumed that after such a long time most of the benzenethiol molecules were adsorbed on the substrates. So about 1.8×10^8 benzenethiol molecules were adsorbed within a $1 \text{ }\mu\text{m}^2$ area, which is the excitation area of the laser. In comparison, Raman spectra of 10^{-1} M benzenethiol solution were measured using a laser intensity of 1.7 mW, which has the effective excitation volume of $400 \text{ }\mu\text{m}^3$, to give N_{solution} of 2.4×10^{10} . In this way, the EF of Cu nanorod arrays can be estimated as 8×10^4 . Similarly, the Raman spectra result of 10^{-15} M benzenethiol adsorbed on the Ag/Cu hybrid nanostructure arrays was chosen for EF calculation (Figure 8b), and the value is 1.0×10^{10} according to the method mentioned above.

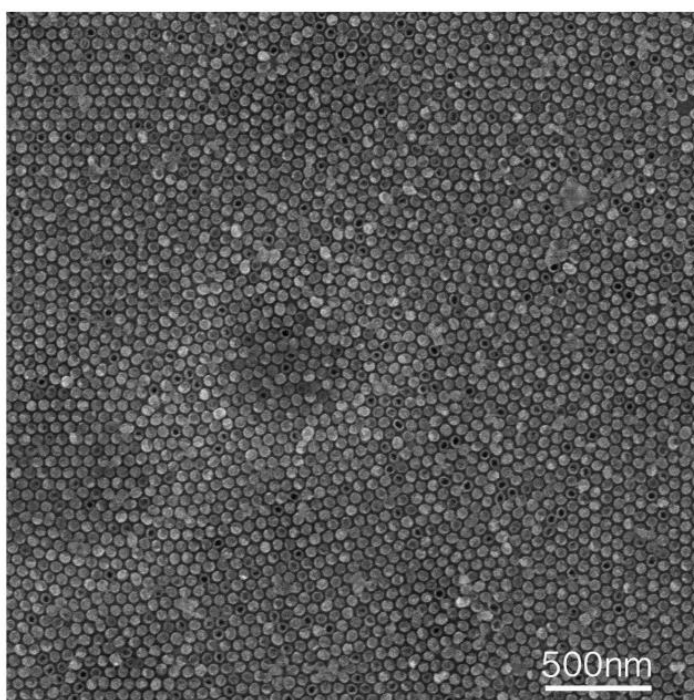


Figure S7. SEM image of Cu nanorod arrays.

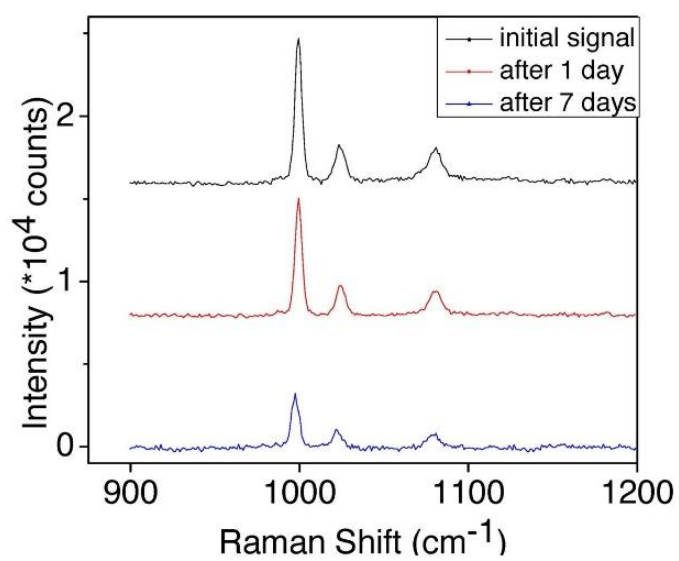


Figure S8. Raman signal variations over time.

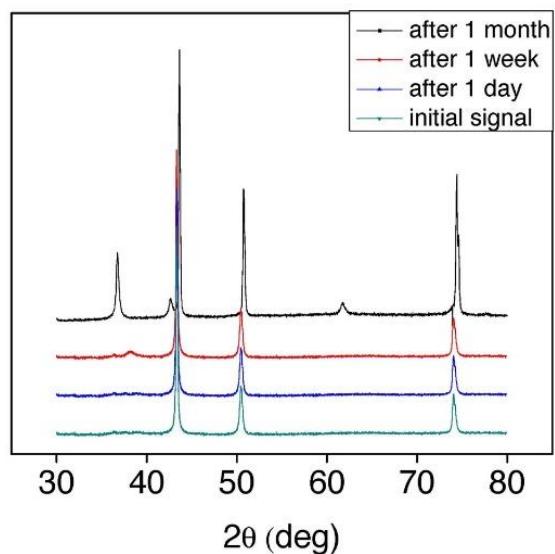


Figure S9. XRD spectra of Cu substrate over time.

XRD results (Figure S9) show that after one day there is no difference in XRD signals. After one week, there is a tiny peak of CuO, which means the substrate is partially oxidized. After one month, the substrate was severely oxidized, indicating that the synthesized Cu substrates are relatively stable only in a short period of time.

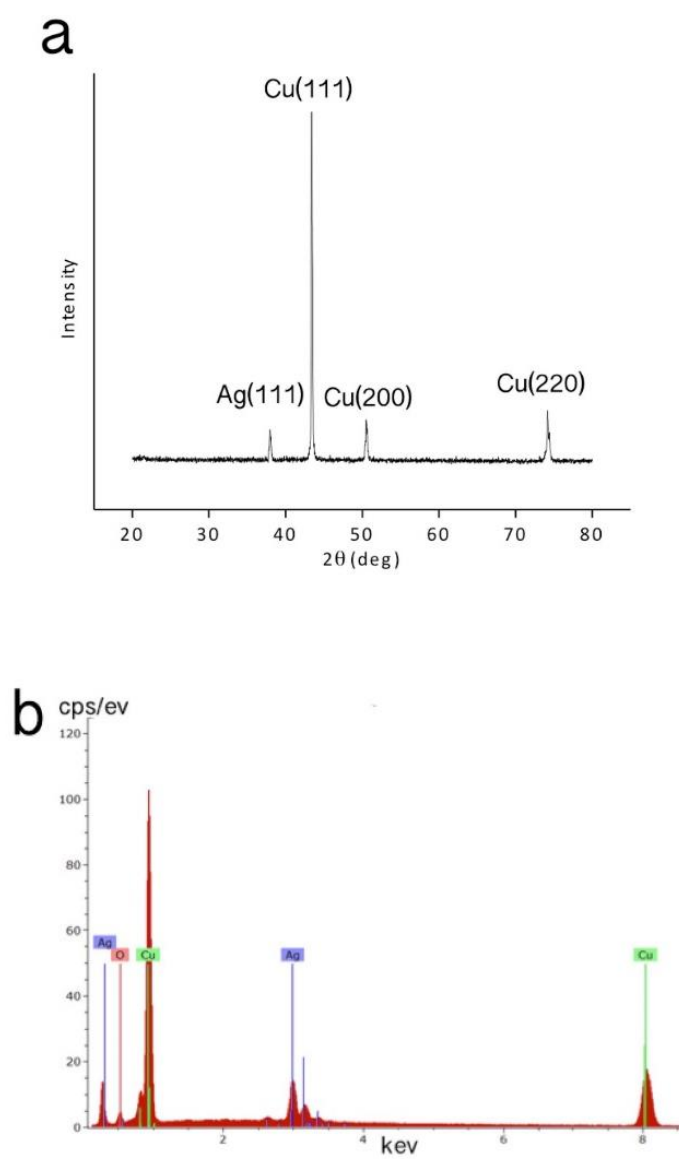


Figure S10. (a-b) XRD and EDS of Ag/Cu hybrid nanostructure arrays.

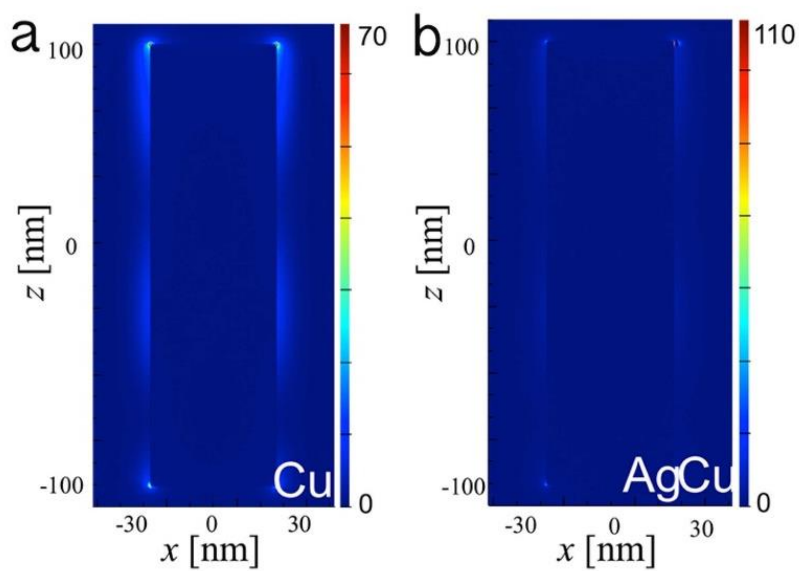


Figure S11. The side views of the electric field distribution in the xz for Cu (a) and Ag/Cu (b) hybrid nanorods.

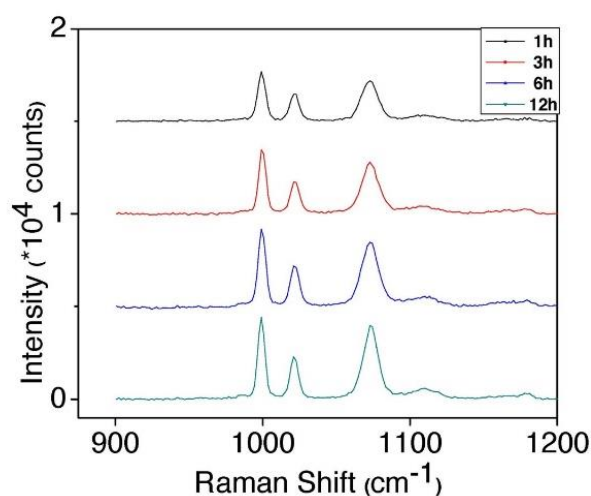


Figure S12. Variation of SERS intensity of Ag/Cu hybrid nanostructure arrays in 10^{-13} M benzenethiol solution with different immersion time.

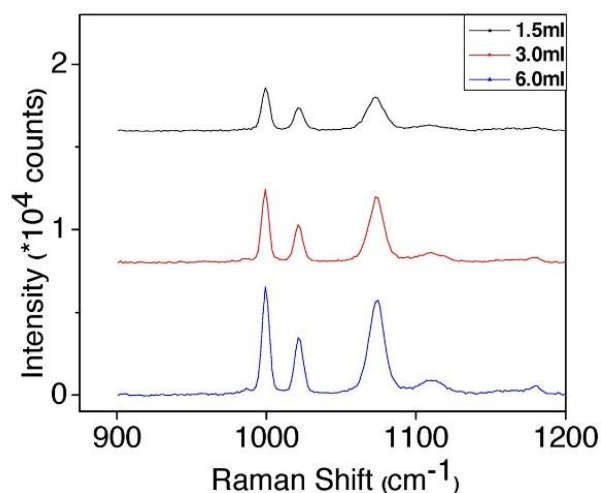


Figure S13. Variation of SERS intensity of Ag/Cu hybrid nanostructure arrays in different volumes of 10^{-13} M benzenethiol solution.

Figure S12 shows that the SERS intensity increases with longer immersion time until the system reaches equilibrium after 6 h, which justifies our use of longer immersion time. Figure S13 indicates that even using 12 h immersion time, when the volume is increased, the SERS intensity also increases accordingly, which proves that most of the benzenethiol molecules in the solution are actually adsorbed on the surface of the substrate.

[1] F. Chen, Q. Zhang, Y. Zhan, D. Ma, K. Xu, Y. Zhao, *ACS appl. mater. interfaces* 2015, 7, 5725-5735.

Chapter 3

**Ultrasensitive surface-enhanced Raman
scattering detection of urea by highly
ordered Au/Cu hybrid nanostructure
arrays**

Chapter Overview

The following chapter is a paper titled “Ultrasensitive surface-enhanced Raman scattering detection of urea by highly ordered Au/Cu hybrid nanostructure arrays” published in *Chemical Communication* in 2017. In this chapter, the nanostructure developed in chapter 2 was used for a real world medical application. Because Au is similarly SERS sensitive as Ag but is much more stable, an Au coating was employed in this study.

A drop method was used to load to urea samples onto the substrates. By effectively adjusting the gap size between neighbouring nanorods into the sub-10 nm regime, a high density of hot-spots was generated, enabling the substrates to detect urea signals at a concentration as low as 1 mM with great reproducibility. This chapter demonstrates the potential of using a highly ordered Au/Cu hybrid nanostructure as a new platform for fast and reliable detection of urea. This SERS substrate has the advantage of low cost, easy fabrication, and excellent reproducibility. Besides, these substrates can be recycled easily and remain SERS active for a long period of time.



Ultrasensitive surface-enhanced Raman scattering detection of urea by highly ordered Au/Cu hybrid nanostructure arrays†

Cite this: DOI: 10.1039/c7cc03523c

Received 6th May 2017,
Accepted 23rd June 2017

DOI: 10.1039/c7cc03523c

rsc.li/chemcomm

Kun Chen,^a Xinyi Zhang^b and Douglas R. MacFarlane^{c*}

We report a simple approach to fabricate cost-effective and highly sensitive surface-enhanced Raman scattering substrates based on Au/Cu hybrid nanostructure arrays for the detection of urea, an important molecule in biological and medical fields. By effectively adjusting the gap size between neighbouring nanorods into the sub-10 nm regime, a high density of hot-spots was generated, enabling the substrates to detect urea signals at a concentration as low as 1 mM with great reproducibility.

Urea is an important compound both in the metabolism of nitrogen-containing compounds as well as in many applications in agriculture, medicine and the chemical industry.^{1,2} The detection of urea is crucial in clinical analysis since it can reveal hidden risks.^{3,4} It can be analysed and quantified by a number of different methods, including colorimetric methods and the Berthelot reaction.^{5–8} Colorimetric analysis is by far the most common, but requires reagent mixing and multiple incubation steps, rendering it unsuitable for rapid monitoring.⁶ Hence there is a strong interest in developing a fast and cost-effective approach to the detection of urea.

Surface-enhanced Raman Spectroscopy (SERS) has attracted attention in biological, chemical, and environmental fields because of its ultrasensitive fingerprint identification of chemicals.^{9–15} It is widely accepted that the high sensitivity of the substrates can be mainly attributed to the much enhanced local electromagnetic fields resulting from nano-scaled gaps (also known as “hot spots”) between neighbouring noble-metal nanostructures.^{16,17} Therefore, significant effort has been focused on making ultra-sensitive SERS nanostructures including Ag microflowers, Ag nanocubes, and Au nanodimer arrays.^{18–20} Although the sensitivity of these synthesised nanostructures are generally very good, the random distribution of these nanostructures makes it very difficult to achieve highly reproducible SERS signals.²⁰ Also, noble metals such as Au and Ag make

these nanostructures unsuitable for large-scale fabrication. Thus the main challenge in this field is to fabricate SERS substrates in a cost-effective way while maintaining high sensitivity and excellent reproducibility.^{21,22}

The porous anodic aluminium oxide (AAO) template method is well known in the fabrication of highly uniform nanostructures.^{23,24} The thickness of the pore walls can be readily adjusted by chemical etching. When the gap between resulting neighbouring nanorods is in the sub-20 nm regime, Raman signals can be exponentially increased due to the much enhanced electromagnetic field excited by the localized surface plasmon coupling between them.¹² However, to lower the thickness of the wall to below 10 nm is challenging because the resultant template is too fragile to use and the corresponding nanorod arrays are not very ordered. Therefore, many researchers chose to use Ag or Au sputtering to adjust the gap size to the sub-10 nm regime.^{23,25} This method significantly increases the SERS sensitivity, not only by decreasing the gap size between adjacent nanorods, but also by using the best SERS active materials.²³

Although the SERS sensitivities of Ag and Au substrates are generally the best, Cu is also an interesting and lower cost SERS material.²⁵ A recent study has shown that the enhancement factor (EF) of an all-copper plasmonic sandwich system can be as high as 1.9×10^7 , which is remarkable comparable to the EF of Au.²⁶ Our recent work also confirms that ordered Cu nanorod arrays can be used as cheap and effective SERS substrates with a detection limit of 10^{-10} M for benzenethiol.²⁷

Considering the importance of urea detection, it is very worthwhile to employ SERS active substrates for this application. Choi and his colleagues used Ag-coated nanodome structures to monitor the urea concentration in a flow cell. However, their detection limit of urea (about 25 mM) is higher than the lower limit of urea concentration in the human body.³ The gap between adjacent nanodomains was usually more than 20 nm, rendering their material not sufficiently SERS active.^{3,27} In this research, we use highly ordered Au/Cu nanostructure arrays as a SERS substrate for urea detection (Fig. 1a). By effectively tuning the gap size between neighbouring nanorods *via* Au sputtering coating, the

School of Chemistry, Monash University, Clayton, VIC 3800, Australia.

E-mail: [redacted]

† Electronic supplementary information (ESI) available. See DOI: 10.1039/c7cc03523c

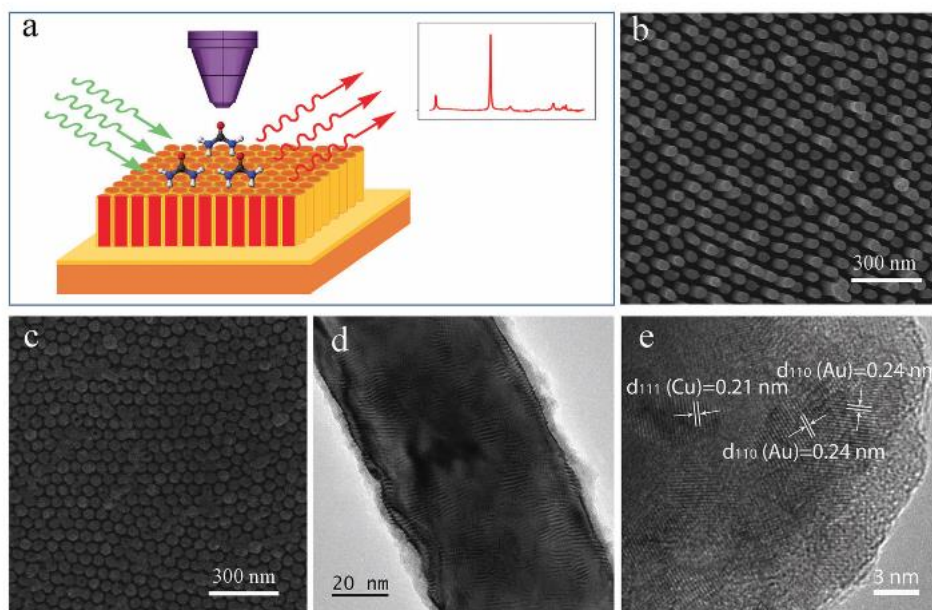


Fig. 1 (a) An overview of the SERS experiment; (b and c) SEM images of ordered Cu nanorod arrays (b) Au/Cu hybrid nanostructure arrays (c); (d and e) TEM images of Au/Cu hybrid nanostructure arrays.

number of “hot spots” were increased, thus significantly enhancing the SERS detection limit. We demonstrate that by using our Au/Cu hybrid nanostructure arrays, the detection limit of urea can be as low as 1 mM.

The scanning electron micrograph (SEM) and transmission electron micrographs (TEM) and X-ray diffraction (XRD) pattern of the obtained nanostructures are shown in Fig. 1 and Fig. S1 and S2 (ESI[†]). Highly ordered Cu nanorod arrays were achieved after a potentiostatic electro-deposition process inside the nanochannels of the AAO template (Fig. 1b). The length of the nanorods can be controlled by adjusting the total electrical charge passed during the process. In this case, 200 nm length was chosen to get high SERS sensitivity while the whole structure still remains highly ordered.¹² The ordered Cu nanorod arrays were subsequently sputter-coated with a layer of Au to enhance the SERS sensitivity. As previous research has shown,^{23,27} the smaller the gap size, the higher the sensitivity. So a 5 min Au sputter coating at a rate of 15 nm min⁻¹ was used to effectively adjust to gap size below 10 nm, as shown in Fig. 1c. Further coating results in the blocking of the nanogaps, thus reducing the SERS sensitivity of the substrates. Fig. 1d shows the TEM images of a Au coated Cu nanorod, the lattice pattern of Au can be clearly observed in Fig. 1e. EDS reveals that the surface has indeed been coated with a layer of gold (Fig. S3, ESI[†]).

The SERS performance of the nanostructured Cu arrays was measured and only a very weak Raman peak was detected when using 0.1 M urea as an analyte (Fig. S4, ESI[†]). As shown in

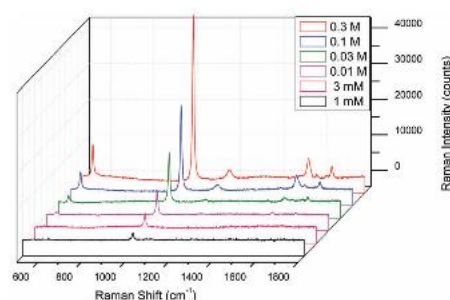


Fig. 2 SERS spectra of Au/Cu hybrid nanostructure arrays loaded with urea with concentration ranging from 0.3 M to 1 mM.

Fig. 2, the synthesized Au/Cu hybrid nanostructure arrays were able to detect urea at a concentration of 1 mM, which is well below the clinically relevant value. As many as 5 characteristic Raman peaks of urea can be observed in the spectra, while in the previous research, the detection limit of urea was 25 mM and only one Raman peak could be observed.³ The intensity of the Raman signal at 1000 cm⁻¹ as a function of urea concentration is plotted in Fig. 3. A linear fit with R^2 value of 0.995 was obtained, which clearly demonstrates that the synthesized Au/Cu hybrid nanostructure arrays can be used to reliably detect these concentrations of urea.

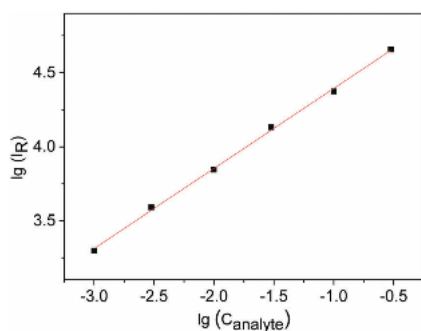


Fig. 3 Raman intensity at 1000 cm^{-1} of urea adsorbed on Au/Cu hybrid nanostructure arrays as a function of urea concentration.

This enhanced sensitivity of urea detection can be attributed to several factors. First, due to the small diameter of the nanorods (about 50 nm), the density of nanogaps is very high, which increases the density of hot spots. Second, when the nanogaps become smaller, the plasmonic coupling among the neighbouring nanorods become more pronounced, thus increasing the SERS sensitivity.²⁴ Besides, Au is a much better material for SERS application than Cu,²³ therefore by coating a thin layer of Au on top of the Cu substrates, the SERS sensitivity is enhanced.

The reusability and chemical stability of the Au/Cu hybrid nanostructure arrays were measured and evaluated. After the SERS measurement, the substrate was washed with deionized water for 1 min and immersed in water for 10 min before being dried in an oven at $50\text{ }^{\circ}\text{C}$ for 15 min. Fig. S5 (ESI[†]) shows that no Raman signal could be observed after this. When using this recycled substrate for urea detection again, it can be observed that most of the Raman signals are again observable, demonstrating good reusability of the substrates.

After the SERS measurement, the sample was put in a glove box for 15 days and then retested under the same conditions, and it was found that the intensity of the signal remained at about 85%, exhibiting a good stability. Even when the sample was kept in the air for 15 days, 75% of the signal intensity was retained, as shown in Fig. S6 (ESI[†]).

A statistical analysis was carried out to examine the SERS intensity variation at different spots on one substrate (spot-to-spot) and different substrates (substrate-to-substrate). Fig. 4a shows the spot-to-spot variation of Raman intensities at 1000 cm^{-1} for a randomly selected Au/Cu hybrid nanostructure substrate. The standard variation is 9.5%, exhibiting remarkable SERS reproducibility. Five separate Au/Cu hybrid nanostructure substrates were used to test the substrate-to-substrate SERS reproducibility. The substrates were loaded with $10\text{ }\mu\text{L}$ of 1 mM urea solution and SERS measurements were carried out at 10 different spots on each substrate to obtain an average Raman intensity. Fig. 4b shows the substrate-to-substrate variation at 1000 cm^{-1} in the Raman spectra for the 5 substrates with a coefficient of variation of 5.6%.

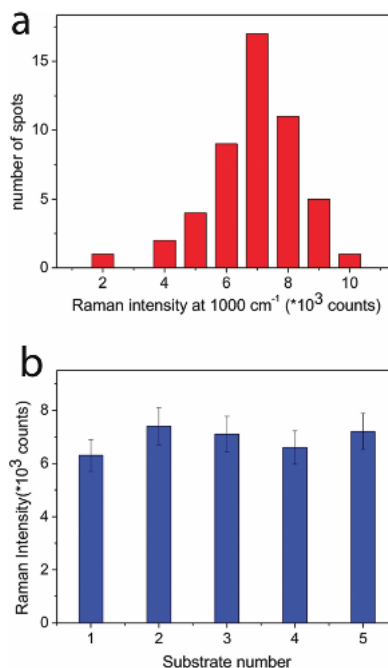


Fig. 4 (a) Histogram of spot-to-spot Raman intensity variation at 1000 cm^{-1} for the Au/Cu hybrid nanostructure arrays. (b) Substrate-to-substrate Raman intensity variation at 1000 cm^{-1} measured for 5 Au/Cu hybrid substrates. Each intensity value represents the average (and standard deviation) of 10 independently measured results at different spots. For all the measurements in (a) and (b), the urea concentration and loading volume are 1 mM and $10\text{ }\mu\text{L}$, respectively.

In summary, we have demonstrated the potential of using a highly ordered Au/Cu hybrid nanostructure as a new platform for fast and reliable detection of urea with concentration as low as 1 mM . This SERS substrate has the advantage of low cost, easy fabrication, and excellent reproducibility. Besides, these substrates can be recycled easily and remain SERS active for a long period of time. The work demonstrated here represents a novel proof-of-concept approach of SERS substrates for medical and clinical applications.

Notes and references

- C.-P. Huang, Y.-K. Li and T.-M. Chen, *Biosens. Bioelectron.*, 2007, **22**, 1835–1838.
- A. Radomska, R. Koncki, K. Pyrzyńska and S. Głab, *Anal. Chim. Acta*, 2004, **523**, 193–200.
- C. J. Choi, H.-Y. Wu, S. George, J. Weyhenmeyer and B. T. Cunningham, *Lab Chip*, 2012, **12**, 574–581.
- B. Premanode and C. Toumazou, *Sens. Actuators, B*, 2007, **120**, 732–735.
- G. Broderick and J. Kang, *J. Dairy Sci.*, 1980, **63**, 64–75.
- Y. Morishita, K. Nakane, T. Fukatsu, N. Nakashima, K. Tsuji, Y. Soya, K. Yoneda, S. Asano and Y. Kawamura, *Clin. Chem.*, 1997, **43**, 1932–1936.
- I. Basu, R. V. Subramanian, A. Mathew, A. M. Kayastha, A. Chadha and E. Bhattacharya, *Sens. Actuators, B*, 2005, **107**, 418–423.

- 8 J. De Melo, S. Cosnier, C. Mousty, C. Martelet and N. Jaffrezic-Renault, *Anal. Chem.*, 2002, **74**, 4037–4043.
- 9 J. L. Abell, J. D. Driskell and Y. Zhao, *Chem. Commun.*, 2014, **50**, 106–108.
- 10 S. Nie and S. R. Emory, *Science*, 1997, **275**, 1102–1106.
- 11 A. Chen, A. E. DePrince, A. Demortière, A. Joshi-Imre, E. V. Shevchenko, S. K. Gray, U. Welp and V. K. Vlasko-Vlasov, *Small*, 2011, **7**, 2365–2371.
- 12 B. Chen, G. Meng, Q. Huang, Z. Huang, Q. Xu, C. Zhu, Y. Qian and Y. Ding, *ACS Appl. Mater. Interfaces*, 2014, **6**, 15667–15675.
- 13 J. Su, D. Wang, L. Nörbel, J. Shen, Z. Zhao, Y. Dou, T. Peng, J. Shi, S. Mathur and C. Fan, *Anal. Chem.*, 2017, **89**, 2531–2538.
- 14 X. Yan, P. Li, B. Zhou, X. Tang, X. Li, S. Weng, L. Yang and J. Liu, *Anal. Chem.*, 2017, **89**, 4875–4881.
- 15 Y. Yuan, Y. Lin, B. Gu, N. Panwar, S. C. Tjin, J. Song, J. Qu and K.-T. Yong, *Coord. Chem. Rev.*, 2017, **337**, 1–33.
- 16 J. Feng, X. Wu, W. Ma, H. Kuang, L. Xu and C. Xu, *Chem. Commun.*, 2015, **51**, 14761–14763.
- 17 J. Huang, F. Chen, Q. Zhang, Y. Zhan, D. Ma, K. Xu and Y. Zhao, *ACS Appl. Mater. Interfaces*, 2015, **7**, 5725–5735.
- 18 Y. Zheng, L. Rosa, T. Thai, S. H. Ng, D. E. Gómez, H. Ohshima and U. Bach, *J. Mater. Chem. A*, 2015, **3**, 240–249.
- 19 G. Mettela, S. Siddhanta, C. Narayana and G. U. Kulkarni, *Nanoscale*, 2014, **6**, 7480–7488.
- 20 P. H. Camargo, M. Rycenga, L. Au and Y. Xia, *Angew. Chem., Int. Ed.*, 2009, **48**, 2180–2184.
- 21 Y. J. Oh and K. H. Jeong, *Adv. Mater.*, 2012, **24**, 2234–2237.
- 22 K. Sun, Q. Huang, G. Meng and Y. Lu, *ACS Appl. Mater. Interfaces*, 2016, **8**, 5723–5728.
- 23 Z. Huang, G. Meng, Q. Huang, Y. Yang, C. Zhu and C. Tang, *Adv. Mater.*, 2010, **22**, 4136–4139.
- 24 X. Zhang, Y. Zheng, X. Liu, W. Lu, J. Dai, D. Y. Lei and D. R. MacFarlane, *Adv. Mater.*, 2015, **27**, 1090–1096.
- 25 L. Chen, T. Fujita, Y. Ding and M. Chen, *Adv. Funct. Mater.*, 2010, **20**, 2279–2285.
- 26 X. Li, X. Ren, Y. Zhang, W. C. Choy and B. Wei, *Nanoscale*, 2015, **7**, 11291–11299.
- 27 K. Chen, X. Zhang, Y. Zhang, D. Y. Lei, H. Li, T. Williams and D. R. MacFarlane, *Adv. Mater. Interfaces*, 2016, **3**, 1600115.

SUPPORTING INFORMATION

Ultrasensitive surface-enhanced Raman scattering detection of urea by highly ordered Au/Cu hybrid nanostructure arrays

Kun Chen,^a Xinyi Zhang,^a Douglas R. MacFarlane*^a

a. School of Chemistry, Monash University, Clayton, Victoria, 3800, Australia

E-mail: douglas.macfarlane@monash.edu

b. Monash Centre for Electron Microscopy, Monash University, VIC 3800, Australia

Materials and methods

The porous AAO templates used in this work were fabricated by employing a well-known two-step anodization process.¹ The starting material used is 0.5 mm thick aluminum foil with ultra-high purity (99.999%). The thickness of the walls and the diameter of the nanochannels are about 40 and 20 nm, respectively. By simply immersing the AAO templates in a 5 % H₃PO₄ for a certain amount of time, the diameter of the nanochannels can be easily adjusted. In this work, 15 mins of immersion time was used to make the diameter of the nanochannels around 45 nm. The Cu nanorod arrays were made using an aqueous bath containing 0.2 M CuSO₄, 0.1 M H₂SO₄ and 0.1 M H₃BO₃. The pH of the solution was about 4.5. The electrodeposition of Cu was carried out at a constant potential of 0.1 V (vs Ag/AgCl) at room temperature. A platinum wire was used as the counter electrode. By controlling the charged passed, the length of the nanorods can be adjusted. When the electro-deposition was done, the samples were cleaned with deionized water and ethanol. After that, a very thick layer of copper was deposited on the backside of the samples to prevent the Cu nanorods from disintegrating after the full removal of the AAO membrane. Finally, the samples were immersed in 5% H₃PO₄ at 30°C for 2h to completely remove the AAO membrane. A Q-150TS sputtering machine was

employed to coat Au nanoparticles on top of the Cu nanorod arrays. By controlling the sputtering coating time, the gap size between neighbouring nanorods was effectively adjusted. All chemical reagents used in this study were of analytical grade and were supplied by Sigma-Aldrich (Australia).

The structure and morphology of the samples were characterized by scanning electron microscopy (SEM, Nova 450), energy dispersive X-ray spectroscopy (EDS), X-ray diffraction (XRD, BRUKER D8-ADVANCE PXRD) and transmission electron microscopy (TEM, Tecnai T20). The SERS measurements were conducted using urea as the analyte. Following the literature methodology, 10 μl of the analyte of different concentrations was dropped on the surface of the Au/Cu hybrid nanostructure arrays.² Then the substrates were put in the oven at 50°C for 20 mins to dry the substrates prior to the SERS measurement. A confocal Raman spectrometer (RENISHAW Invia Raman Microscope) was employed to detect the SERS spectra. All the Raman spectra were collected from a 1 μm^2 area of the samples excited at 532 nm with a laser power of 1.7 mW. The exposure time for urea detection was 10 s.

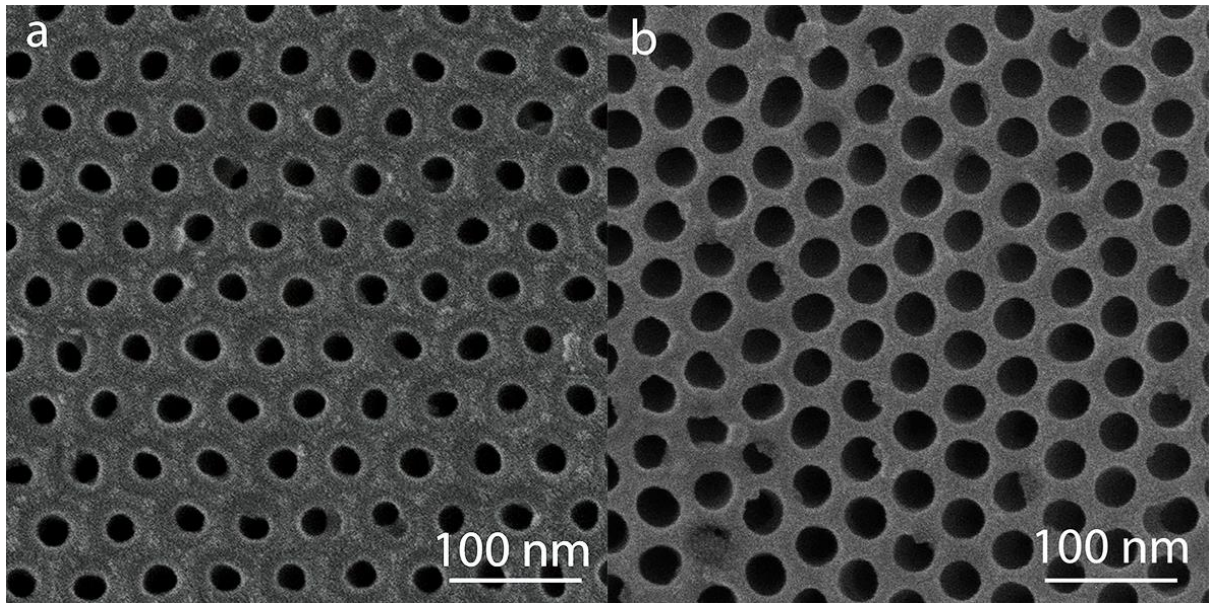


Fig. S1 SEM images of AAO membranes prepared in sulfuric acid electrolyte with different pore sizes.

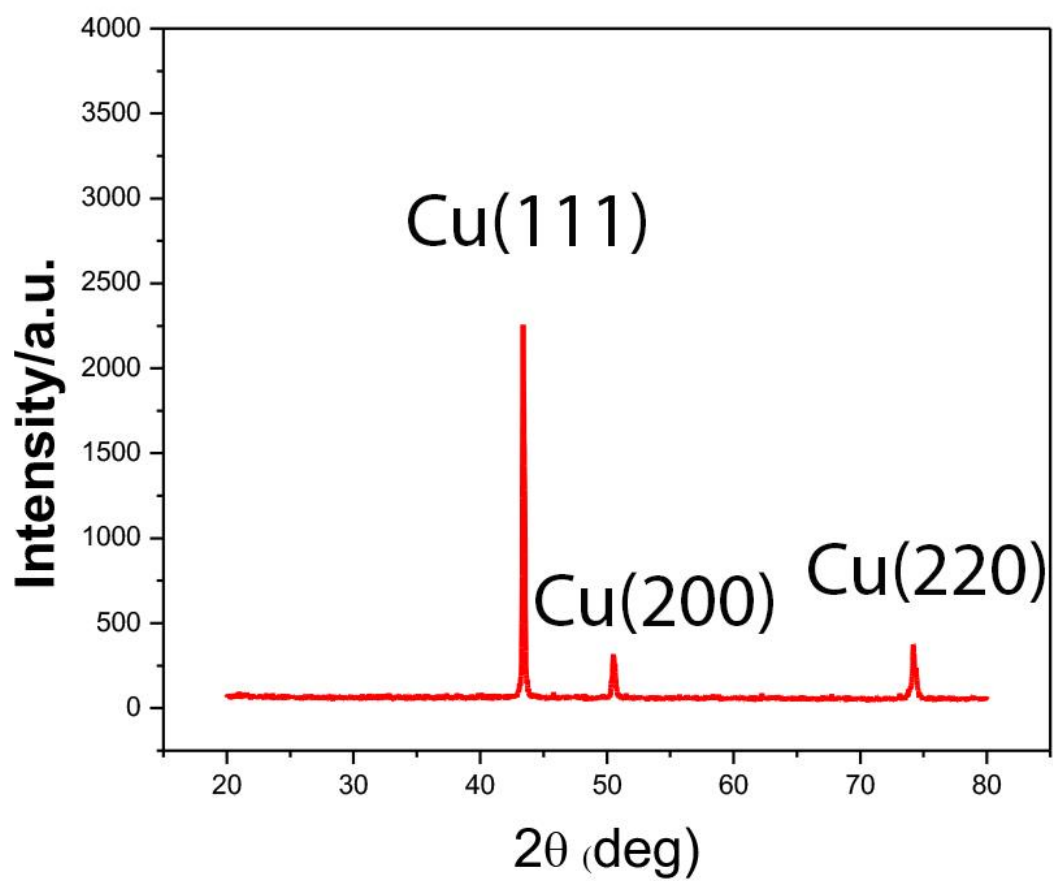


Fig. S2 XRD pattern of the Cu nanorod arrays.

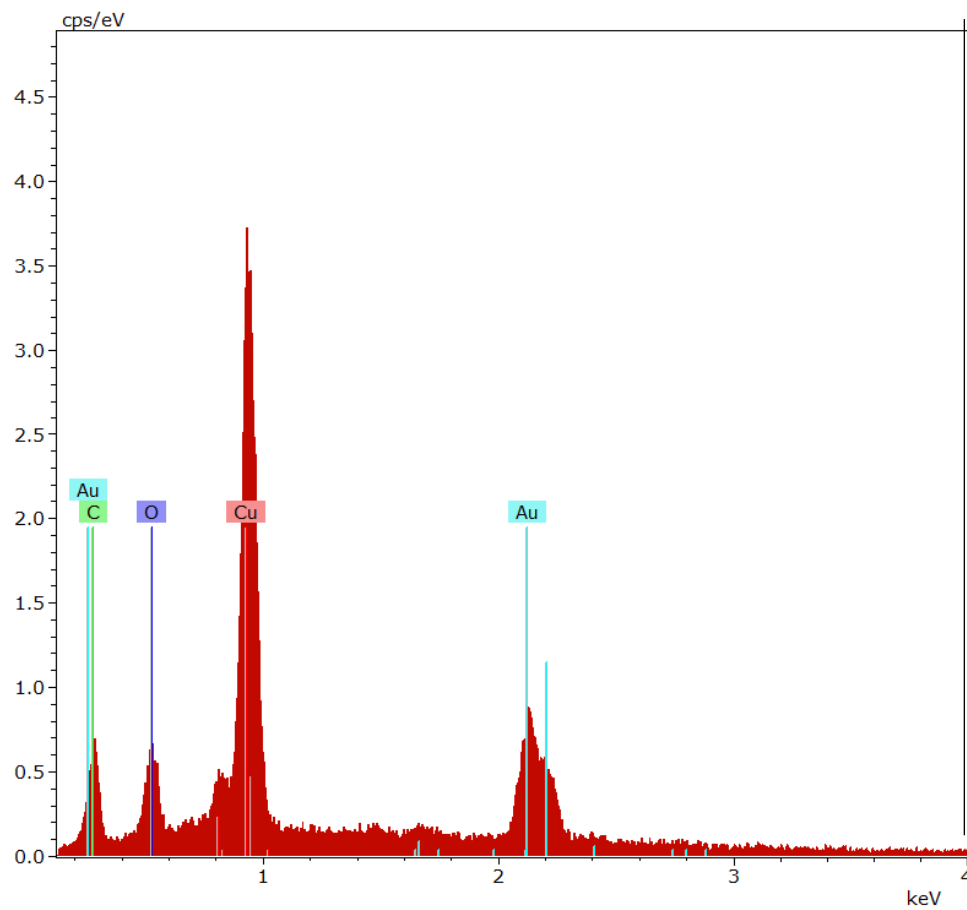


Fig. S3 EDS of the Au/Cu hybrid nanorod arrays.

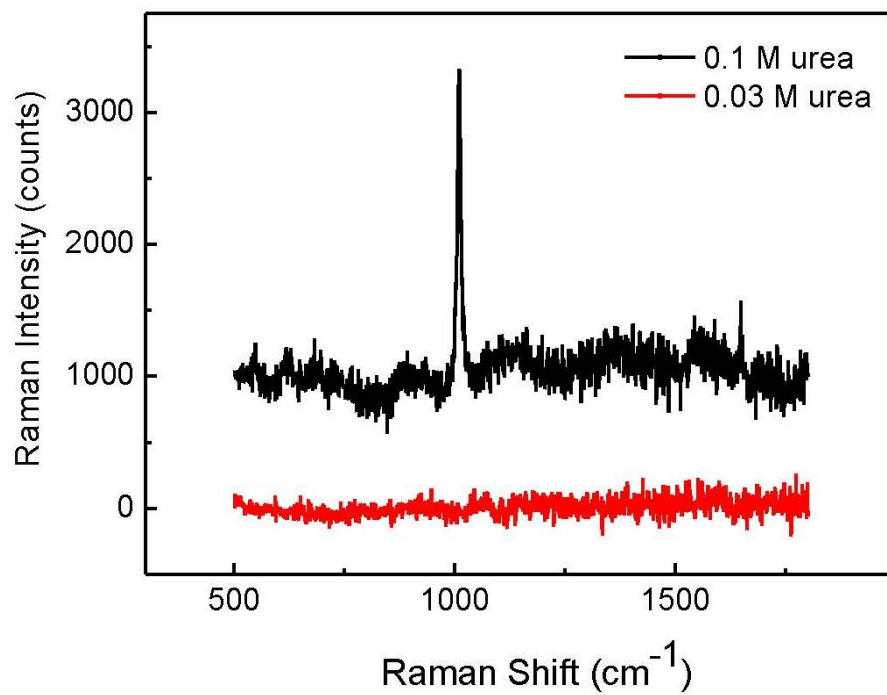


Fig. S4 SERS spectra of pure Cu nanostructured arrays loaded with urea with different concentrations.

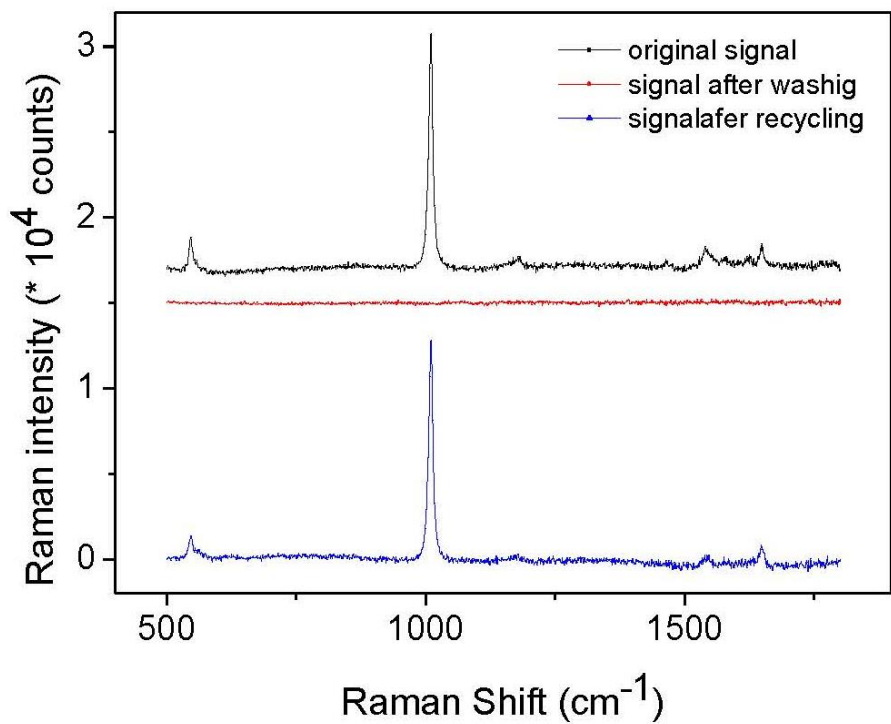


Fig. S5 Reusability test of Au/Cu hybrid nanostructure arrays by using 0.03 M urea as an analyte. This concentration was chosen because it gives relatively strong signals while all peaks can be observed.

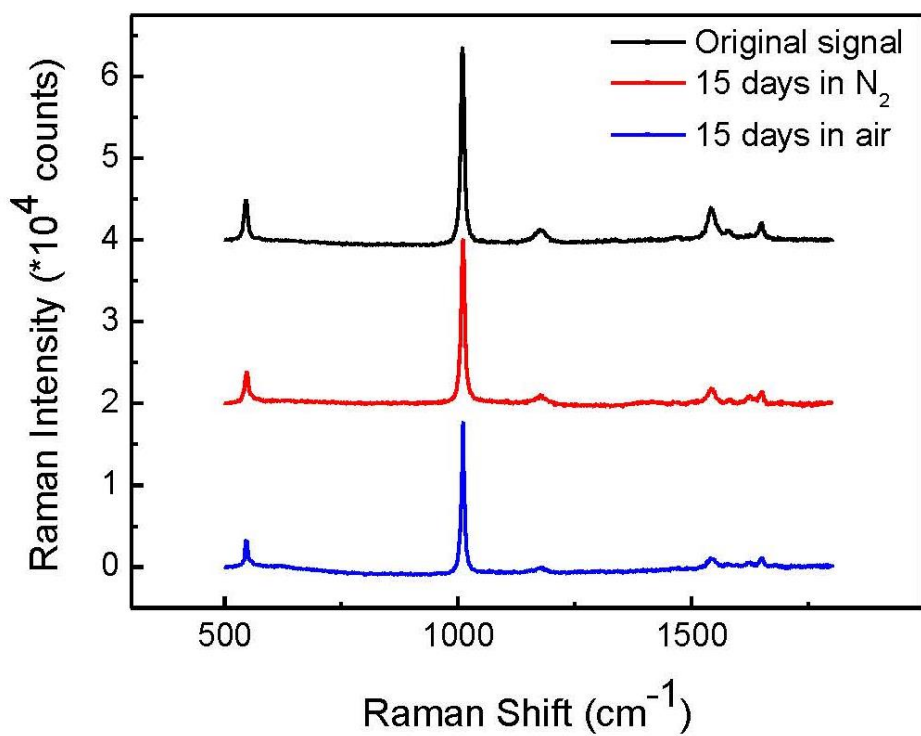


Fig. S6 Raman signal variations under different conditions over time using 0.1 M urea as an analyte. This concentration was chosen because it gives relatively strong peaks, which makes it easy for the comparison of the peak intensities.

Chapter 4

**Syngas production through
electrochemical reduction of CO₂ on
Au-coated Cu nanowires**

Chapter Overview

The following chapter is a paper titled “Syngas production through electrochemical reduction of CO₂ on Au-coated Cu nanowires” published in *Electrochimica Acta* in 2017. In this chapter, the Cu nanorod arrays synthesised in chapter 2 were tested for CO₂ reduction. The results show that the current density of the Cu nanowires electrode was much higher, due to the much-enhanced surface area. But the synthesised Cu nanowires tended to favour H₂ evolution a lot. By sputtering coating a layer of Au on top of the Cu nanowires, the FE of CO was increased. At an overpotential of 540 mV, the catalyst was capable of producing syngas with high efficiency and stability. The much higher current density was attributed to the surface morphology of the catalyst, while the thin layer of Au coating was responsible for increasing the CO Faradaic efficiency. The Au-coated Cu nanowires electrode may pave a way for producing syngas efficiently.



Electrochemical reduction of CO₂ on core-shell Cu/Au nanostructure arrays for syngas production



Kun Chen^a, Xinyi Zhang^b, Tim Williams^c, Laure Bourgeois^c, Douglas R. MacFarlane^{a,*}

^aARC Centre of Excellence for Electromaterials Science, School of Chemistry, Monash University, Clayton, Victoria 3800, Australia

^bSchool of Chemistry, Monash University, Clayton, Victoria 3800, Australia

^cMonash Centre for Electron Microscopy, Monash University, Clayton, Victoria 3800, Australia

ARTICLE INFO

Article history:

Received 19 December 2016

Received in revised form 4 April 2017

Accepted 4 April 2017

Available online 4 April 2017

Keywords:

CO₂ reduction
faradaic efficiency
core-shell Cu/Au nanostructures
syngas

ABSTRACT

Electrocatalytically converting CO₂ to hydrocarbons is a very attractive way to use the excess electricity generated from renewable energies. In this paper, we report the electrochemical reduction of CO₂ based on Cu nanowire arrays. The Cu nanostructured electrode shows much higher current density than polycrystalline Cu. By sputter coating a thin layer of Au on the Cu nanowires, the Faradaic efficiency (FE) of CO can exceed 30%. At an overpotential of 540 mV with respect to the formation of CO, the Cu/Au core-shell nanowire array electrode catalyses the formation of syngas, a very useful gas mixture, with a stable CO/H₂ ratio.

© 2017 Elsevier Ltd. All rights reserved.

1. Introduction

As one of the main end products of combustion, carbon dioxide is considered as the primary cause of global warming. The concentration of atmospheric CO₂ has reached unprecedented levels due to the increased use of fossil fuels [1–6]. If unstopped, it is projected to inflict catastrophic impacts on the world climate, causing irrevocable damages [7]. In view of the inevitable depletion of fossil fuels, it is therefore essential to have a future energy source that is safe and CO₂-neutral. Solar, wind and geothermal energies are all very promising energy sources. But currently the transportation and storage of these green energies is still a huge challenge. One possible solution to this problem is to electrocatalytically convert CO₂ to hydrocarbon fuels to store excess electricity generated from renewable energies, which could not only provide valuable energy sources in a sustainable manner, but also help mitigate the global warming effect caused by rising atmospheric CO₂ levels [8–10].

Over the past few decades, various materials have been studied for electrochemical conversion of CO₂. However, none is efficient and selective enough for practical application. The primary reason is that CO₂ is extremely stable and the hydrogen evolution reaction (HER) usually prevails over CO₂ reduction in aqueous solutions [11,12]. To date, the majority of the CO₂ reduction studies have been

focused on Cu electrodes because Cu is capable of producing hydrocarbons (methane and ethylene), which are much more valuable than CO [13]. Recent research indicates that the morphology and roughness of the Cu electrode surface play a significant role in the catalytic activity and product selectivity of the electrodes [14–18]. Li et al. demonstrated that by reduction of thick Cu₂O films, the overpotentials for CO₂ reduction are significantly reduced [15]. Reske and colleagues reported that the size of Cu nanoparticles has a dramatic influence on the CO₂ reduction path [16]. Ma et al. show that CuO-derived Cu nanowires could selectively reduce CO₂ to CO [19].

Among the materials being tested, Au has also attracted particular interest due to the fact that it can selectively convert CO₂ to CO under very low overpotentials [11,20]. Recent research has shown that the catalytic activity for CO₂ reduction can be further enhanced through controlling the structure of metallic nanocrystals [21–28]. Among them, the Cu/Au core-shell nanoparticles are of great interest, which give insights into the intermediate binding and geometric effect of bimetallic nanostructures in CO₂ reduction [29–31]. Considering the importance of Cu electrodes for CO₂ reduction and the fact that both the size and structure of the electrodes could have massive impacts on the CO₂ reduction path, it is worthwhile to explore the catalytic activity of three-dimensional nanostructured Cu electrodes. In this study, we show for the first time the reduction of CO₂ on Cu/Au core-shell nanowire arrays. Compared with polycrystalline Cu, the current density of the electrochemical reduction of CO₂ on Cu nanowire arrays is dramatically increased. By sputter coating a thin layer of

* Corresponding author.

E-mail address: [redacted] (D.R. MacFarlane).

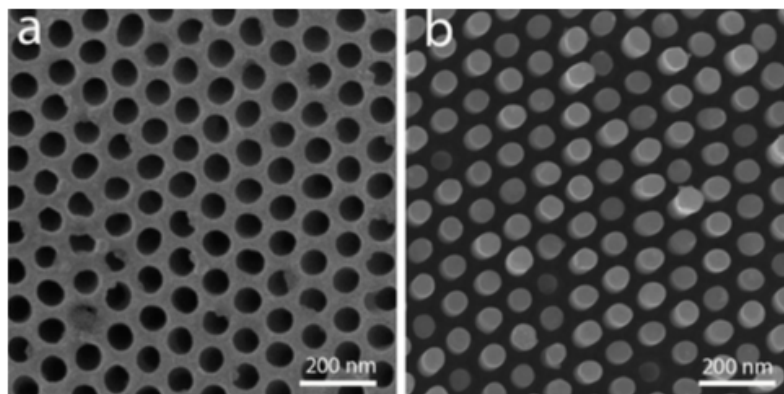


Fig. 1. SEM images of AAO membrane prepared in oxalic acid electrolyte and corresponding Cu nanowires.

Au on top of the Cu nanowires, we demonstrate that the current density can be further increased, as is the FE of CO production. At -0.65 V RHE, the molar ratio of CO and H_2 in the product is about 1:2, which is the composition of syngas. Therefore, the synthesized gas mixture can be readily used as a source gas for the Fischer-Tropsch process [32], which is an essential gas-to-fuel technology used to produce various liquid hydrocarbon fuels.

2. Experimental

The porous AAO templates used in this work were fabricated by employing a well-known two-step anodization process [33]. The starting material used is 0.5 mm thick aluminum foil with ultra-high purity (99.999%). A thin layer of Au (around 10 nm) was sputter coated onto the back side of the AAO membrane to make it conductive. An aqueous bath was prepared with 0.2 M $CuSO_4$ and 0.1 M H_3BO_3 , 0.1 M H_2SO_4 solution was used to adjust the pH of the solution to around 4.5. Cu nanowires were electrodeposited into the nanochannels of the AAO membrane under a constant current of 1 mA with a platinum wire serving as the counter electrode. The length of the Cu nanowires can be readily controlled by simply changing the electrodeposition time. After electrodeposition, the AAO membrane was thoroughly washed with deionized water. Then the backside was electrodeposited with a very thick layer of Cu in order to produce the electrode for the CO_2 reduction reaction. After that, the sample was immersed in a 5% H_3PO_4 solution at $30^\circ C$ for 1.5 h to fully remove the AAO membrane. Then the back side of the Cu nanowires was soldered together with a copper conductor and subsequently sealed with glue. The surface area of the electrode is around 0.8 cm^2 . A Q-150TS sputtering machine was employed to coat a thin layer of Au on top of the Cu nanowires at a current density of 40 mA.

Scanning electron microscopic (SEM) images and energy dispersive spectra (EDS) were obtained from a FEI Nona NanoSEM 450 FEG SEM Instrument equipped with a Bruker Quantax 400 X-ray analysis system. Transmission electron microscopic (TEM) images were collected on a FEI Tecnai G2 T20 TWIN TEM Instrument. X-ray diffraction (XRD) data was collected on a Philip X-ray power diffractometer. An Agilent 7820 A gas chromatography (GC) system equipped with a HP-plot molesieve (5A) column was employed for GC measurements. Helium (99.99%) and nitrogen (99.99%) were used as carrier gas for CO and H_2 analysis respectively. All the electrochemical experiments were carried out on a Gamry Electrochemical Instrument under ambient temperature and pressure. CO_2 electrolysis experiments were

carried out in a gas-tight two-compartment electrochemical cell with a glass frit serving as the separator. Each compartment had 15 mL electrolyte and around 15 mL headspace. A platinum wire and an Ag/AgCl (3 M KCl) were used as counter and reference

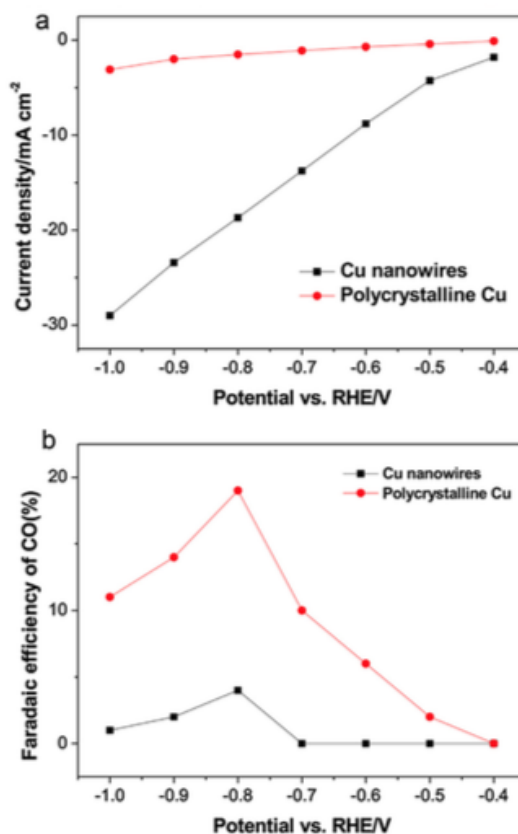


Fig. 2. Current density (a) and FE of CO (b) of Cu nanowires and polycrystalline Cu under different potentials.

electrodes respectively. Linear sweep voltammetry analysis was carried out in a 0.5 M KHCO_3 solution saturated with CO_2 in a conventional three-electrode cell with a platinum wire serving as the counter electrode. The electrolyte (0.5 M KHCO_3) was purged with a constant flow of CO_2 for 30 minutes before electrolysis. The Ohmic resistance between the reference and working electrodes was measured to be around 2Ω , and the Ohmic drop was about 20 mV at -0.65 V (vs RHE), so the effect of Ohmic drop is almost negligible. During the electrolysis, the electrolytes in both compartments were stirred vigorously. After the electrolysis, a gas-tight syringe was used to get 200 μL gas sample from the cell's head space and subsequently analysed by GC. All potentials were converted to a reversible hydrogen electrode (RHE) reference scale. All chemicals used in this study were purchased from Sigma-Aldrich Australia and were used without further purification.

3. Results and Discussion

3.1. Synthesis and characterization of Cu nanowire arrays

A typical SEM image of the AAO membrane is shown in Fig. 1a. The diameter of the nanoholes is around 60 nm with a 40 nm gap between them. Ordered Cu nanowires were fabricated after the electrodeposition of Cu inside the AAO membrane. After full removal of the AAO membrane, ordered Cu nanowires can be clearly observed, as shown in Fig. 1b. The XRD analysis confirms the face centred cubic crystal structure of the Cu nanowires with dominant (111) facets (Fig. S1).

3.2. CO_2 reduction performance of Cu nanowire arrays

Fig. S2 shows the linear sweep analysis of Cu nanowires with different lengths. The 1 μm Cu nanowires show a higher current density in a linear scan compared with 10 μm and 50 μm Cu nanowires. This is probably because when the nanowires become too long they tend to aggregate (as shown in Fig. S3), thus making it very difficult for electrolyte to enter the bottom part of the

nanowires hence decrease availability of the inner surface. Besides, due to the small diameter of the nanowires (around 60 nm), when they are too long, the conductivity also becomes an issue. Therefore, Cu nanowires with a length of around 1 μm were chosen to carry out the CO_2 reduction experiment in this work.

Fig. 2a shows that compared with the polycrystalline Cu electrode, the current density of our Cu nanowires electrode is much higher, which is due to the much increased surface area. But the synthesized Cu nanowires tend to favour H_2 evolution. From -0.4 V to -0.7 V , no other product except H_2 could be detected, as shown in Fig. 2b. At -0.8 V and -0.9 V , CO was detected, but the amount was very low. Although the current density of polycrystalline Cu electrode is quite low, the FE of CO is much higher than the Cu nanowire electrode. Besides, formate, methane and ethylene were also detected when using the polycrystalline Cu electrode, as shown in Fig. S4. For the Cu nanowires electrode, apart from H_2 and CO, no other product could be detected at a potential of -0.9 V . Only when the potential was further decreased to -1.1 V , a tiny amount (around 1%) of methane was detected. One possible explanation is that due to small gap size, large surface area, and high current density the reaction is likely to be mass transfer limited. Therefore, HER (hydrogen evolution reaction) is dominant and the FE of hydrogen production is relatively high since the kinetics of HER are considerably faster than CO_2 reduction [15].

3.3. CO_2 reduction performance of Au coated Cu nanowire arrays

In order to fully utilize the large surface area of the Cu nanowires, a thin layer of Au was sputter coated on top of the nanowires. Various previous studies have shown that Au is capable of converting CO_2 to CO with high efficiency and great selectivity. So by controlling the thickness of Au coating, we aimed to raise the ratio of CO in the gas product to make syngas. Fig. 3a shows the SEM image of the Au coated Cu nanowires. It can be observed that the surface became rough after coating a layer of Au. EDS (Fig. S5) reveals that the surface is indeed covered with a layer of Au. TEM images prove that the side surface is also quite rough (Fig. 3b), and

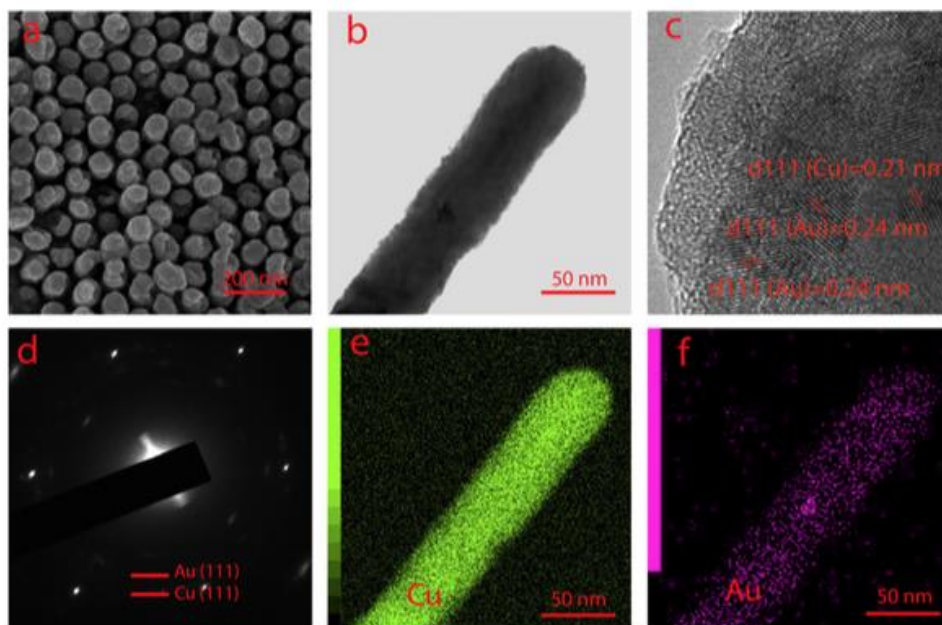


Fig. 3. SEM (a), TEM (b,c), diffraction pattern (d), and elemental mapping (e,f) of Au coated Cu nanowire.

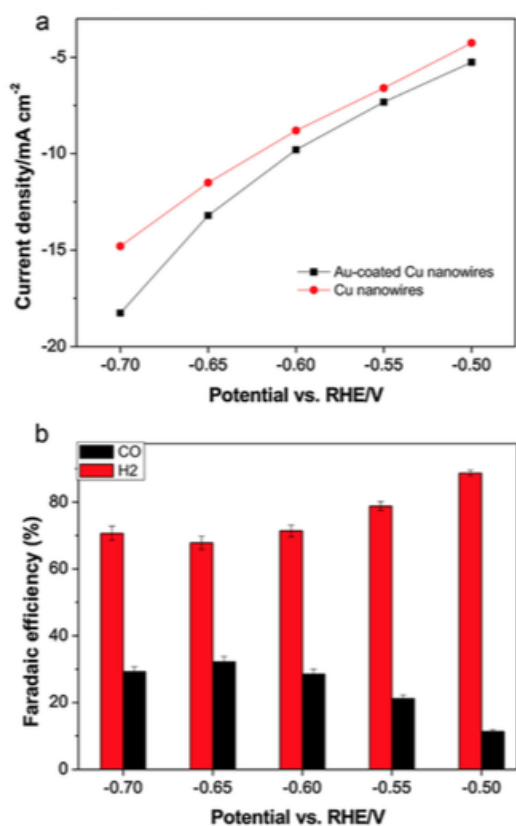


Fig. 4. Current density (a) and Faradaic efficiency for CO and H₂ (b) as a function of potential for Au coated Cu nanowires electrode.

covered with a very thin layer of Au (Fig. S6), as confirmed by the lattice pattern (Fig. 3c) and diffraction pattern (Fig. 3d). Elemental mapping further demonstrates that the Cu nanowire surface is indeed coated with a very thin layer of Au (Fig. 3e, f). Fig. S7 shows the linear sweep voltammetry of core-shell Cu/Au nanostructure arrays in CO₂-saturated and N₂-saturated aqueous 0.5 M KHCO₃ solution at a scan rate of 50 mV/s. The cyclic voltametric (CV) result is provided in Fig. S8.

Fig. 4a shows that by coating a thin layer of Au onto the nanowires, the current density was slightly increased, which is consistent with the literature, as Au electrodes tend to generate higher current than Cu-based ones [19,24]. Although there is only a minor increase in the current density, the FE of CO was increased dramatically, as shown in Fig. 4b. The results show that CO and H₂ are the only products that could be detected, with a combined FE of around 100%. The FE of CO is highly dependent on the potential applied. At an applied potential of -0.5 V (an over-potential of 0.39 V for CO formation), H₂ is the dominant product with a FE of CO of around 11%. As the overpotential increases, the FE of CO also becomes higher, reaching a maximum of 33% at a potential of -0.65 V. Further increase of the overpotential only leads to the decrease of FE of CO. This phenomenon was also observed in various previous reports using Au, Ag, and Cu as catalysts [24]. This is because when the overpotential is very low, HER is kinetically

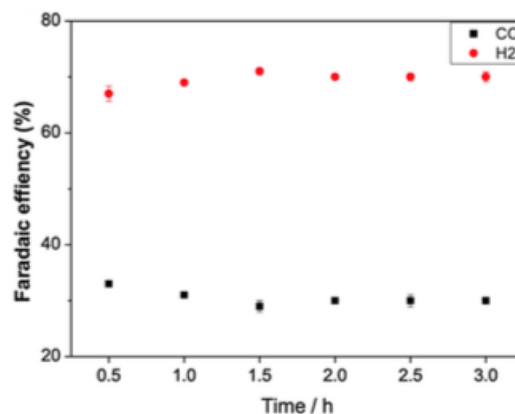


Fig. 5. Faradaic efficiency of H₂ and CO. Potentiostatic electrolysis at -0.65 V in CO₂-saturated 0.5 M aqueous KHCO₃ solution.

and thermodynamically more favourable than CO formation [34]. When the over-potential is in the intermediate range, HER is hindered because of the low desorption of CO from the active sites, thus increasing the FE of CO [35]. When the overpotential is very high, HER becomes dominant again due to the fact that H⁺ is much more abundant and readily available in the KHCO₃ solution. Therefore, the FE of CO starts to decrease after a certain value of overpotential [36,37].

What is especially worth mentioning is that when the applied potential is -0.65 V, the molar ratio of CO and H₂ is around 1:2, which is the composition of syngas. Therefore, this gas mixture can be readily used as the source gas for the Fischer-Tropsch process, which is widely employed in industries to produce various liquid fuels [32]. Although many other catalysts can generate higher FE of CO with lower overpotentials [24], to the best of our knowledge, none of the Cu based ones was capable of generating such a high current density (around 14 mA/cm²) at an applied potential of -0.65 V. This is probably due to the fact that the dimensions of most other metal catalysts are at the microscale, while the dimension of our catalyst is at the nanoscale, thus significantly increasing the current density [24]. According to previous studies, Au electrodes normally lead to maximum FE of CO much higher than 33% (as high as 98% in some cases) [24]. The extremely small gap size and the local pH effects within the gaps are possible explanations for the observed low FE of CO [14,15]. The presence of the Cu nanowires under the Au coating might be another factor facilitating the HER. Au coating cannot cover the whole surface of the nanowires, especially the bottom part. Therefore, Cu still plays a very important role in the reaction, generating a lot of H₂ gas, thereby decreasing the CO/H₂ ratio produced by the thin Au layer coating.

3.4. Durability of the Au coated Cu nanowires

The long term stability of CO/H₂ ratio was tested under the applied potential of -0.65 V, which is the potential to produce the highest FE of CO. As shown in Fig. 5, the FE of CO and H₂ remains highly stable over a three-hour period of electrolysis. Even after 24 h of electrolysis, the CO/H₂ ratio is still around 1:2, although there is an observable decrease in the overall current density. Therefore, our Au coated Cu nanowires have great potential to be used as a cost-effective catalyst for syngas synthesis for the Fischer-Tropsch process. Besides, the long term stability of current

density was also studied under the potential of -0.65 V, as shown in Fig. S9. Although an initial decay of current can be clearly observed during the first three hours of electrolysis, which cannot be simply attributed to adsorption of gaseous products or double layer charging process, this kind of decay is also reported in other Cu electrodes due to the deactivation of catalytic activity of the catalyst [15,17]. But the current density of our catalyst becomes quite stable after three hours. Even after 24 hours, the current density is still around 8 mA/cm^2 at an applied potential of -0.65 V, much higher than most metal based electrodes [24]. More importantly, even though the current is decreased, the FE of CO remains quite constant (Fig. 5), which means that the deactivation of the catalyst is evenly distributed among Cu and Au in our electrode. Fig. S10 shows that after 24 h of electrolysis, no discernible structure change can be observed, demonstrating the stability of the Au coating layer.

4. Conclusions

In summary, we have synthesized an Au-coated Cu nanowires electrode and used it for electrocatalytic reduction of CO_2 to CO in CO_2 saturated KHCO_3 solution. To the best of our knowledge, this kind of core-shell nanostructure has never been reported for syngas production. The results show that much increased surface area can dramatically enhance the current density of the electrode. At an overpotential of 540 mV, our catalyst is capable of producing syngas with high efficiency and stability. The much higher current density is attributed to the surface morphology of our catalyst, while the thin layer of Au coating is responsible for producing CO. Our Au-coated Cu nanowires electrode may pave a way for producing syngas efficiently.

Acknowledgments

This work was financially supported by the Australian Research Council through the ARC Centre of Excellence for Electromaterials Science (GrantNo. CE140100012) and Grant No.: DP120104334. DRM is grateful to the ARC for his Australian Laureate Fellowship. The authors also gratefully acknowledge the contribution of the Monash Centre for Electron Microscopy.

Appendix A. Supplementary data

Supplementary data associated with this article can be found, in the online version, at <http://dx.doi.org/10.1016/j.electacta.2017.04.019>.

References

- [1] A.M. Appel, J.E. Bercaw, A.B. Bocarsly, H. Dobbek, D.L. DuBois, M. Dupuis, J.G. Ferry, E. Fujita, R. Hille, P.J. Kenis, Frontiers, opportunities, and challenges in biochemical and chemical catalysis of CO_2 fixation, *Chemical reviews* 113 (2013) 6621–6658.
- [2] H. Arakawa, M. Aresta, J.N. Armor, M.A. Barteau, E.J. Beckman, A.T. Bell, J.E. Bercaw, C. Creutz, E. Dinjus, D.A. Dixon, Catalysis research of relevance to carbon management: progress, challenges, and opportunities, *Chemical Reviews* 101 (2001) 953–996.
- [3] M. Aresta, A. Dibenedetto, Utilisation of CO_2 as a chemical feedstock: opportunities and challenges, *Dalton Transactions* (2007) 2975–2992.
- [4] M. Aresta, A. Dibenedetto, A. Angelini, Catalysis for the valorization of exhaust carbon: From CO_2 to chemicals, materials, and fuels. *Technological use of CO_2* , *Chemical reviews* 114 (2013) 1709–1742.
- [5] A. Harriman, Prospects for conversion of solar energy into chemical fuels: the concept of a solar fuels industry *Philosophical Transactions of the Royal Society of London A: Mathematical, Physical and Engineering Sciences* 371 (2013) 20110415.
- [6] N.S. Lewis, D.G. Nocera, Powering the planet: Chemical challenges in solar energy utilization, *Proceedings of the National Academy of Sciences* 103 (2006) 15729–15735.
- [7] S.C. Doney, V.J. Fabry, R.A. Feely, J.A. Kleypas, Ocean acidification: the other CO_2 problem, *Marine Science* 1 (2009).
- [8] A.S. Varela, W. Ju, T. Reier, P. Strasser, Tuning the Catalytic Activity and Selectivity of Cu for CO_2 Electroreduction in the Presence of Halides, *ACS Catalysis* 6 (2016) 2136–2144.
- [9] W. Luo, X. Nie, M.J. Janik, A. Asthagiri, Facet Dependence of CO_2 Reduction Paths on Cu Electrodes, *ACS Catalysis* 6 (2015) 219–229.
- [10] H. Mistry, F. Behafarid, R. Reske, A.S. Varela, P. Strasser, B. Roldan Cuenya, Tuning catalytic selectivity at the mesoscale via interparticle interactions, *ACS Catalysis* 6 (2016) 1075–1080.
- [11] Y. Hori, Electrochemical CO_2 reduction on metal electrodes, *Modern aspects of electrochemistry*, Springer, 2008, pp. 89–189.
- [12] J. Schneider, H. Jia, J.T. Muckerman, E. Fujita, Thermodynamics and kinetics of CO_2 , CO, and H^+ binding to the metal centre of CO_2 reduction catalysts, *Chemical Society Reviews* 41 (2012) 2036–2051.
- [13] Y. Hori, A. Murata, R. Takahashi, Formation of hydrocarbons in the electrochemical reduction of carbon dioxide at a copper electrode in aqueous solution, *Journal of the Chemical Society Faraday Transactions 1: Physical Chemistry in Condensed Phases* 85 (1989) 2309–2326.
- [14] S. Sen, D. Liu, G.T.R. Palmore, Electrochemical reduction of CO_2 at copper nanofoams, *ACS Catalysis* 4 (2014) 3091–3095.
- [15] C.W. Li, M.W. Kanan, CO_2 reduction at low overpotential on Cu electrodes resulting from the reduction of thick Cu_2O films, *Journal of the American Chemical Society* 134 (2012) 7231–7234.
- [16] R. Reske, H. Mistry, F. Behafarid, B. Roldan Cuenya, P. Strasser, Particle size effects in the catalytic electroreduction of CO_2 on Cu nanoparticles, *Journal of the American Chemical Society* 136 (2014) 6978–6986.
- [17] R. Kas, R. Kortlever, A. Milbrat, M.T. Koper, G. Mul, J. Baltrusaitis, Electrochemical CO_2 reduction on Cu_2O -derived copper nanoparticles: controlling the catalytic selectivity of hydrocarbons, *Physical Chemistry Chemical Physics* 16 (2014) 12194–12201.
- [18] W. Tang, A.A. Peterson, A.S. Varela, Z.P. Jovanov, L. Bech, W.J. Durand, S. Dahl, J. K. Nørskov, I. Chorkendorff, The importance of surface morphology in controlling the selectivity of polycrystalline copper for CO_2 electroreduction, *Physical Chemistry Chemical Physics* 14 (2012) 76–81.
- [19] M. Ma, K. Djanashvili, W.A. Smith, Selective electrochemical reduction of CO_2 to CO on CuO -derived Cu nanowires, *Physical Chemistry Chemical Physics* 17 (2015) 20861–20867.
- [20] K.P. Kuhl, T. Hatsukade, E.R. Cave, D.N. Abram, J. Kibsgaard, T.F. Jaramillo, Electrocatalytic conversion of carbon dioxide to methane and methanol on transition metal surfaces, *Journal of the American Chemical Society* 136 (2014) 14107–14113.
- [21] X. Min, M.W. Kanan, Pd-catalyzed electrohydrogenation of carbon dioxide to formate: High mass activity at low overpotential and identification of the deactivation pathway, *Journal of the American Chemical Society* 137 (2015) 4701–4708.
- [22] Y. Chen, C.W. Li, M.W. Kanan, Aqueous CO_2 reduction at very low overpotential on oxide-derived Au nanoparticles, *Journal of the American Chemical Society* 134 (2012) 19969–19972.
- [23] Q. Lu, J. Rosen, Y. Zhou, G.S. Hutchings, Y.C. Kimmel, J.G. Chen, F. Jiao, A selective and efficient electrocatalyst for carbon dioxide reduction, *Nature communications* 5 (2014).
- [24] Q. Lu, J. Rosen, F. Jiao, Nanostructured metallic electrocatalysts for carbon dioxide reduction, *ChemCatChem* 7 (2015) 38–47.
- [25] A. Salehi-Khojin, H.-R.M. Jhong, B.A. Rosen, W. Zhu, S. Ma, P.J. Kenis, R.L. Masel, Nanoparticle silver catalysts that show enhanced activity for carbon dioxide electroreduction, *The Journal of Physical Chemistry C* 117 (2013) 1627–1632.
- [26] W. Zhu, R. Michalsky, O.N. Metin, H. Lv, S. Guo, C.J. Wright, X. Sun, A.A. Peterson, S. Sun, Monodisperse Au nanoparticles for selective electrocatalytic reduction of CO_2 to CO, *Journal of the American Chemical Society* 135 (2013) 16833–16836.
- [27] W. Zhu, Y.-J. Zhang, H. Zhang, H. Lv, Q. Li, R. Michalsky, A.A. Peterson, S. Sun, Active and selective conversion of CO_2 to CO on ultrathin Au nanowires, *Journal of the American Chemical Society* 136 (2014) 16132–16135.
- [28] C. Kim, H.S. Jeon, T. Eom, M.S. Jee, H. Kim, C.M. Friend, B.K. Min, Y.J. Hwang, Achieving Selective and Efficient Electrocatalytic Activity for CO_2 Reduction Using Immobilized Silver Nanoparticles, *Journal of the American Chemical Society* 137 (2015) 13844–13850.
- [29] D. Kim, J. Resasco, Y. Yu, A.M. Asiri, P. Yang, Synergistic geometric and electronic effects for electrochemical reduction of carbon dioxide using gold-copper bimetallic nanoparticles, *Nature communications* 5 (2014).
- [30] J. Monzó, Y. Malewski, R. Kortlever, F.J. Vidal-Iglesias, J. Solla-Gullón, M. Koper, P. Rodríguez, Enhanced electrocatalytic activity of Au@Cu core-shell nanoparticles towards CO_2 reduction, *Journal of Materials Chemistry A* 3 (2015) 23690–23698.
- [31] J. Christophe, T. Doneux, C. Buess-Herman, Electroreduction of carbon dioxide on copper-based electrodes: activity of copper single crystals and copper-gold alloys, *Electrocatalysis* 3 (2012) 139–146.
- [32] Y. Zhang, G. Jacobs, D.E. Sparks, M.E. Dry, B.H. Davis, CO and CO_2 hydrogenation study on supported cobalt Fischer-Tropsch synthesis catalysts, *Catalysis today* 71 (2002) 411–418.
- [33] X. Zhang, Y. Zheng, X. Liu, W. Lu, J. Dai, D.Y. Lei, D.R. MacFarlane, Hierarchical Porous Plasmonic Metamaterials for Reproducible Ultrasensitive Surface-Enhanced Raman Spectroscopy, *Advanced Materials* 27 (2015) 1090–1096.
- [34] C. Delacourt, P.L. Ridgway, J. Newman, Mathematical modeling of CO_2 reduction to CO in aqueous electrolytes I. kinetic study on planar silver and gold electrodes, *Journal of The Electrochemical Society* 157 (2010) B1902–B1910.

- [35] P. Kedzierzawski, J. Augustynski, Poisoning and Activation of the Gold Cathode during Electroreduction of CO₂, *Journal of The Electrochemical Society* 141 (1994) L58–L60.
- [36] T. Hatsukade, K.P. Kuhl, E.R. Cave, D.N. Abram, T.F. Jaramillo, Insights into the electrocatalytic reduction of CO₂ on metallic silver surfaces, *Physical Chemistry Chemical Physics* 16 (2014) 13814–13819.
- [37] Y. Hori, A. Murata, K. Kikuchi, S. Suzuki, Electrochemical reduction of carbon dioxides to carbon monoxide at a gold electrode in aqueous potassium hydrogen carbonate, *Journal of the Chemical Society, Chemical Communications* (1987) 728–729.

Supplementary Information

Electrochemical reduction of CO₂ on core-shell Cu/Au nanostructure arrays for syngas production

Kun Chen,^{a*} Xinyi Zhang,^b Tim Williams,^c Laure Bourgeois,^c Douglas R MacFarlane^a

^aARC Centre of Excellence for Electromaterials Science, School of Chemistry, Monash University, Clayton, Victoria 3800, Australia

^bSchool of Chemistry, Monash University, Clayton, Victoria 3800, Austral

^cMonash Centre for Electron Microscopy, Monash University, Clayton, Victoria 3800, Australia

*Corresponding Author: [REDACTED]
[REDACTED]

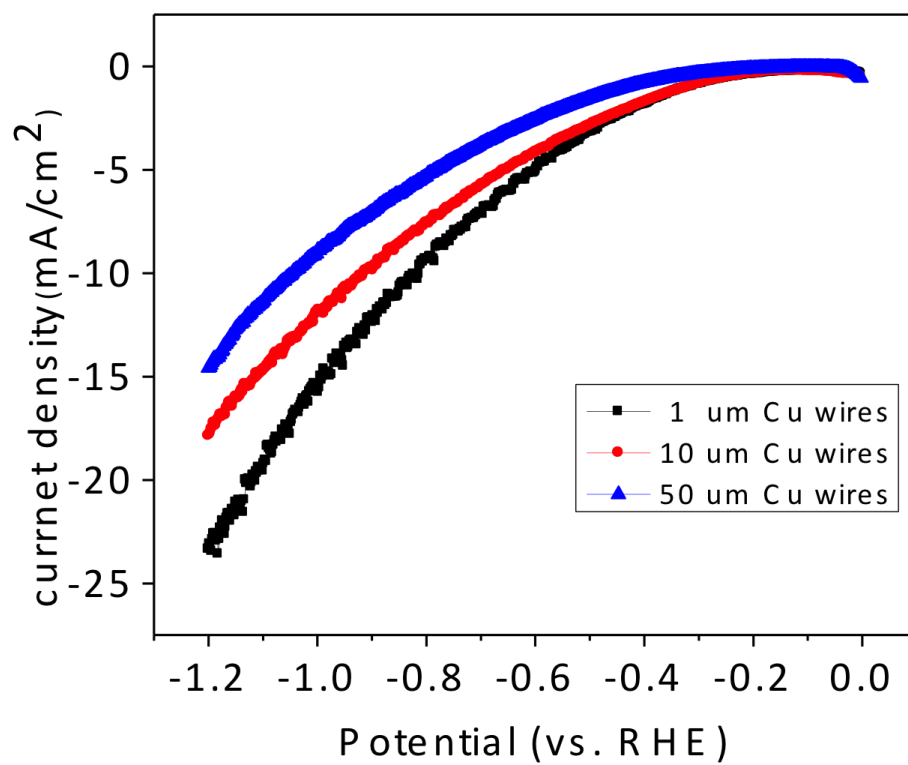


Figure S2. Linear sweep analysis of Cu nanowires with different lengths with a scan rate of 50 mV/s.

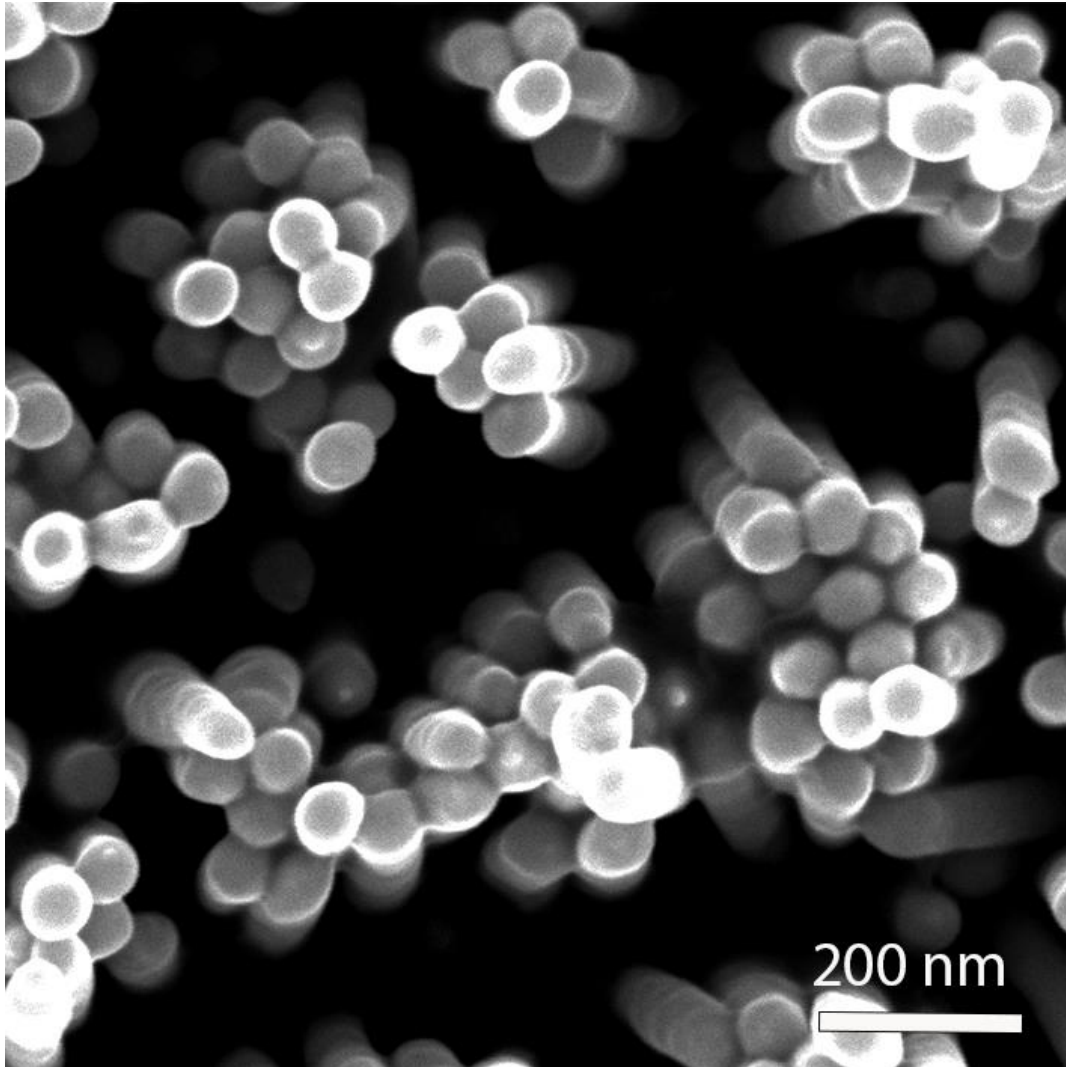


Figure S3. SEM image of Cu nanowires with a length of 10 μm .

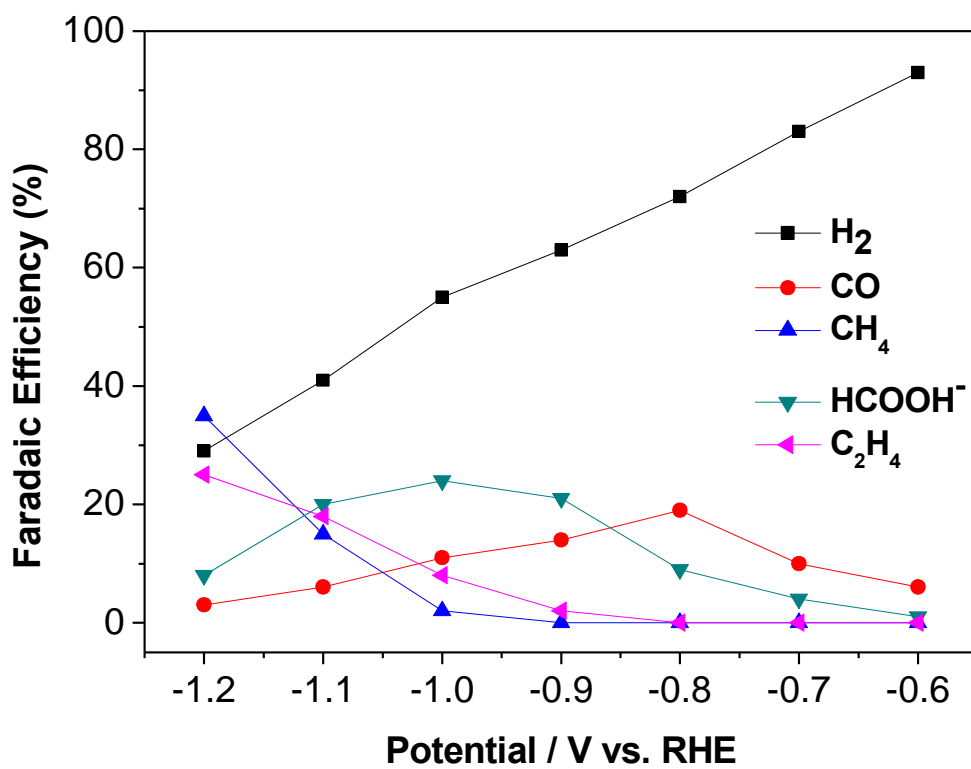


Figure S4. Variation of the Faradaic efficiencies of the products in electrochemical reduction of CO₂ in 0.1 M KHCO₃ solution.

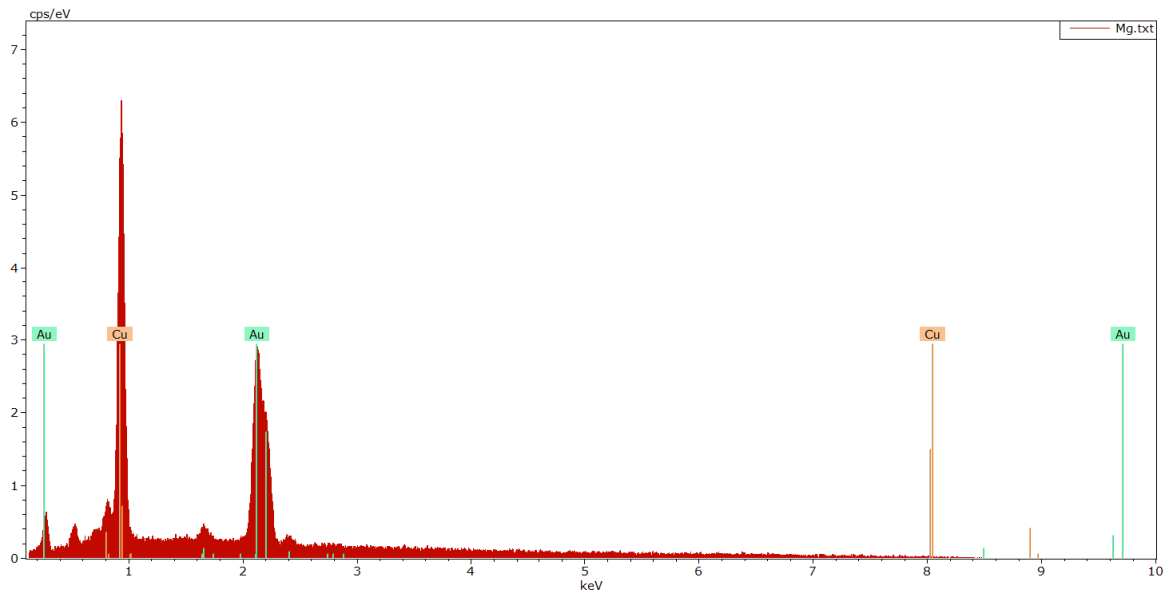


Figure S5. EDS of the Au-coated Cu nanowires.

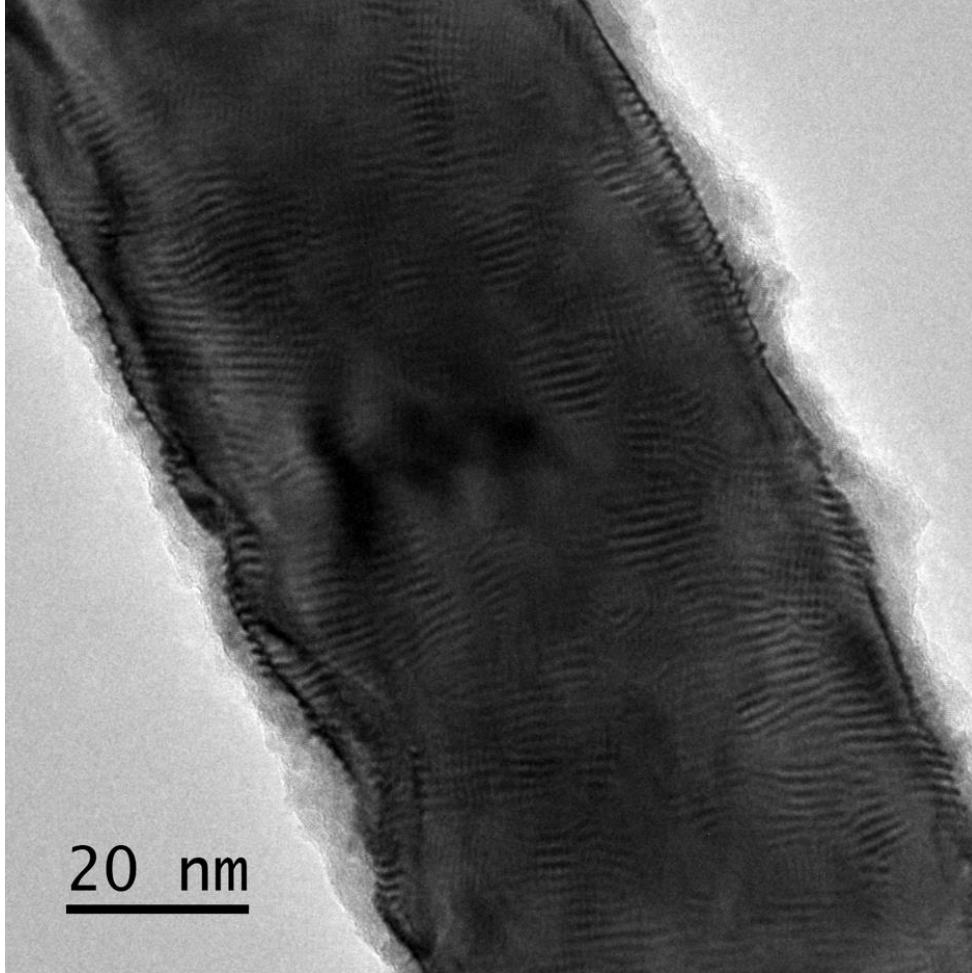


Figure S6. TEM image of Au coated Cu nanowire.

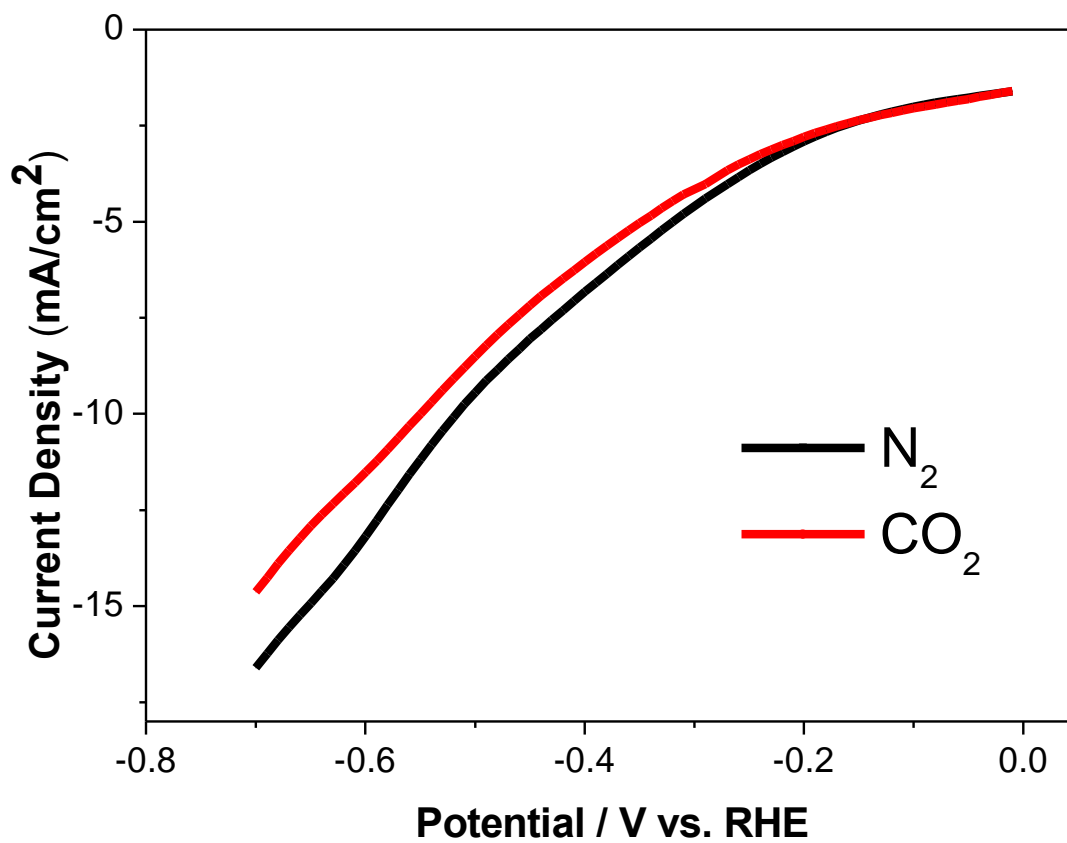


Figure S7. Linear sweep voltammetry of Au coated Cu nanowire arrays in CO₂-saturated and N₂-saturated aqueous 0.5 M KHCO₃ solution at a scan rate of 50 mV/s.

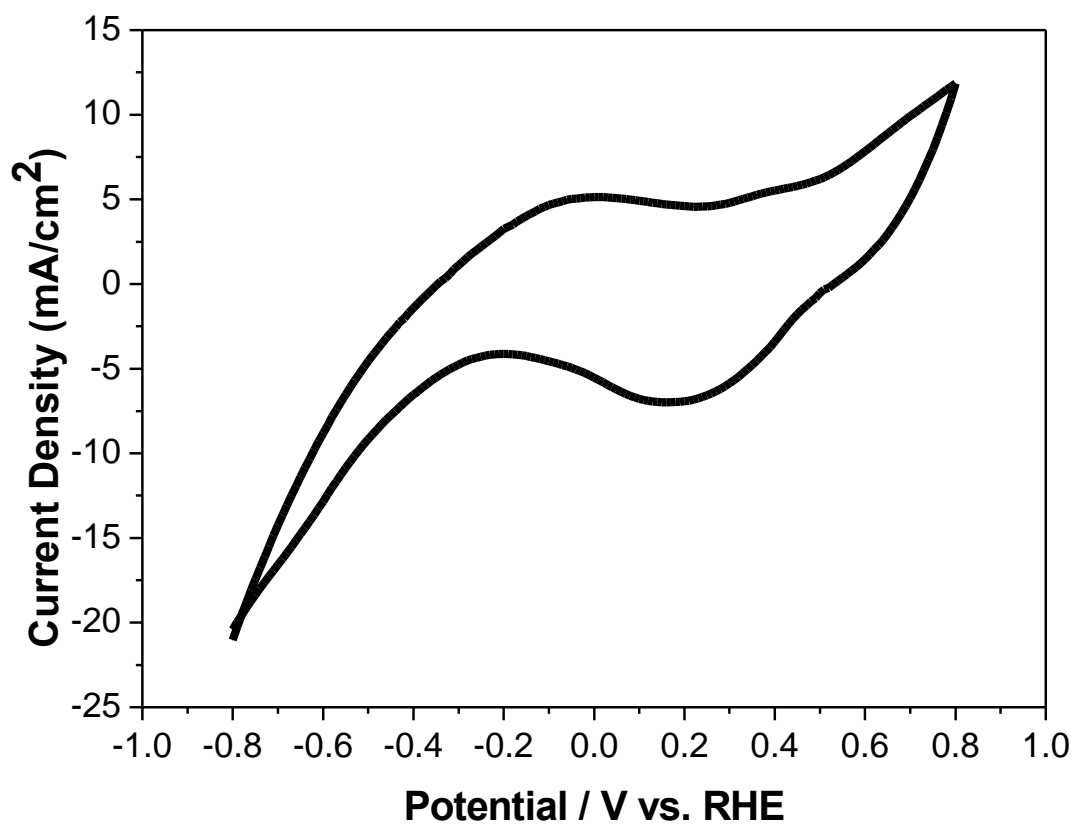


Figure S8. Cyclic voltammetric (CV) of Au coated Cu nanowire arrays in CO₂-saturated and N₂-saturated aqueous 0.5 M KHCO₃ solution at a scan rate of 50 mV/s.

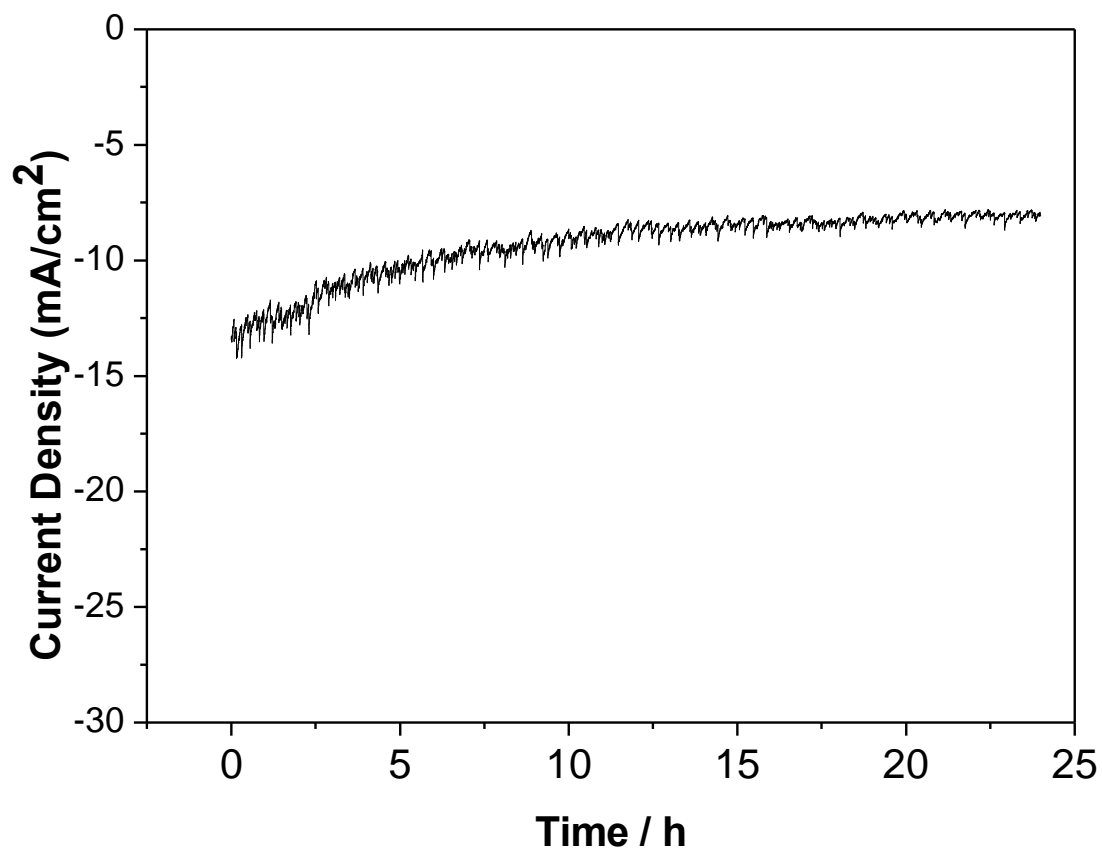


Figure S9. Current density vs. time curve during electrolysis at -0.65 V vs. RHE.

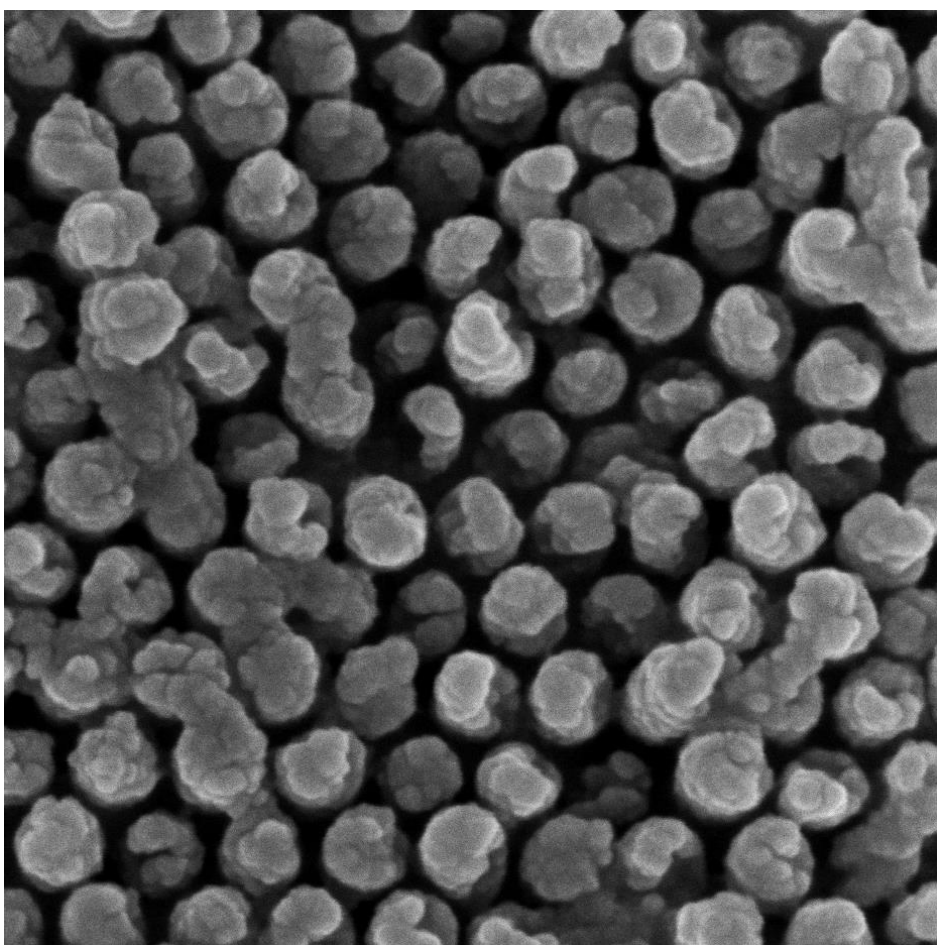


Figure S10. SEM image of core-shell Cu/Au nanostructure arrays after 24h of electrolysis

Chapter 5

**Electrochemical production of syngas
from CO₂ on nanoporous flow-through
Cu membranes in ionic liquid electrolyte**

Chapter Overview

The following chapter is a paper titled “Electrochemical production of syngas from CO₂ on nanoporous flow-through Cu membranes in ionic liquid electrolyte” submitted to PCCP. In this chapter, the effects of membrane configuration and electrolyte on the electrocatalytic performance of nanostructured Cu membranes for CO₂ reduction was investigated. The non-flow-through Cu membrane was able to produce a very high current density, but the product was almost entirely H₂, implying that the reaction was mass-transfer limited. When ionic liquid was used as the electrolyte, this Cu membrane catalysed formation of CO at an overpotential as low as 90 mV. By making the flow-through Cu membrane, with pores open at both ends, and using ionic liquid electrolyte, the catalyst was able to produce syngas with high efficiency and stability at an overpotential of 390 mV. This novel system may pave a way for producing syngas efficiently

Electrochemical production of syngas from CO₂ on nanoporous flow-through Cu membranes in ionic liquid electrolyte

Kun Chen,^a Xinyi Zhang,^a Douglas R. MacFarlane^{a*}

Received 00th January 20xx,
Accepted 00th January 20xx

DOI: 10.1039/x0xx00000x

www.rsc.org/

We report the effects of membrane configuration and electrolyte on the electrocatalytic performance of nanostructured Cu membranes for CO₂ reduction. In aqueous electrolyte, non-flow-through Cu membranes gave very high current densities, but produced only H₂, suggesting that the reaction was mass-transfer limited. When ionic liquid was added to the electrolyte, these flow-through membranes could catalyse formation of CO at an overpotential as low as 90 mV. The combination of a flow-through Cu-membrane catalyst and ionic liquid in the electrolyte produced syngas with high efficiency and stability at an overpotential of 390 mV.

1 Introduction

Global warming has become one of the biggest worldwide concerns. With the CO₂ concentration in the atmosphere rising to a record high level, actions are urgently needed to tackle this problem. One promising approach is to use renewable electricity to reduce CO₂ into hydrocarbons,¹⁻⁵ as a means of replacing use of fossil fuels.

Over the past few decades, various electrocatalysts have been tested for the electrochemical reduction of CO₂.⁶⁻⁹ Among them, Cu is of particular interest, because it is the only material known to be capable of producing hydrocarbons.¹⁰ Although huge efforts have been devoted to using Cu for CO₂ reduction, none of the reported electrocatalysts is selective or efficient enough for practical applications.¹¹⁻¹⁷ Besides this, because of the various paths involved in the CO₂ reduction process, the underlying mechanisms are also not fully understood.¹⁸⁻²⁰ Synthesizing novel Cu structures with high efficiency and selectivity for CO₂ reduction is critical, from both practical and fundamental viewpoints.

Ordered nanoporous Cu membranes are promising candidates for this purpose. Zhang et al. made highly ordered metal nanostructures via a double-template method.²¹ Using a similar method for Cu could allow the preparation of membranes with very large surface areas, greatly increasing the current density. Metal nanostructures often have very different catalytic activity compared with that of their bulk counterparts,²⁰ due to the presence of many edge and corner sites so the nanoporous Cu membrane might also have better product selectivity. Nanoporous membranes may also be used

in a flow-through configuration, which would make CO₂ more readily available to the catalyst surface, and further enhance the reduction process.

Previous research has also demonstrated that adding ethylmethylimidazolium tetrafluoroborate (EMIM-BF₄) ionic liquid (IL) into the electrolyte tends to reduce the energy barrier and increase the efficiency for CO₂ reduction.²² Rosen et al. revealed that the EMIM cation is also capable of inhibiting the competing hydrogen evolution reaction (HER), even at very high water concentrations.²³ Thus, by adding ionic liquid into the electrolyte, it is possible to increase the efficiency and selectivity of the Cu catalyst.

Therefore, in this study, ordered nanoporous Cu membranes were synthesised and applied to CO₂ reduction for the first time. Non-flow-through Cu membranes sustained very high current densities, but yielded largely H₂, probably because the reaction was mass transfer limited. In contrast, a flow-through copper membrane with an ionic-liquid containing electrolyte yielded some CO at overpotentials as low as 90 mV. At an overpotential of 390 mV with respect to the formation of CO, syngas, a very useful industrial gas mixture with a stable CO/H₂ ratio, was formed.

2 Experimental

2.1 Fabrication of Nanoporous Cu Membranes

Anodic aluminium oxide (AAO) membranes were fabricated in 0.3 M oxalic acid solution by using an established two-step anodization process.²⁴ Aluminium foil (99.999%, 0.5 mm thick) was the starting material. Then, a Au layer, around 10 nm thick, was sputter-coated onto one side of the AAO membrane to make it conductive. A reverse porous poly (methyl methacrylate) (PMMA) replica of the AAO membrane was then prepared by immersing the AAO membrane in a solution of 5

a. School of Chemistry, Monash University, Clayton, Victoria, 3800, Australia

† Footnotes relating to the title and/or authors should appear here. Electronic Supplementary Information (ESI) available: [details of any supplementary information available should be included here]. See DOI: 10.1039/x0xx00000x

wt% benzoyl peroxide in methyl methacrylate monomer.²⁴ The monomer-impregnated sample was polymerized by heating at 60 °C for 12 h. A concentrated NaOH solution was then used to fully remove the AAO membrane, leaving behind a negative replica PMMA template. Cu electrodeposition was carried out at room temperature, in an electrolyte containing 0.2 M CuSO₄ and 0.1 M H₃BO₃, adjusted to pH 4.5 with H₂SO₄. A constant current of -3 mA was used, and the counterelectrode was a platinum wire. Two different electrodeposition times were used: around 3 hours gave a mechanically robust electrode, with pores closed on one end (non-flow-through membrane), while around 10 minutes gave a far thinner membrane with open pores (flow-through membrane). After electrodeposition, the membranes were immersed in CHCl₃ to fully dissolve the PMMA. Figure S1 shows a schematic of the procedures involved in fabricating the porous Cu membranes. For comparison, a non-flow-through membrane with larger pores was also prepared in a similar way, starting with commercial AAO from Whatman as the template.

2.2 Characterization

An FEI Nova NanoSEM 450 FEG SEM instrument was used to collect scanning electron microscopic (SEM) images and energy dispersive spectra (EDS). A Philips X-ray power diffractometer was used to collect X-ray diffraction (XRD) data. Gas chromatography (GC) was performed on an Agilent 7820 A GC system equipped with a thermal conductivity detector and an HP-plot molesieve (5A) column. Helium (99.99%) was used as the carrier gas for CO analyses, while the carrier gas for H₂ detection was nitrogen (99.99%). The retention times were compared with those of known compounds. The electrochemical experiments were conducted on a CHI 760E electrochemical workstation (CH Instruments, Austin, Texas, USA) at room temperature.

Copper conductors were soldered onto the non-porous faces of the non-flow-through membranes, and subsequently sealed with glue. The surface areas of the non-flow-through and flow-through electrodes were around 0.5 cm². CO₂ electrolysis experiments for these membranes were carried out in a gas-tight two-compartment electrochemical cell with a glass frit serving as the separator. Each compartment had 15 mL electrolyte and around 15 mL headspace. Counter and reference electrodes were platinum wire and Ag/AgCl (3 M KCl), respectively. The electrolyte (0.5 M KHCO₃ for initial tests, EMIM-BF₄ solutions in later tests) was purged with a constant flow of CO₂ for 30 minutes before electrolysis. During the electrolysis, the electrolytes in both compartments were stirred vigorously. After electrolysis, a gas-tight syringe was used to take 100 µL gas samples from the cell's head space for subsequent analysis by GC.

A different cell (shown in Figure S2), was fabricated to test the flow-through Cu membrane. The flow rate of CO₂ was 0.3 mL/min. After 10 mins of reaction, around 3 mL of the gas product was collected and analysed by GC.

In this study, all potentials were converted to a reversible hydrogen electrode (RHE) reference scale. EMIM-BF₄ was purchased from Proionic. All other chemicals in this study were purchased from Sigma-Aldrich Australia and were used without further purification.

3 Experimental Results and Discussion

3.1. Non-flow-through Cu membrane with 70 nm pore size

Figure 1 shows the SEM image of an ordered nanoporous Cu membrane made using home-made AAO as the template. The nanopores are around 70 nm in diameter, and the walls are around 10 nm thick. The order within this membrane structure is clearly apparent. EDS confirmed that the membrane is indeed made of Cu, as shown in Figure S3. XRD (Figure S4) reveals three peaks in the spectra, namely (111), (200), and (220).

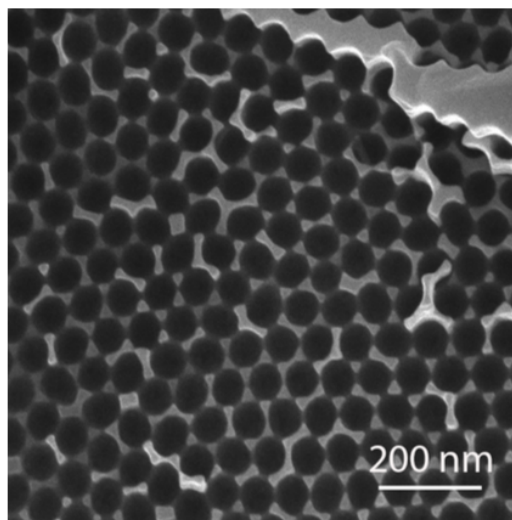


Figure 1. SEM image of an ordered nanoporous Cu membrane with 70 nm pore size.

Figure 2a shows that the nanoporous Cu membrane could sustain a similar current density to that produced by the Cu nanowire arrays investigated in our previous work.²⁵ However, the Faradaic Efficiency (FE) for CO production on the nanoporous Cu membrane had slightly better performance, but the overall efficiency was still extremely low. The highest FE of CO was only around 5%, as shown in Figure 2b, with the remaining product being H₂. Compared with Hori's results on polycrystalline Cu foil, the FE of CO is much lower. Besides, formate, methane and ethylene were also detected when the bulk Cu electrode was used.²

One possible explanation for this poor performance is that because of the extremely small size of the nanopores and the high current density, the reaction is mass transfer limited. Since H⁺ is much more abundant and readily available in the electrolyte, the HER becomes dominant over CO₂ reduction.

Besides, previous study on density functional (DFT) calculation indicates that the (111) surface of Cu is more likely to be involved in the HER than in the CO₂ reduction reaction.¹⁴ Since Cu (111) dominates the structure of the Cu membrane (as shown in Figure S4), the production of various CO₂ reduction products is severely suppressed while the HER gets promoted.

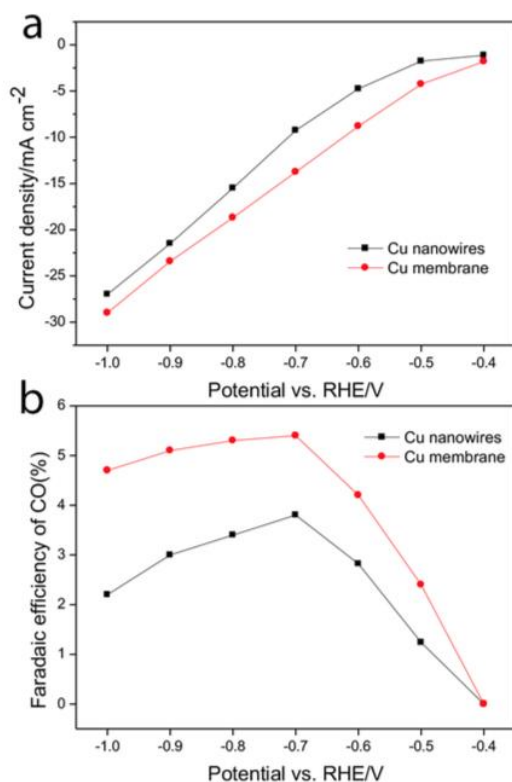


Figure 2. Current density (a) and FE of CO (b) of non-flow-through Cu membrane and Cu nanowires under different potentials.

3.2. Performance of Cu membranes with 200 nm pores

Since it is possible that the poor performance of the non-flow-through Cu membrane for CO₂ reduction is caused by the small size of the nanopores, non-flow-through Cu membranes with larger pores were also tested. In this case, commercially available AAO membranes were used as templates.

A typical SEM image of the commercial AAO membrane is shown in Figure S5. The diameter of the nanopores is around 200 nm and the thickness of the pore wall is about 40 nm. The overall membrane thickness is around 50 μm (Figure S5b).

Figure 3 shows the SEM image of this Cu membrane after removal of the polymer. EDS confirms that the main composite of the membrane is Cu, as shown in Figure S6. The membrane was then made into an electrode, as previously described.

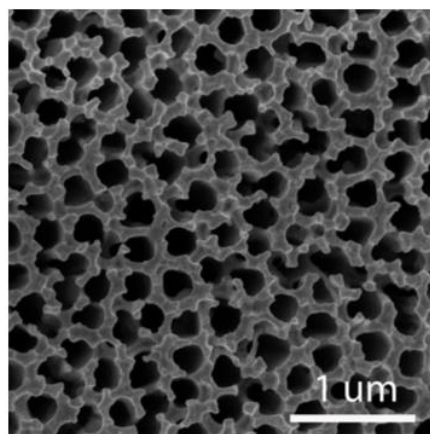


Figure 3. SEM image of non-flow-through Cu membrane with bigger pores.

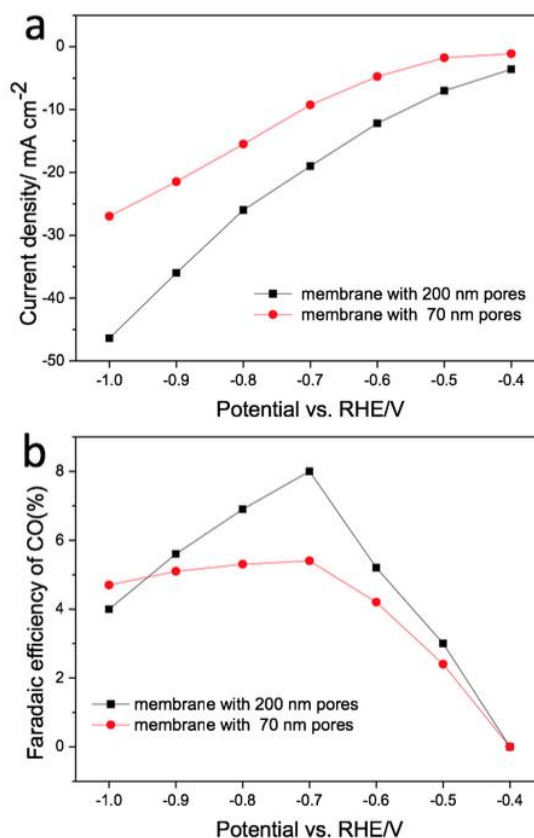


Figure 4. Current density (a) and FE of CO (b) of non-flow-through Cu membranes with different pore sizes at different potentials.

Figure 4a shows that the magnitude of the current density obtained with this porous Cu membrane is considerably higher than that obtained with the membrane with smaller pores. At -0.5 V vs. RHE, CO was first detected, but the amount was very low, as shown in Figure 4b. At a potential range of -0.6 to -1 V vs. RHE, the majority of the product was H₂ with less than 8% of CO detected. At that potential range, no other product apart from CO and H₂ could be detected. One possible reason for this poor performance is that even though the nanopores in this membrane were much bigger than those in the previous Cu membrane, it is quite possible that they were still too small for the electrolyte to move freely during the experiment, meaning that the reaction might still be mass transfer limited, and therefore dominated by the HER. Since HER is kinetically faster, H₂ became the main product of the reaction.

3.3. Effect of EMIM-BF₄ addition on CO₂ reduction

Previous research has demonstrated that it is possible to reduce the energy barrier and increase the efficiency for CO₂ reduction by simply adding EMIM-BF₄ ionic liquid (IL) into the electrolyte.²² So EMIM-BF₄ mixed with deionized water was used as the electrolyte for CO₂ reduction. Because 50 vol % EMIM-BF₄ has been suggested to have the highest conductivity, this electrolyte composition was first examined.²⁵ The electrolyte was purged with CO₂ before use, as described for the aqueous electrolyte.

As shown in Figure 5a, the magnitude of the current density produced by the non-flow-through Cu membrane in 50 vol % EMIM-BF₄ electrolyte was very high. At -1 V vs RHE, the current density was around 50 mA/cm², even higher than seen in the aqueous electrolyte. When the concentration of EMIM-BF₄ was raised to 75 vol %, the current density remained relatively high. But, at 95 vol %, the current density dropped dramatically. This is mainly because when the concentration of EMIM-BF₄ becomes higher, the conductivity of the electrolyte decreases, thus reducing the overall current density.

Figure 5b shows the FE of CO at different concentrations of EMIM-BF₄. At 50 vol %, the Cu membrane started to catalyse the formation of CO at a potential of -0.2 V, corresponding to 90 mV overpotential for this product. This increased activity is mainly due to the presence of the ionic liquid, which significantly reduces the energy barrier. A peak FE of around 12 % for CO production is obtained at potential of -0.5 V RHE. When the IL concentration was increased to 75 vol %, the peak FE for CO became 18%. At a concentration of 95 vol %, the peak FE for CO was as high as 50 %.

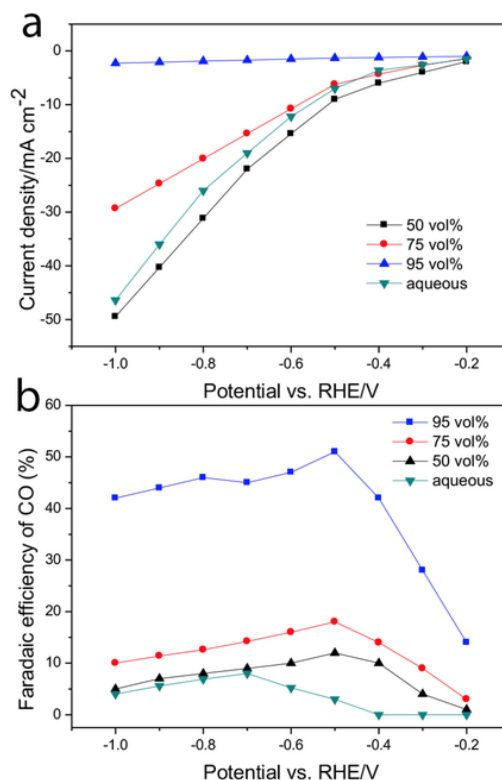


Figure 5. Current density (a) and FE of CO (b) of non-flow-through Cu membrane with smaller pores, obtained with different concentrations of EMIM-BF₄ in the electrolyte, under different potentials.

This result demonstrates that the presence of ionic liquid significantly reduces the overpotential for CO production. However, EMIM-BF₄ does not dramatically suppress the HER. In an ionic liquid electrolyte, H₂ remains the dominant product.

3.4. CO₂ reduction by flow-through Cu membranes in aqueous medium

To increase the mass transfer efficiency, a flow-through chemical cell was specially designed and manufactured, as shown in Figure S2. The flow-through Cu membrane was fabricated by using a much shorter electrodeposition time. Figure 6 shows SEM images of both faces of the flow-through Cu membrane. The nanopore diameter is around 200 nm.

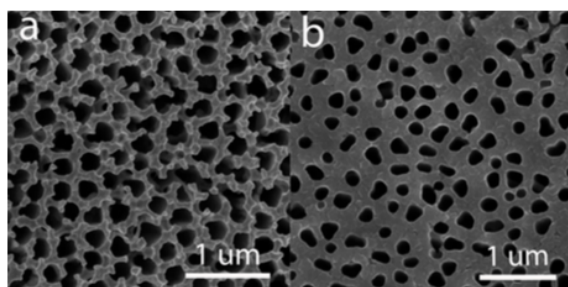


Figure 6. (a, b) SEM images of both faces of the Cu membrane.

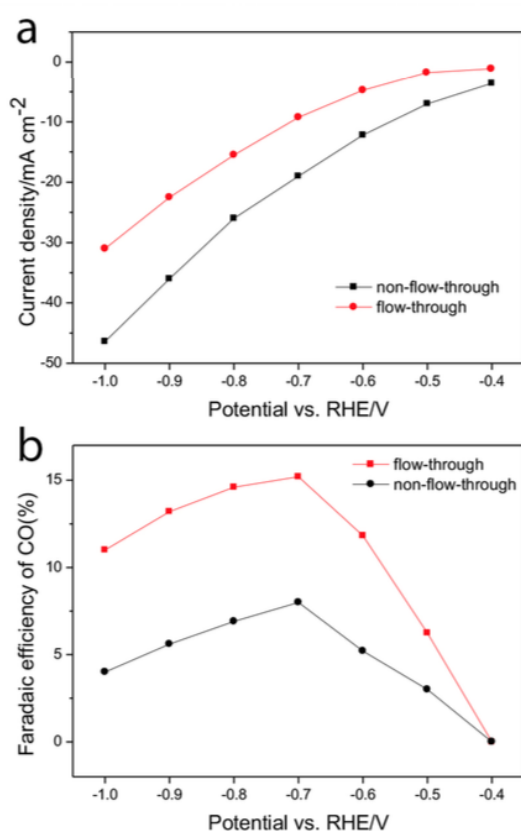


Figure 7. Current density (a) and FE of CO (b) of flow-through and non-flow-through Cu membranes under different potentials in aqueous medium.

Figure S7 shows the cross-sectional SEM image of the flow-through Cu membrane, demonstrating that pores extend through the Cu membrane. The performance of the flow-

through membrane is shown in Figure 7. The current density sustained by the flow-through membrane was lower than that for the non-flow-through Cu membrane. This is because the flow-through membrane is much thinner, and thus has a smaller surface area, leading to a reduced current density. The flow-through Cu membrane had a much higher FE of CO than its non-flow-through counterpart, presumably because CO₂ is more readily available in the flow-through configuration, facilitating the CO₂ reduction reaction. But the highest FE of CO that could be achieved was still only about 15%, with the remainder being H₂. No other products could be detected under the potentials tested.

3.5. CO₂ reduction performance of flow-through Cu membranes in ionic liquid medium

To further increase the FE of CO, the performance of the flow-through Cu membrane was investigated in water-ionic liquid mixture electrolytes. Figure 8a shows that the current density of the flow-through Cu membrane in 80 vol % EMIM-BF₄ electrolyte is much lower than that obtained in the aqueous medium. This can again be attributed to the lower conductivity of the electrolyte. Figure 8b shows that the flow-through Cu membrane started to catalyse the formation of CO at a potential of -0.2 V, corresponding to 90 mV overpotential for this product, demonstrating the high catalytic activity of the membrane in ionic liquid medium. As the potential increases, the FE of CO also becomes higher, reaching a peak value of around 34% at a potential of -0.5 V RHE. Further increase of in potential slightly decreases the FE of CO.

As can be clearly observed from Figure 8b, when the applied potential was -0.5 V, the molar ratio of CO/H₂ was about 1:2, which is the composition of syngas. This gas mixture is of particular interest because it can be readily used as the source gas for the Fischer-Tropsch process, a widely used industrial technique to produce many types of fuel.²⁵ Besides, even at such a modest overpotential, the current density was over 2 mA/cm², higher than most reported values for Cu electrodes.^{10,12,16} This high current density is mainly due to the large true surface area of the nanoporous Cu membrane.

A potential of -0.5 V was used to investigate the long-term stability of the CO/H₂ ratio. After 6 hours of electrolysis, the ratio remained quite stable (as shown in Figure 8c), demonstrating the high stability of the catalyst. Besides, the long-term stability of the current was also studied under an applied potential of -0.5 V. Figure 8d shows, that apart from the initial drop, the current density remained quite stable during 24 h of electrolysis. This long-term stability can be attributed to the very solid nanostructure as well as the large surface area of the nanoporous Cu membrane.

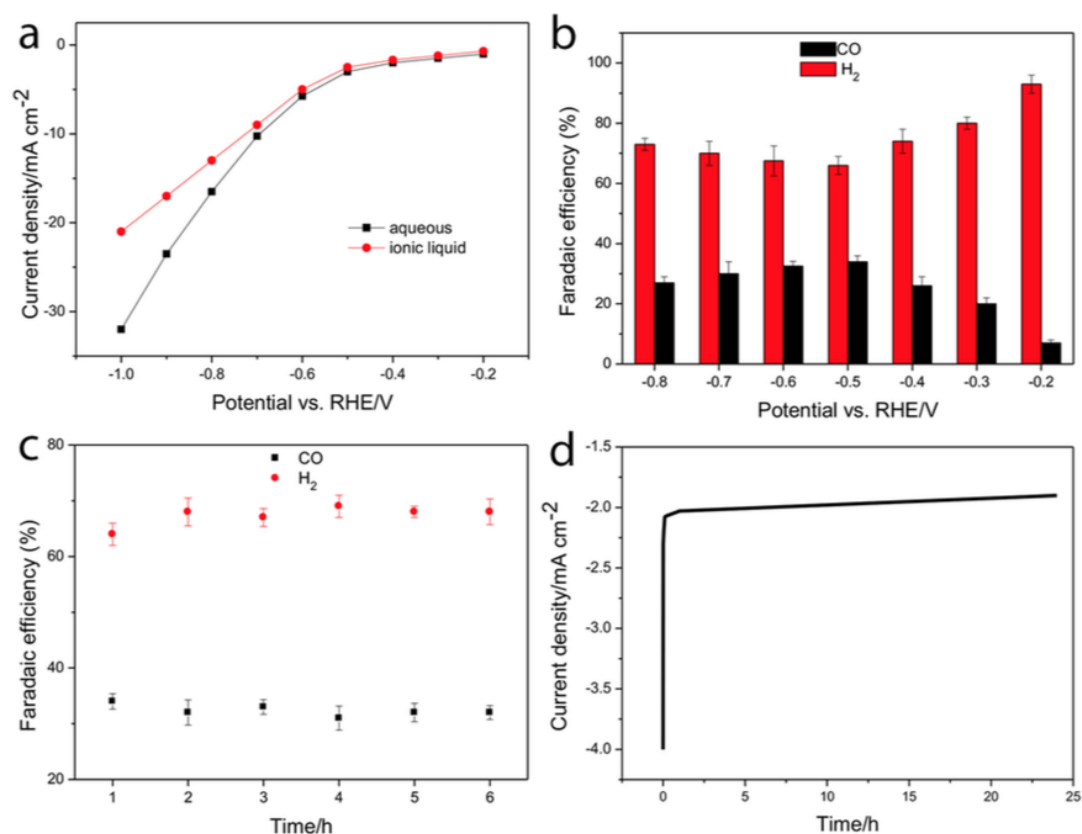


Figure 8. Current densities (a) and Faradaic efficiencies for CO and H₂ (b) as a function of potential. (c) Faradaic efficiencies for CO and H₂ over time. (d) current density at a potential of -0.5 V vs RHE over time. All tests were carried out in a flow-through cell with 80 vol% EMIM-BF₄, 20 vol% water used as electrolyte.

4 Conclusions

In conclusion, ordered nanoporous Cu membranes were synthesised and used as electrodes in CO₂ reduction for the first time. The non-flow-through Cu membrane was able to produce a very high current density, but product was almost entirely H₂, implying that the reaction was mass-transfer limited. When ionic liquid was used as the electrolyte, this Cu membrane catalysed formation of CO at an overpotential as low as 90 mV. By making the flow-through Cu membrane, with pores open at both ends, and using ionic liquid electrolyte, the catalyst was able to produce syngas with high efficiency and stability at an overpotential of 390 mV. This novel system may pave a way for producing syngas efficiently.

Acknowledgements

This work was financially supported by the Australian Research Council through the ARC Centre of Excellence for Electromaterials Science (Grant No. CE140100012) and Grant

No.: DP120104334. DRM is grateful to the ARC for his Australian Laureate Fellowship. The authors also gratefully acknowledge the contribution of the Monash Centre for Electron Microscopy.

Notes and references

1. J. Xie, Y. Huang and H. Yu, *Frontiers of Environmental Science & Engineering*, 2015, **9**, 861-866.
2. Y. Hori, A. Murata and R. Takahashi, *Journal of the Chemical Society, Faraday Transactions 1: Physical Chemistry in Condensed Phases*, 1989, **85**, 2309-2326.
3. K. P. Kuhl, E. R. Cave, D. N. Abram and T. F. Jaramillo, *Energy & Environmental Science*, 2012, **5**, 7050-7059.
4. C. Costentin, M. Robert and J.-M. Savéant, *Chemical Society Reviews*, 2013, **42**, 2423-2436.
5. S. Zhang, P. Kang and T. J. Meyer, *Journal of the American Chemical Society*, 2014, **136**, 1734-1737.
6. H. Wang, J. Jia, P. Song, Q. Wang, D. Li, S. Min, C. Qian, L. Wang, Y. F. Li and C. Ma, *Angewandte Chemie International Edition*, 2017.

7. W. Luc, C. Collins, S. Wang, H. Xin, K. He, Y. Kang and F. Jiao, *Journal of the American Chemical Society*, 2017, **139**, 1885-1893.
8. W. Lu, B. Jia, B. Cui, Y. Zhang, K. Yao, Y. Zhao and J. J. Wang, *Angewandte Chemie International Edition*, 2017, 10.1002
9. Y. Chen, C. W. Li and M. W. Kanan, *Journal of the American Chemical Society*, 2012, **134**, 19969-19972.
10. Y. Hori, in *Modern aspects of electrochemistry*, Springer, 2008, pp. 89-189.
11. T. T. Hoang, S. Ma, J. I. Gold, P. J. Kenis and A. A. Gewirth, *ACS Catalysis*, 2017, **7**, 3313-3321.
12. C. W. Li and M. W. Kanan, *Journal of the American Chemical Society*, 2012, **134**, 7231-7234.
13. X. Nie, M. R. Esopi, M. J. Janik and A. Asthagiri, *Angewandte Chemie International Edition*, 2013, **52**, 2459-2462.
14. S. Sen, D. Liu and G. T. R. Palmore, *Acs Catalysis*, 2014, **4**, 3091-3095.
15. W. Luo, X. Nie, M. J. Janik and A. Asthagiri, *ACS Catalysis*, 2015, **6**, 219-229.
16. M. Ma, K. Djanashvili and W. A. Smith, *Physical Chemistry Chemical Physics*, 2015, **17**, 20861-20867.
17. W. Tang, A. A. Peterson, A. S. Varela, Z. P. Jovanov, L. Bech, W. J. Durand, S. Dahl, J. K. Nørskov and I. Chorkendorff, *Physical Chemistry Chemical Physics*, 2012, **14**, 76-81.
18. K. Schouten, Y. Kwon, C. Van der Ham, Z. Qin and M. Koper, *Chemical Science*, 2011, **2**, 1902-1909.
19. P. Hirunsit, W. Soodsawang and J. Limtrakul, *The Journal of Physical Chemistry C*, 2015, **119**, 8238-8249.
20. Q. Lu, J. Rosen and F. Jiao, *ChemCatChem*, 2015, **7**, 38-47.
21. X. Zhang, Y. Zheng, X. Liu, W. Lu, J. Dai, D. Y. Lei and D. R. MacFarlane, *Advanced Materials*, 2015, **27**, 1090-1096.
22. B. A. Rosen, A. Salehi-Khojin, M. R. Thorson, W. Zhu, D. T. Whipple, P. J. Kenis and R. I. Masel, *Science*, 2011, **334**, 643-644.
23. B. A. Rosen, W. Zhu, G. Kaul, A. Salehi-Khojin and R. I. Masel, *Journal of The Electrochemical Society*, 2013, **160**, H138-H141.
24. K. Chen, X. Zhang, Y. Zhang, D. Y. Lei, H. Li, T. Williams and D. R. MacFarlane, *Advanced Materials Interfaces*, 2016, **3**.
25. K. Chen, X. Zhang, T. Williams, L. Bourgeois and D. R. MacFarlane, *Electrochimica Acta*, 2017, **239**, 84-89.

Supporting Information for

Electrochemical production of syngas from CO₂ on nanoporous flow-through Cu membranes in ionic liquid electrolyte

Kun Chen,^a Xinyi Zhang,^a Douglas MacFarlane^{a*}

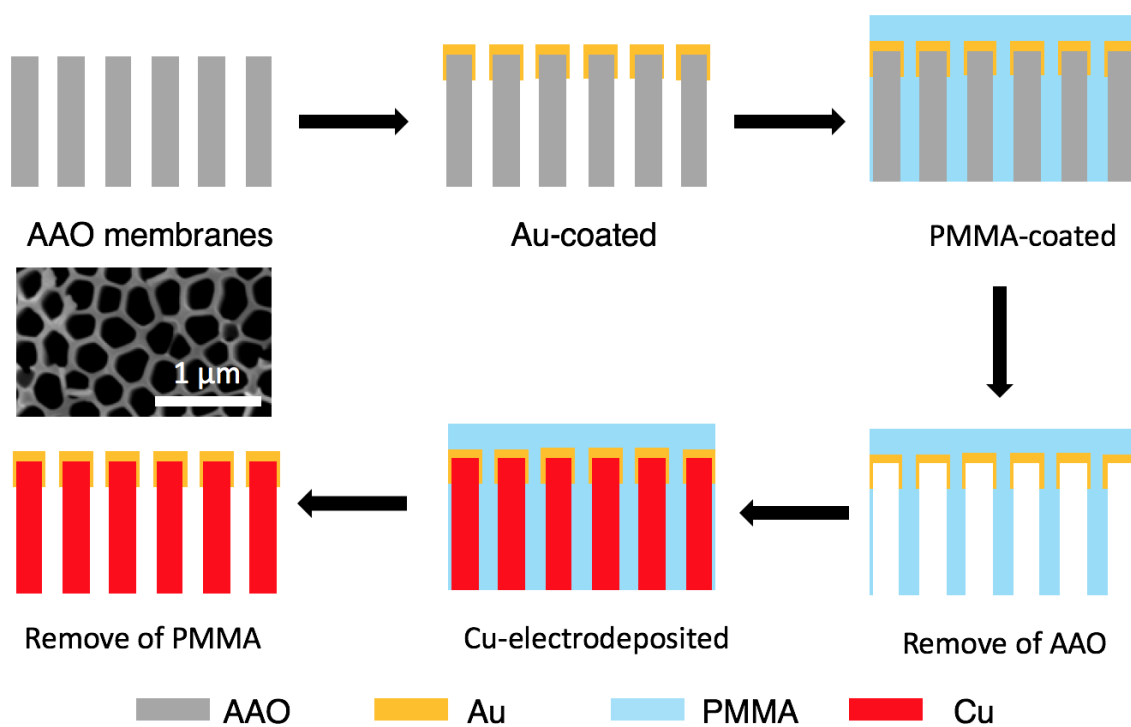


Figure S1. Schematic diagrams for the fabrication procedure of hole-through Cu membrane.

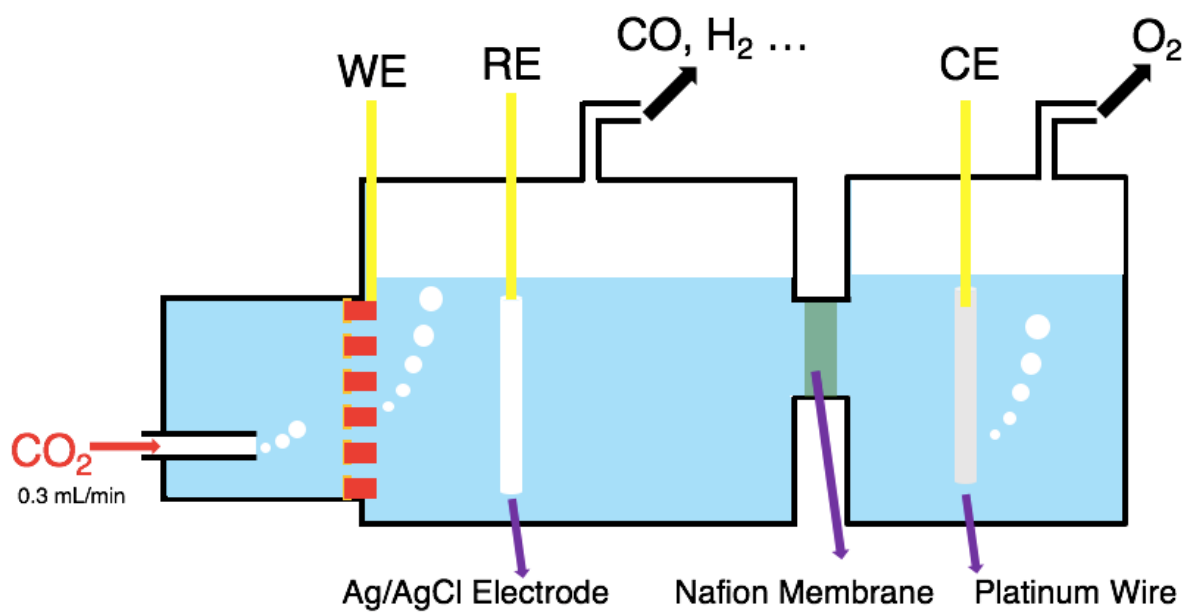


Figure S2. Schematic diagrams of the flow through cell.

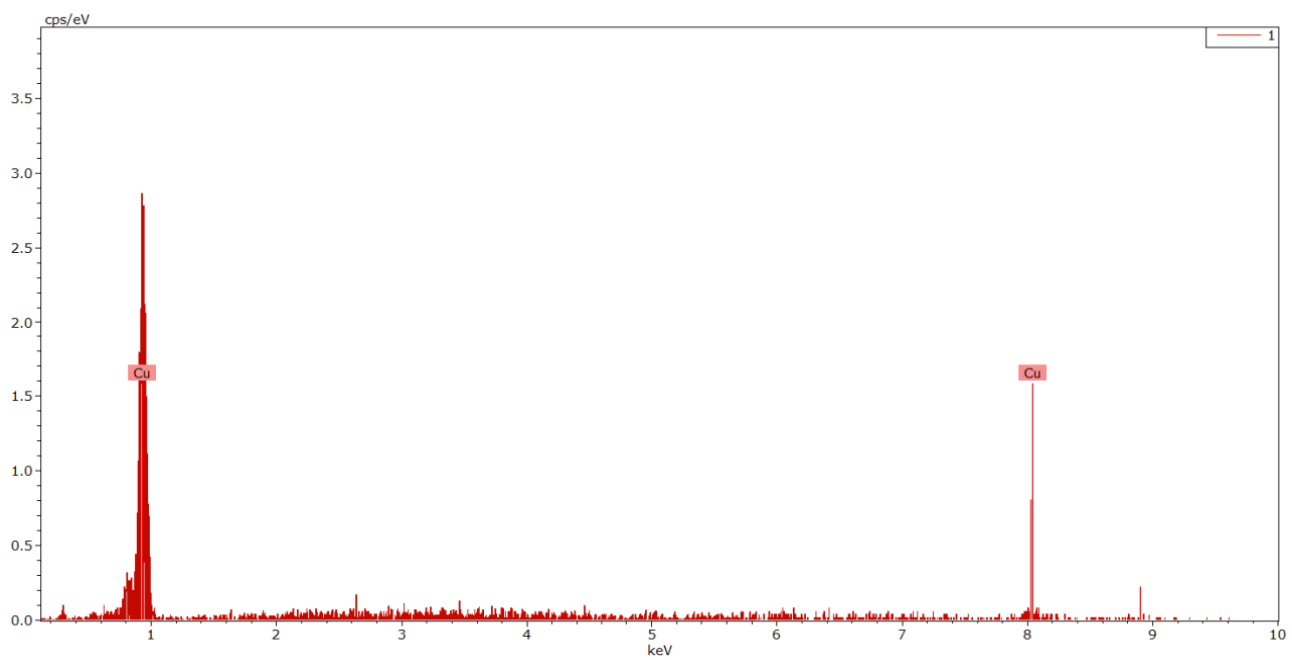


Figure S3. EDS of an ordered nanoporous Cu membrane.

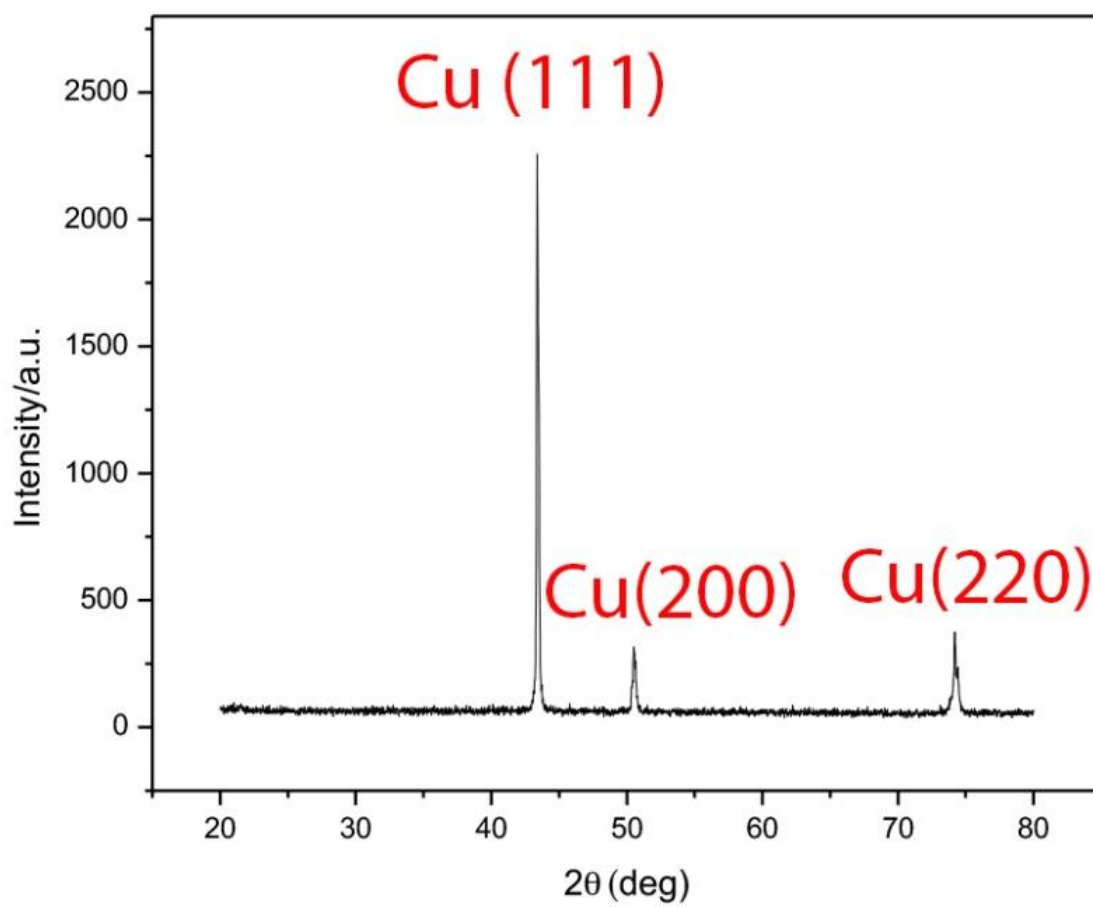


Figure S4. XRD of ordered nanoporous Cu membrane.

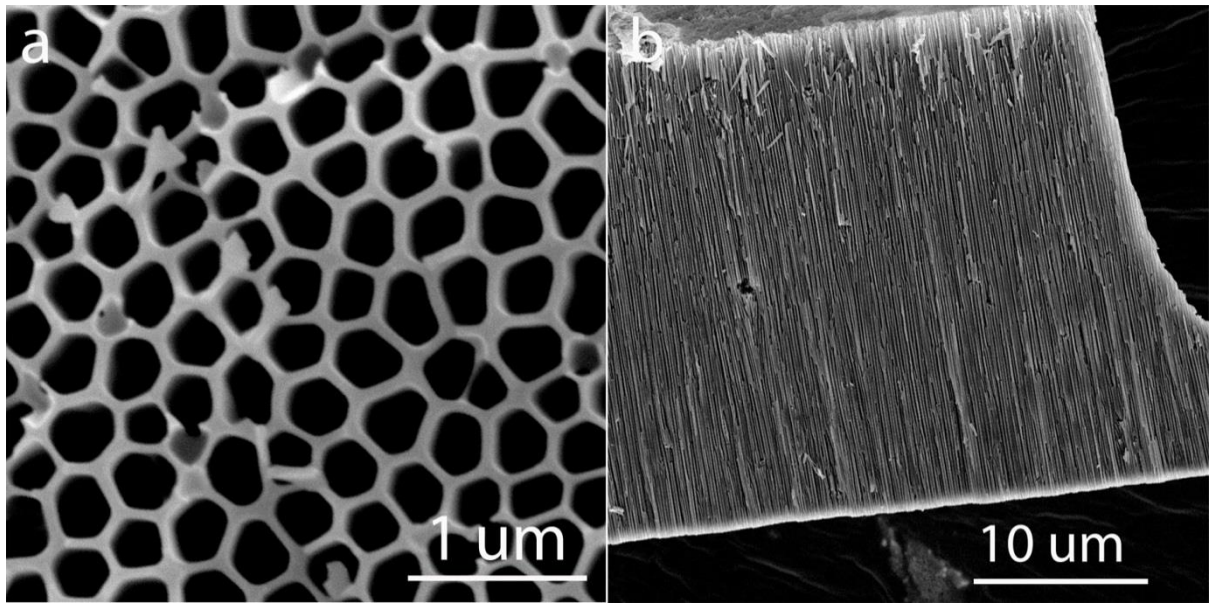


Figure S5. Front (a) and cross-section (b) SEM images of the commercial AAO membrane.

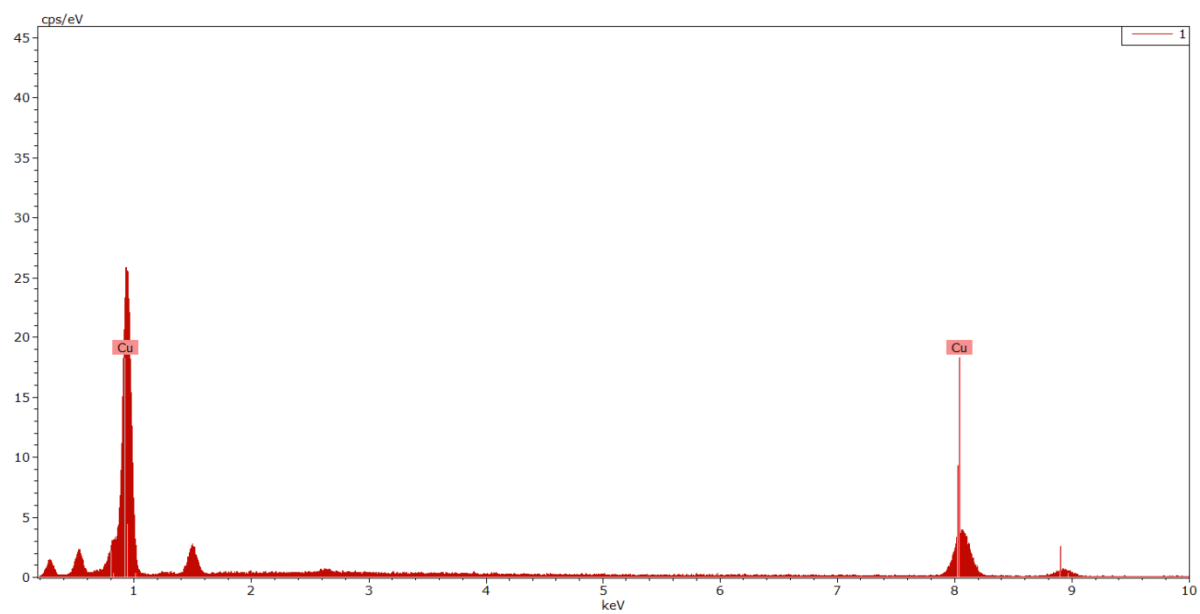


Figure S6. EDS of the ordered nanoporous Cu membrane with bigger pore size.

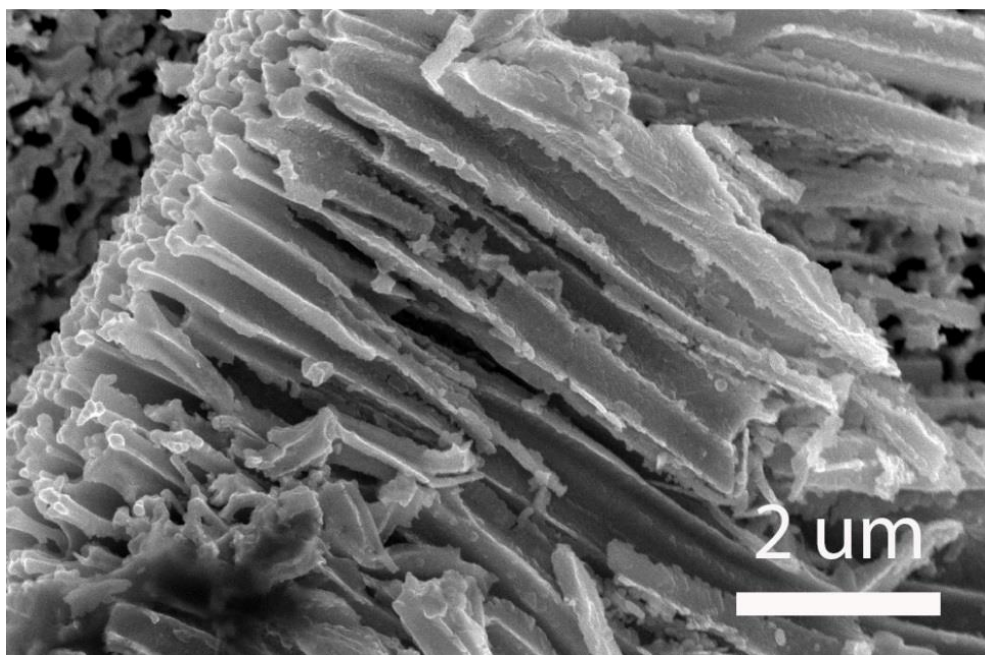


Figure S7. Cross-section SEM image of the hole-through Cu membrane.

Chapter 6

Conclusions and Future Work

6.1. Conclusions

This thesis has discussed the fabrication of Cu-based ordered nanostructures as well as their applications in surface-enhanced Raman spectroscopy (SERS) and electrochemical reduction of CO₂. Chapter 2 demonstrated a simple approach for the fabrication of Ag/Cu hybrid nanostructure arrays as highly sensitive and cost-effective substrates for SERS application. By effectively tuning the gap size between neighboring nanorods to sub-10 nm and increasing the packing density of nanorods, ordered Cu nanorod arrays can be used as cheap and effective SERS substrates in their own right. After sputtering a very thin layer of Ag nanoparticles on the surface of the Cu nanorods to achieve sub-5 nm gaps, further field enhancement is enabled. The Ag/Cu hybrid nanostructure arrays exhibit a detection limit down to 10⁻¹⁵ M for non-resonant molecules such as benzenethiol.

Chapter 3 presented a paper published in Chemical Communication to demonstrate that SERS can be used in real world medical applications. In this paper, a simple approach was explored to fabricate cost-effective and highly sensitive surface-enhanced Raman scattering substrates based on Au/Cu hybrid nanostructure arrays for the detection of urea, an important molecule in biological and medical fields. By effectively adjusting the gap size between neighbouring nanorods into the sub-10 nm regime, a high density of hot-spots was generated, enabling the substrates to detect urea signals at a concentration as low as 1 mM with great reproducibility.

Electrocatalytically converting CO₂ to hydrocarbons is a very attractive way to use the excess electricity generated from renewable energies. In chapter 4, Cu nanowires fabricated with an anodic aluminium oxide (AAO) membrane were used as the electrode CO₂ reduction for the first time. By sputter coating a thin layer of Au on top, the current density as well as Faradaic efficiency (FE) of CO were further enhanced. At an overpotential of 540 mV with respect to the formation of CO, the Au-coated Cu nanowires catalysed the formation of syngas, a very useful gas mixture, with high efficiency and stability.

In Chapter 5 ordered nanoporous Cu membranes were synthesised to improve the performance of CO₂ reduction. The Cu membrane was able to produce a very high current density, but the main product was H₂ since the reaction was likely to be mass transfer limited. When ionic liquid was used as the electrolyte, the Cu membrane was capable of catalysing the formation of CO at an overpotential as low as 90 mV. By making the Cu membrane flow-through and using ionic liquid as electrolyte, the catalyst was able to produce syngas with high efficiency and stability at an overpotential of 390 mV.

6.2. Future work

There are a number of research pathways that will expand upon the work presented in this thesis in a meaningful way. In the following sections, several suggestions for future work will be presented.

6.2.1. Ordered nanoporous Fe membranes for N₂ reduction

The fabrication method developed in chapter 5 is highly versatile. The same method can also be applied to synthesise Fe membranes. Fe is known to be a very good catalyst for N₂ reduction reaction. To the best of my knowledge, nobody has investigated ordered nanoporous Fe membranes in ionic liquid media for N₂ reduction yet. Considering the very large surface area of the Fe membrane and the great value of N₂ reduction, it is worth exploring this field. Ideally, this would create a catalyst with low overpotential and high efficiency to convert N₂ into ammonia, an important ingredient for fertilizer.

6.2.2. Hybrid metal membranes for the electrochemical reduction of CO₂

Although the study in chapter 5 shows that Cu membrane is not a particularly good structure for CO₂ reduction, the hole-through metal membrane structure still has many advantages due to its extremely large surface area. So in future work, hybrid metallic metal membranes could be synthesised to improve the performance of CO₂ reduction.

6.2.3. Cu membranes for water splitting

The Cu membranes have a current density comparable to other catalysts for hydrogen evolution in water splitting. The main issue for water splitting is that the Nafion membrane used to separate the electrodes is extremely expensive. It might be possible to use our Cu membrane to separate the gas products, getting rid of the expensive organic membrane in the middle all together. If successful, this could significantly bring down the cost of water electrolysis cells.

6.2.4. nanostructured metal oxide for photo catalysis

The nanostructures developed in this thesis have very large surface area and good catalytic activity. Therefore, cheap and effective photo-catalysts can be potentially be made to convert CO₂ and N₂ into useful organic products by using a renewable energy source such as solar energy.

6.2.5. Flow-through metal membranes as molecular sieves

The diameters of many biological molecules are in the range of 20-300 nm. Therefore, the flow-through nanostructure developed in Chapter 5 can be potentially be used as a molecular sieve to separate molecules of different size, which is a vital process in many biological procedures